CONTROLLED-RELEASE OF MOSQUITO REPELLENTS

FROM MICROPOROUS POLYMER STRANDS

by

Alcides Everildo José Sitoe

Thesis submitted in partial fulfilment of the requirements for the degree of

Doctor of Philosophy

in

Chemical Technology

In the Faculty of Engineering, Built and Environment and Information

Technology

University of Pretoria

Pretoria

2019

DECLARATION

I, Alcides Everildo José Sitoe, Student No. 16401426, do hereby declare that this research is my original work and that to the best of my knowledge and belief, it has not been previously in its entirety or in part been submitted and is not currently being submitted either in whole or in part at any university for a degree or diploma, and that all references are acknowledged.

SIGNED on this 31st day of July 2019

_____

A.E.J. Sitoe

CONTROLLED-RELEASE OF MOSQUITO REPELLENTS FROM MICROPOROUS POLYMER STRANDS

Author: Alcides Everildo José Sitoe

Supervisor: Prof. Walter W. Focke

Degree: PhD (Chemical Technology)

Department: Chemical Engineering

SYNOPSIS

Malaria parasite infects more than 200 million people and about 435 000 succumb to the illness annually (WHO, 2019). Victims are mostly young children and pregnant women. It is transmitted by the bite of the infected female *Anopheles* mosquitoes. Indoor protection is provided by bed nets and residual spraying of insecticides. Mosquitoes typically bite ankles and feet most of the time (93%) whilst in outdoor settings. Long lasting insect-repellent anklets/bracelets/footlets may provide a strategy for reducing mosquito bites outdoors in the lower limb regions. This study considered long-lasting repellent anklets that may be used for outdoor protection against mosquito bites. Experiments were performed to investigate the incorporating of mosquito repellents into the thermoplastic polymers, poly(ethylene-co-vinyl acetate) (EVA) and linear low-density

polyethylene (LLDPE). Two different mosquito repellents, namely DEET and Icaridin, were employed. The target was to develop cost-effective bracelets with long-lasting efficacy, i.e., slow release of the active ingredient over extended periods. In this way, it is expected to protect people from acquiring mosquito-borne diseases during the time they spend outdoors. The proposed concept utilises microporous polymer strands manufactured via conventional plastic extrusion processes. The internal open-cell polymer foam structure serves both as a reservoir and a protective environment for the active ingredient trapped inside. An outer dense skin layer covering the strands may provide the necessary diffusion barrier that controls the release of repellent at effective levels over a considerable period. The objective was achieved by phase separation via spinodal decomposition (SD), triggered by extruding the molten strands directly into ice-cold water. Thermogravimetric analysis (TGA) and solvent extraction confirmed that all of the repellents were embedded in the polymer matrices. Scanning Electronic Microscopy (SEM) confirmed the porous co-continuous repellent-polymer microstructure. The stability of the polymer matrix was studied by estimating the swelling and shrinkage of the polymer matrix. The release of the active ingredient in the polymer/repellent system was followed as a function of oven-ageing temperature and time. The kinetics of the release rate of the repellent from microporous polymer matrix strands was mathematically modelled using semi-empirical models. The performance of the repellent-based strands was evaluated using foot-in-cage repellence testing. Finally, an attempt was made to predict the phase diagrams of the LLDPE/repellent system on the basis of alkane/repellent systems data.

The results confirmed that EVA and LLDPE are suitable scaffold matrices, acting as reservoirs, for liquid repellents that were released at a constant rate. As expected, the repellent swelled EVA more than LLDPE. As a result, it also shrank significantly more when the repellent was released, i.e. EVA showed poor dimensional stability compared to LLDPE.

The semi-empirical repellent release models were found valuable as they provided insights into the way that the repellent was being released. They allowed differentiating between diffusion and relaxation mechanisms. It was found that repellence efficacy can be maintained for more than 90 days. Future developments of sandals and anklets based on this approach may assists in preventing outdoor mosquito bites, thereby decreasing malaria infection rates.

Keywords: Malaria, vector control; polymer-repellent solution; spinodal decomposition;

DEDICATION

Dedicated to my beloved wife, Evelina Sitoe and my inspirational sons that

were born during my studies, Jessé and Jonathan Sitoe

ACKNOWLEDGEMENTS

I gratefully thank God Almighty, because "through him, all things were made; without him, nothing was made that has been made" - John 1:3.

I sincerely thank my supervisor, Prof. Walter W. Focke for his patience, guidance and encouragement during my studies and throughout my stay at the University of Pretoria.

I would also like to thank the following people for their assistance:

Mr Benjamim Mapossa (Compounding and Bioassay testing)

Prof. Leo Braack (Providing mosquitoes for Bioassay testing)

Dr Shepherd Tichapondwa (Guidance, encouragement and moral support)

Mr Joseph Sebekedi (Compounding)

Prof. James Wesley-Smith (Electron Microscopy analysis)

Dr Eudri Venter (Scanning Electron Microscopy)

Ms Erna van Wilpe (Scanning Electron Microscopy)

Mr Victor (Thermogravimetric analysis)

Mr Cyril Ndonyane (Providing mosquitoes for Bioassay testing)

Ms Isbe van der Westhuizen (Thermogravimetric analysis and DSC facilities)

Mr Robert Tewo (Compounding and Bioassay testing)

Mr Tatenda Madzorera (Bioassay testing)

Ms Chanita Sungkapreecha (Thermogravimetric analysis)

Ms Suzette Seymore (Administration)

Dr Mthokozisi Sibanda (Experimental discussion)

Mr Sifiso Skosana (Compounding)

I would like to extend my sincere gratitude to my parents, José Johane Sitoe and Mariana Salvador Tivane and my brothers Nelson Sitoe, Claúdio Sitoe, Ándre Sitoe and my sister Alcília Sitoe, for encouraging me and for their moral support. I want to thank my colleagues at Eduardo Mondlane University (UEM), Carvalho Madivate, Arão Manhique and Herminio Muiambo, for giving me this opportunity to go further with my studies. I would also like to thank my friends Arlindo Wate, Óscar Nhabanga, Eutilério Chaúque, Joaquim Simbine, Moisés Matlombe Elísio Macarringue Lucréncio Macarringue and Isaias Face.

TABLE OF CONTENTS

LIST OF FIGURES

LIST OF TABLES

LIST OF ACRONYMS AND ABBREVIATIONS

3D	Three-dimensional
AFR	WHO African Region
Al 3-14244	Cyclohexanepropionic acid
Al 3-35765	1-(3-Cyclohexen-1-ylcarbonyl)piperidine
Al 3-37220	Cyclohex-3-en-1-yl-(2-methylpiperidin-1-yl)methanone
AMR	WHO Region of the Americas
ANOVA	Analysis of variance
AS	Repellent-based EVA strand samples
ATR	Attenuated total reflection
BEPD	2-Butyl-2-ethyl-1,3-propanediol
BET	Brunauer–Emmett–Teller
BHT	Butylated hydroxytoluene
BM	Repellent-based LLDPE strand samples
BnBzO	Benzyl benzoate
CAS	Chemical abstracts service
DBP	Dibutyl phthalate
DEET	N,N-Diethyl-3-methylbenzamide
DEPA	*N,N*-diethyl phenylacetamide
DF	Dengue fever
DFG	Deutsche Forschungsgemeinschaft
DIPS	Diffusion induced phase separation
DMC	Dimethyl carbate
DMP	Dimethyl phthalate
DNA	Deoxyribonucleic acid
DOP	Dioctyl phthalate

DSC	Differential scanning calorimetry
EA	Ethyl anthranilate
EMR	WHO Eastern Mediterranean Region
EOs	Essential oils
EUR	WHO European Region
EVA	Poly(ethylene-co-vinyl acetate)
FESEM	Field Emission Scanning Electron Microscope
F-H	Flory-Huggins
FTIR	Fourier Transform infrared spectroscopy
GPC	Gel permeation chromatography
HSP	Hansen solubility parameter
HT-SEC	High-Temperature Size Exclusion Chromatography
Icaridin	KBR3023: sec-butyl 2 – (2-hydroxyethyl piperidine -1) carboxylate
Indalone	Butopyronoxyl
IR3535	Ethyl 3-[acetyl(butyl)amino] propanoate
IRS	Indoor residual spraying
ITNs	Insecticide-treated mosquito nets
LCST	Lower critical solution temperature
L-L	Liquid-liquid
LLDPE	Linear low-density polyethylene
LLIN	Long-lasting insecticide-treated net
LOI	Loss on Ignition
MA	Methyl anthranilate
Metofluthrin	2,3,5,6-Tetrafluoro-4-(methoxymethyl)benzyl-2,2-dimethyl-3-(prop-1-en-1-yl)cyclopropanecarboxylate
MFI	Melt flow index
MGK Repellent 11	4,5a,6,9,9a,9b-hexahydro-1H-dibenzofuran-4a-carbaldehyde

MGK Repellent 264	*N*-octyl bicycloheptene dicarboximide
MGK Repellent 326	Di-n-propyl isocinchomeronate
MNDA	*N*-Methylneodecanamide
Nepetalactone	4,7-dimethyl-5,6,7,7*a*-tetrahydro-4*aH*-cyclopenta[c]pyran-1(4aH)-one
NICD	National Institute for Communicable Diseases
NIPS	Non-solvent induced phase separation
PIPS	Pressure-induced phase separation
PNC	Polymer nanocomposites
RI	Refractive index
RNA	Ribonucleic acid
Rutgers 612	2-Ethyl-1,3-hexanediol
SD	Spinodal decomposition
SEAR	WHO South-East Asia Region
SEM	Scanning Electron Microscopy
SIPS	Solvent-induced Phase Separation
S-L	Solid-liquid
TAEPS	Thermally assisted evaporation phase separation
TCB	1,2,4-trichlorobenzene
TGA	Thermogravimetric analysis
TIPS	Thermally induced phase separation
UCST	Upper critical solution temperature
UK	United Kingdom
UV	Ultraviolet
VA	Vinyl acetate
WHO	World Health Organization
WNV	West Nile virus

WPR   WHO Pacific Region

LIST OF SYMBOLS

ΔS_m^{comb} Combinatorial change in entropy of mixing [J·K^{-1}]

ΔG_m Change in Gibbs free energy of mixing [J·mol^{-1}]

ΔH_V Molar enthalpy of vaporisation [J]

ΔH_m Change in enthalpy (or heat) of mixing [J]

ΔS_m Change in entropy of mixing [J·K^{-1}]

Δ_T Lyderson correction [-]

ϕ_2 Volume fraction of solute or polymer [-]

D_f Diameters after shrinkage process of strands [mm]

D_i Diameters before shrinkage process of strands [mm]

E_D Dispersion cohesive energy [-]

E_H Hydrogen bond cohesive energy [-]

E_P Polar cohesive energy [-]

E_T Total cohesive energy [-]

E_{coh} Cohesive energy [-]

G_1 Solvent Gibbs free energy [J·mol^{-1}]

G_{12} Gibbs free energy for the mixture [J·mol^{-1}]

G_2 Solute or polymer Gibbs free energy [J·mol^{-1}]

M_w Molar mass [g·mol^{-1}]

N_1 Number of solvent molecules [-]

N_2 Number of solute or polymer molecules [-]

N_A Avogadro constant [mol^{-1}]

N_C Number of mosquitoes landing on and/or probing the untreated leg [-]

N_T Number of mosquitoes landing on and/or probing the treated leg [-]

$S_R(\%)$ Shrinkage of polymer strands in percentage [-]

T_b	Boiling temperature [K]
T_c	Critical temperature [K]
T_{cloud}	Cloud point Glass temperature [^{o}C]
T_g	Glass transition temperature [^{o}C]
T_m	Melting temperature [^{o}C]
W_1	Numbers of distinguishable spatial arrangements of the solvent molecules
W_{12}	Numbers of distinguishable spatial arrangements of the molecules in the mixture
W_2	Number of distinguishable spatial arrangements of the solute molecules
W_f	Weight of the strand after extraction of the repellent [g]
W_i	Weight of the strands before extraction of the repellent [g]
X_1	Mole fraction of solvent [-]
X_2	Mole fraction of solute or polymer [-]
m_0	Weight of dried polymer pellets [g]
m_t	Weight of swollen polymer pellets at time t [g]
n_1	Number of moles of solvent [mol]
n_2	Number of moles of solute or polymer [mol]
p^H	Scale of acidity [-]
δ_1	Solubility parameter of solvent [$J^{1/2}.m^{-3/2}$]
δ_2	Solubility parameter of solute or polymer [$J^{1/2}.m^{-3/2}$]
δ_D	Dispersion interactive (London) force [$J^{1/2}.m^{-3/2}$]
δ_H	Hydrogen bond forces [$J^{1/2}.m^{-3/2}$]
δ_P	Dipole-dipole interactive forces [$J^{1/2}.m^{-3/2}$]
δ_T	Hansen or total solubility parameter [$J^{1/2}.m^{-3/2}$]
χ_H	Entropic component of χ [-]
χ_S	Enthalpic component of χ [-]
χ_c	Critical Flory-Huggins polymer-solvent interaction parameter [-]

ϕ_1	Volume fraction of solvent [-]
ϕ_{2c}	Critical composition [-]
ϕ_2' or ϕ_2^α	Volume fraction in the polymer poor phase [-]
ϕ_2'' or ϕ_2^β	Volume fraction in the polymer-rich phase [-]
n	Shape parameter [-]
$E(\%)$	Estimated repellent amount in mass per cent [-]
F	Molar attraction constant [-]
P	Constant pressure [kPa]
R	Universal gas constant [J·K^{-1}.mol^{-1}]
S	Entropy [J·K^{-1}]
$S(\%)$	Estimated polymer matrix swelling by repellents in percentage [-]
T	Absolute temperature [K]
V or V_m	Molar volume of the mixture [m^3]
$X(t)$	Time-dependent repellent released [g]
$X(t)$	Total amount of repellent released [%]
a	Entropic component of χ [J]
b	Enthalpic component of χ [J·K^{-1}]
k	Kinetic rate constant [-]
$p(\%)$	Protection in percentage [-]
t	Time [days]
x	Total number of segments in a polymer chain [-]
$\boldsymbol{k}$	Boltzmann constant [J·K^{-1}]
$\boldsymbol{n}$	Diffusional exponent [-]
ρ	Mass density [g·cm^{-3}]
τ	Dimensionless time constant/ scale parameter [-]

THESIS OUTLINE

In total, the thesis comprises of five chapters and references. Appendices are also included.

An introduction to the study, as well as a description of the novel product and methodology used in the present work are given in *Chapter One*.

Chapter Two introduces polymers, polymer solutions, polymer nanocomposites (PNC) and microporous structures as well as their preparation and application. In addition, a description of tropical diseases is provided. The weaknesses of the current vector control focused on malaria are discussed. The chapter introduces the reader to different methods of preparing microporous polymer structures. However, the emphasis is on the thermal-induced phase separation (TIPS) method, as it was the method used. A new product concept is presented to address the weakness(es) mentioned above in the fight against malaria. The principle of controlled-release technology and the mathematical model for repellent release from the new product are also presented.

Chapter Three outlines the experimental design and presents the raw materials and the instruments that were implemented in the laboratory work. The methods and procedures followed in the laboratory are also described in this chapter. It describes how the polymer strands were produced and characterised.

The results are presented and discussed in *Chapter Four*. The following aspects are dealt with:

- The effect of the nanofiller (fumed silica and clay) as well as the type and concentration of repellent in the microporous polymer structure;

- The morphology of the microporous polymer strands as revealed through micrographs;

- The swelling of the polymer matrix by repellents and shrinkage of polymer strands;

- The time-dependent release of the repellents from microporous matrices and its mathematical modelling. This includes the different factors (temperature, polymer, nature and concentrations of repellent, the diameter of strand and nanofiller) that affected the release of the repellent from the microporous polymer matrix;

- The repellency bioassay results of the polymer strands; and

- The modelling of the phase behaviour of polymer/repellent systems.

Chapter Five summarises the key findings of the study together with recommendations.

The *Reference* section provides a record of the literature consulted during this study, which was also used to elucidate the findings of the study.

Additional relevant information and data are given in the *Appendices*.

CHAPTER ONE

INTRODUCTION

1.1 Background

The human capacity to deal with infectious diseases has seen tremendous advancements in recent decades. Even so, some infectious diseases have managed to cope with these medical and scientific developments. Although medical progress has been made and modern response systems are constantly being designed, developed and improved, humanity is nonetheless continually confronted with new and re-emerging diseases. Mosquitoes and arthropods, distributed worldwide but mostly found in tropical and sub-tropical areas, are the usual disease transport vectors responsible for infectious diseases (Rivero *et al.*, 2010, Morens and Fauci, 2016, Murugan and Sathishkumar, 2016).

Mosquitoes are one of the most dominant disease-causing vectors and are one of the most fatal animals in the world. Every year, mosquitoes cause millions of deaths due to their capacity to carry and transmit a variety of diseases. Dengue, chikungunya, yellow fever and Zika are transmitted to humans by the female *Aedes aegypti* mosquito, while malaria and West Nile Virus (WNV) are transmitted by *Anopheles* spp and *Culex* spp, respectively. The most dreaded mosquito-borne disease is malaria, which caused 435 000 deaths globally in 2017 alone (WHO, 2019). More than 50% of the population of the world live in regions where it is nearly impossible to eliminate mosquitoes. Therefore, sustainable mosquito controls using novel interventions are necessary to

avoid outbreaks of these diseases (Winstanley, 2001, Tiwary *et al.*, 2007, Benelli, 2016, Murugan and Sathishkumar, 2016, WHO, 2019).

Due to the high cost involved, countries with limited resources are discouraged from using topically-applied repellents on exposed body areas (DEET in most cases) and from wearing cloths impregnated with insecticides to reduce mosquito bites while outdoors. However, essential oils (EOs) like citronella oil extracted from plants that are used as insect repellents have high volatility that limits their use in topical formulations. The use of these EOs could potentially be a cost-effective solution (Fradin and Day, 2002, Cisak *et al.*, 2012, Van Zyl, 2016).

In impoverished tropical and sub-tropical countries, a two-pronged approach is always used in the effort to control malaria. The first is parasite control by means of diagnosing malaria parasite and treating infected people as well as intermittent preventive therapy in pregnant woman, and the second is vector control by means of indoor residual spraying (IRS) of insecticides as well as the use of long-lasting insecticide-treated bed nets (LLINs).

The over-reliance on parasite control and vector control using the approaches outlined above has resulted in many reports expressing concerns about the current situation of drug and insecticide resistance, as well as environmental concerns regarding malaria control and the need to explore new tools and new strategies (Hemingway *et al.*, 2006, Pang *et al.*, 2009, Rivero *et al.*, 2010, David *et al.*, 2013, Benelli *et al.*, 2015, Benelli, 2016, Benelli and Mehlhorn, 2016, Molla, 2016, Ranson and Lissenden, 2016, Yewhalaw and Kweka, 2016). Strategies for vector control are further compromised by the fact that no convincing mechanism exists anywhere in the world for reducing

mosquito bites outdoors in impoverished rural communities living in tropical and sub-tropical areas, where malaria incidences are high. Introducing new approaches or tools in the armoury to combat mosquito-borne diseases would represent a major contribution to the improvement in public health and human well-being in the most affected areas of the world, where development continues to be held back by the simple inability to prevent mosquito bites and where infectious diseases have made headway.

The main malaria vectors are attracted by the smell of short-chain fatty acids (which smell like Limburger cheese) produced by bacteria living mainly on the human foot. As a result, malaria mosquitoes prefer to bite the ankle area (Knols and De Jong, 1996, Knols, 1996, Knols *et al.*, 1997, Dekker *et al.*, 1998).

A recent study conducted to analyse the mosquito bite behaviour of the mosquito's main malaria vector showed that approximately 93% of bites occur on the ankles and feet, whether people are seated or standing. The study also showed that if feet and ankles are covered or protected in some way, the mosquitoes do not feed but rather search for alternative hosts whose ankles or feet are not covered. Importantly, it was also found that mosquitoes biting ankles and feet are related to the height above ground level, and not to a specific body part (Braack *et al.*, 2015).

Therefore, a long-life, repellent-impregnated polymer product (anklets or sandals) may possibly help to reduce mosquito bites at ground level. The repellent would have to be incorporated in a thermoplastic polymer, poly(ethylene-co-vinyl acetate) (EVA) and linear low-density

polyethylene (LLDPE). It could be possible to make the products cost-effectively with a conventional plastic extrusion process.

It would be possible to trap large amounts of repellents in microporous matrices. Such reservoirs can be obtained by controlled phase separation of polymer solutions. Thermally induced phase separation is a possible route to trap liquid mosquito repellent in a polymer matrix, where phase separation can initiate in unstable regions by spinodal decomposition (SD) mechanisms forming interconnections with uniform structures (Castro, 1981, Lloyd *et al.*, 1990, Song and Torkelson, 1995, Wenjun *et al.*, 1995, Li *et al.*, 2006, Chen *et al.*, 2007, Kim *et al.*, 2016, Liu *et al.*, 2016).

The idea proposed is to use thermally induced phase separation (TIPS) as a route to trap liquid mosquito repellent in a polymer matrix. Here, non-soluble repellent in the polymer matrix at ambient temperature will be used. Trapping of such repellents in the polymer matrix can be achieved by SD of the polymer-liquid repellent system. At sufficiently high-temperatures, a homogeneous solution is formed and rapid cooling of such solution to well below the upper critical solution temperature leads to the formation of co-continuous phase structure. The polymer then forms an open-cell structure with the repellent trapped inside. The repellents considered in this study are listed in Table 1.1 and Table 1.2 below.

Table 1.1: Natural insect repellents identified for consideration in this study

Repellent
p-menthane-3,8-diol (Citriodiol)
Citronella oil
Neem oil
Birch oil
Limonene
Lippia javanica essential oil
Catnip (Nepeta) oil
Clove oil

Table 1.2: Synthetic insect repellents identified for consideration in this study

Repellent	
DEET	*N,N*-Diethyl-3-methylbenzamide
Icaridin	1-piperidinecarboxylic acid 2-(2-hydroxyethyl)-1-methylpropylester
IR3535	Ethyl 3-[acety(butyl)amino] propanoate
MGK Repellent 11	4,5a,6,9,9a,9b-hexahydro-1H-dibenzofuran-4a-carbaldehyde
MGK Repellent 264	*N*-octyl bicycloheptene dicarboximide
MGK Repellent 326	Di-n-propyl isocinchomeronate
MNDA	*N*-Methylneodecanamide
Al 3-35765	1-(3-Cyclohexen-1-ylcarbonyl) piperidine
Al 3-37220	Cyclohex-3-en-1-yl-(2-methylpiperidin-1-yl) methanone
Rutgers 612	2-Ethyl-1,3-hexanediol
Indalone	Butopyronoxyl
MA	Methyl anthranilate
EA	Ethyl anthranilate
BEPD	2-Butyl-2-ethyl-1,3-propanediol
Al 3-14244	Cyclohexanepropionic acid
Metofluthrin	2,3,5,6-Tetrafluoro-4-(methoxymethyl)benzyl-2,2-dimethyl-3-(prop-1-en-1-yl)cyclopropanecarboxylate
Nepetalactone	4,7-dimethyl-5,6,7,7a-tetrahydro-4*aH*-cyclopenta[c]pyran-1(4aH)-one
DMP	Dimethyl phthalate
DBP	Dibutyl phthalate
DOP	Dioctyl phthalate
DMC	Dimethyl carbate
BnBzO	Benzyl benzoate
DEPA	*N,N*-diethyl phenylacetamide

Table 1.3 lists the criteria that should be considered in the development of a polymer/repellent system.

Table 1.3: Criteria for selection of repellents

Selection criteria	Comment
Efficiency to repel mosquitoes	The repellents will be tested regarding their ability to inhibit mosquito attraction to a host.
Volatility	An effective repellent will be the least volatile and offer long-lasting protection. Volatility is usually associated with vapour pressure and also the contribution of the diffusivity in the air.
Thermal stability	Thermal stability is required to withstand polymer processing temperatures often exceeding 180°C.
Toxicity and acceptance	Repellent must not be toxic to humans, be odourless or with a pleasant or annoyance odour and with non-effect to the skin, clothes, etc. A natural repellent will be preferred compared to synthetic repellents.
Costs	Repellents need to be cost-effective to make the final product affordable to poor nations and rural communities where mosquito-borne diseases are most prevalent
Phase behaviour	At room temperature, solid repellents will be easier to formulate into long-life controlled release polymer systems than liquid. Repellents must be non-soluble in the polymer matrix at ambient temperature.

The aim of this study was to develop technology and repellent-impregnated polymer products (anklets or sandals) that act as reservoirs for mosquito repellents, which efficiently and optimally release the repellent into the environment at a controlled rate. This will reduce the frequency of

mosquito bites on humans and would have the potential to become a new tool for malaria control, especially in outdoor conditions.

Incorporating a membrane-like structure on the surfaces of the open-cell polymer-repellent system could help to control the repellent-release rate. If necessary, the permeability of the polymer membranes with respect to particular repellent can be adjusted by the membrane thickness, the polymer chemistry and the addition of clay nanofillers.

It is important to note that ethical clearance was required for the study. This was due to the use of laboratory bioassays of the product, i.e. foot-in-cage repellence testing.

If successful, these products will not only be effective against malaria-transmitting mosquitoes but will also reduce the biting frequency of different types of mosquitoes transmitting other diseases. This, in turn, will contribute to the improvement of the public health and social well-being of the population overall, thereby making a significant difference in reducing incidences of disease.

1.2 Hypothesis

The premature loss of effectiveness of repellent active ingredients that are currently used in malaria vector control for mosquito outdoor biting is due to their high volatility. The aim of this study was to develop technology and repellent-impregnated polymer products (anklets or sandals) that will act as reservoirs for mosquito repellents, which efficiently and optimally release the repellent to the environment at a controlled rate. The target was to reduce mosquito bites on humans, thereby providing a new tool for malaria control, especially in outdoor settings. In this regard, the following hypotheses have been investigated:

- Large amounts of repellent can be trapped inside a microporous polymer matrix;

- The required microporous scaffold can be generated by SD of a homogeneous repellent-containing polymer melt. This can be achieved by direct extrusion of the exiting melt into ice-cold water to facilitate rapid cooling;

- Incorporating an outer skin membrane layer can control the repellent release to low values that will provide long-term repellence efficacy (> six months); and

- Both stiff and flexible polymer matrices are possible.

1.3 Research objectives

(1) To determine the swelling of the polymer by the liquid repellents and the shrinkage of polymer matrix strands after complete release of repellents;

(2) To estimate the phase diagrams of the LLDPE/repellent system using the model systems of alkane/repellent systems;

(3) To prepare repellent-containing strands by melt-compounding and extrusion. Induce phase separation by SD to generate the required open-cell scaffold structures;

(4) To characterise the core microporous structure of the polymer/repellent system;

(5) To estimate and optimise the release rate of the active ingredient in the polymer/repellent system as a function of oven-ageing temperature and time;

(6) To evaluate the amount of repellent trapped by microporous polymer matrix strands by thermogravimetric analysis (TGA) and solvent extraction methods;

(7) To mathematically model the kinetics of the release rate of the repellent from microporous polymer matrix strands;

(8) To test effectiveness of mosquito repellent products using the foot-in-cage test (bioassays).

1.4 Methodology

The research methodology will include the following activities:

(a) Determine the swelling of the polymer by DEET and Icaridin and the shrinkage of polymer matrix strands after complete release of DEET and Icaridin;

(b) Formation of open-cell micro-structures via SD by extrusion process into ice-water. TGA and solvent extraction will be used to estimate the quantity of repellent trapped and Scanning Electron Microscopy (SEM) to confirm the microporous structure formed;

(c) The release rate of the active ingredient will be studied using a convection oven, changing the temperature profile of the oven, type and concentration of the repellent, type of polymer, adding different types of nanofiller (silica and organoclay) as well as the concentration;

(d) The data used to model phase behaviour thermodynamically of alkanes/repellent systems will be obtained by differential scanning calorimetry (DSC) and hot stage microscopy. Alkanes represent different molar mass components [Hexadacane (C16), Eicosane (C20) and Tetracontane (C40)]. Finally, the modelled systems of alkanes/repellent will be used to predict the phase equilibrium of LLPDE-repellent systems;

(e) The models describing the release rate kinetics will be evaluated;

(f) For repellent efficacy of the product, bioassays tests will be carried out in foot-in-cage tests over a period of 12 weeks. Statistical analysis will be used to check the reliability of the results.

CHAPTER TWO

LITERATURE REVIEW

2.1 Infectious tropical diseases

Many infectious diseases are transmitted by vectors. Most of the vectors are bloodsucking organisms and they include flies, ticks, fleas, aquatic snails and mosquitoes. The latter has, for centuries, been the origin of diverse illnesses affecting humans. Female mosquitoes require protein for reproduction and get it from the blood of host animals. The different species target different vertebrate host. Some mosquitoes are highly specific with respect to their choice of host species (Reiter, 2001, Tolle, 2009, Petersen *et al.*, 2013, Murugan and Sathishkumar, 2016). The transmission occurs when the female mosquito consumes disease-producing microorganisms along with blood ingestion from an infected host and passes it to another host in a subsequent bloodsucking act (Tolle, 2009, Murugan and Sathishkumar, 2016).

Mosquitoes can be found all over the world except in areas enduringly or continuously frozen. Around the world, the tropical and subtropical zones are greatly affected by mosquito-borne diseases (Reiter, 2001, Tolle, 2009).

Mosquitoes are inevitably connected to water sources in their first life stage (larvae). Consequently, mosquito-borne disease is intrinsically correlated to the presence of water (freshwater or brackish water) (Norris, 2004, Murugan and Sathishkumar, 2016). Human activities can change the environment, such that it alters mosquito reproduction habitats. Beyond climate change, human activities and their impact on ecology are significant factors increasing the

transmission scale and expanding geographic areas of mosquitoes borne diseases (Martens and Hall, 2000, Reiter, 2001, Norris, 2004, Iturbe-Ormaetxe *et al.*, 2011, Patel *et al.*, 2011, Kouadio *et al.*, 2014).

There are numerous infectious diseases caused by mosquitoes but those responsible for the most deaths worldwide are malaria, dengue, and chikungunya (Murugan and Sathishkumar, 2016). Malaria is considered a very old human affliction. It continues to be the dominant infectious tropical disease, in spite of the major progress in malaria control during the past few decades. There are different ways in which malaria can be spread. However, virtually all malaria cases derive from the bite of infected female *Anopheles* mosquitoes. Malaria is caused by parasites that are transmitted to humans through the blood-feeding of an infected mosquito. Malaria is considered to be the most serious parasitic illness in humans. Among the five parasites species that can transmit malaria, *Plasmodium falciparum* and *Plasmodium vivax* are the most dangerous, causing the vast majority of deaths. The former is responsible for malaria prevalence in Africa and deaths globally while the latter is the dominant parasite in most countries outside Africa (Winstanley, 2001, Tolle, 2009, Cowman *et al.*, 2016, Molla, 2016, Selvaretnam *et al.*, 2016, WHO, 2019).

In 2017, almost 219 million cases of malaria occurred globally, with 435 000 deaths (WHO, 2019). Although there were an estimated 20 million fewer malaria cases in 2017 than in 2010, data for the period 2015–2017 highlight that no significant progress in reducing global malaria cases was made in this timeframe. Most malaria cases in 2017 were in the WHO African Region (200 million

or 92% of global cases), followed by the WHO South-East Asia Region with 5% of the cases and the WHO Eastern Mediterranean Region with 2%. Fifteen countries in sub-Saharan Africa plus India carried almost 80% of the global malaria burden. Five countries accounted for nearly half of all malaria cases worldwide: Nigeria (25%), the Democratic Republic of the Congo (11%), Mozambique (5%), India (4%) and Uganda (4%).

Although the WHO African Region was home to the highest number of malaria deaths in 2017, it also accounted for 88% of the 172 000 fewer global malaria deaths reported in 2017 (when compared with 2010) (Figure 2.1). Nearly 80% of global malaria deaths in 2017 were concentrated in 17 countries in the WHO African Region plus India. Seven of these countries accounted for 53% of all global malaria deaths: Nigeria (19%), Democratic Republic of the Congo (11%), Burkina Faso (6%), United Republic of Tanzania (5%), Sierra Leone (4%), Niger (4%) and India (4%). Approximately 61% of global deaths are estimated to have occurred in children under 5 years of age (WHO, 2019).
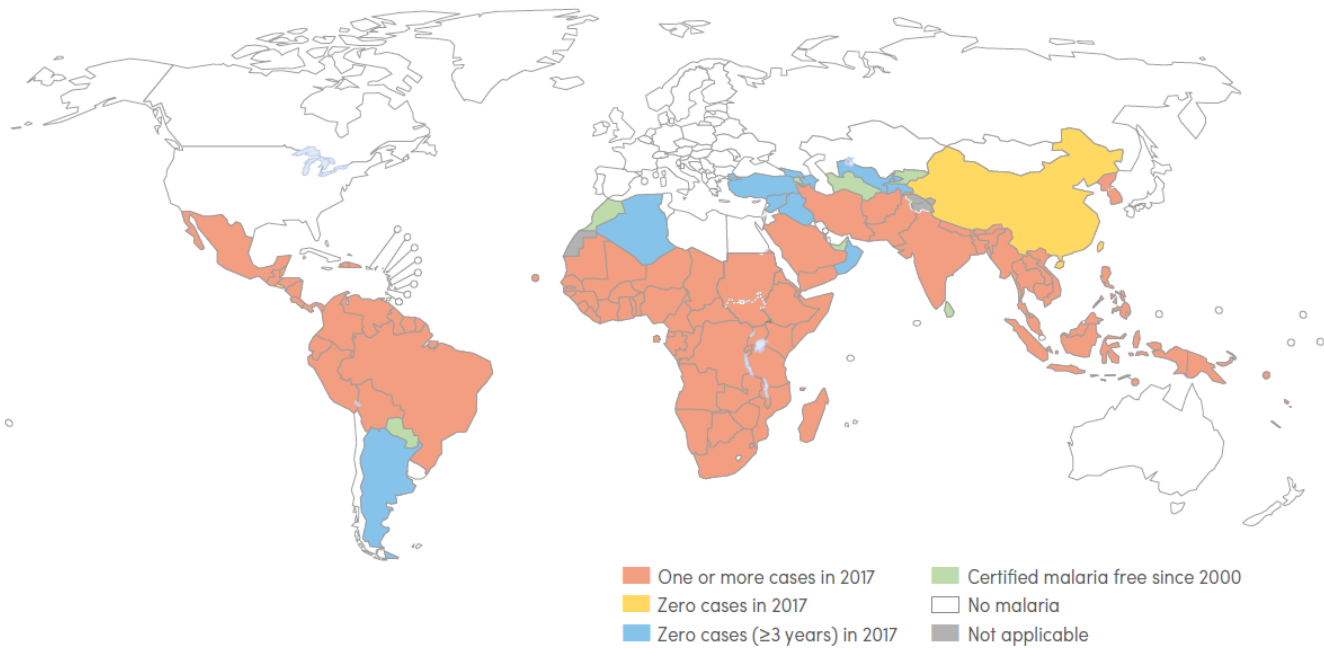
Figure 2.1: Malaria endemic countries in 2000 and their status by 2017 (WHO, 2019).

Dengue is also a mosquito-borne disease. Dengue is caused by a virus, which is mainly transmitted by the bite of infected female mosquitoes of the species *Aedes aegypti* and *Aedes albopictus*. The disease is spread throughout the world but commonly found in tropical and sub-tropical regions. It infects between 50-100 million people each year. It is estimated that 40% of people residing in tropical and sub-tropical regions of Africa, America, and Asia are at risk of infection (Lai *et al.*, 2017, Beltrán-Silva *et al.*, 2018). Although dengue has no particular treatment, early diagnosis and suitable treatment can nevertheless reduce the fatality rate (Gubler, 1997, Reiter, 2001, Favier *et al.*, 2006, Tolle, 2009, Monath *et al.*, 2016, Selvaretnam *et al.*, 2016). Dengue has turned into a principal global public health problem in those areas with an impact on the paediatric and adolescent population. As a result, in many countries, it is one of the principal origins of paediatric hospitalisation. Dengue has been considered one of the relevant resurgent infectious tropical

diseases with an increasing geographical distribution of the mosquito vector, as well as the viruses (Tolle, 2009, Monath *et al.*, 2016, Lai *et al.*, 2017).

Chikungunya is a viral infection transmitted by female *A. aegypti* and *A. albopictus* mosquitoes. It causes an acute febrile infection that results in painful joint symptoms that can continue for years. Infection by the chikungunya virus was recorded for the first time in Tanzania in 1952 and isolated in 1953 after an epidemic period. Chikungunya means "bent walk" in Makonde or Swahili, referring to the manner in which the patient walks. It occurs widely in tropical and sub-tropical areas of Asia, recently in America and Africa but it is considered to have originated from Africa (Pialoux *et al.*, 2007, Weaver and Lecuit, 2015, Kimani *et al.*, 2016, Madariaga *et al.*, 2016, Morens and Fauci, 2016, Murugan and Sathishkumar, 2016).

Yellow fever was identified initially as a viral infection in 1900; it has also been considered a major public health problem in the last two centuries. It is transmitted principally through the bite of infected female *A. aegypti* mosquitoes. It is distributed in tropical areas of Africa and South America and has been recorded in more than 57 countries. The outbreaks of yellow fever have reached high percentages, namely a 75% fatality rate in hospitalised cases (Monath and Vasconcelos, 2015, Burki, 2016, Monath *et al.*, 2016, Kraemer *et al.*, 2017).

WNV is a mosquito-borne infection that is extensively distributed in many of the temperate and tropical parts of the world such as Australia, the Middle East, southwestern Asia, Africa, and western Russia. Historically, some occasional fatal epidemic outbreaks occurred in western Asia, the Middle East and Africa. There are many routes of WNV infection to humans but the most

common is by the bite of a female *Culex* mosquito which previously bit an infected bird. The WNV was isolated for the first time in a district of Uganda from the infected blood of a woman and later in Egypt from different animals and humans (Hubálek and Halouzka, 1999, Sampathkumar, 2003, Petersen *et al.*, 2013, Coffey and Reisen, 2016, Grubaugh and Ebel, 2016, Soni *et al.*, 2016).

Lymphatic filariasis (elephantiasis) is a neglected parasitic tropical disease transmitted by different kinds of mosquito species such as *Culex*, *Anopheles,* and *Aedes*. Due to its broad geographical distribution and the irreversible disfigurement caused by lymphatic injury, it is becoming a severely troubling public health issue. It occurs widely in Asia and Africa, mainly in regions with a low socioeconomic development standard. Lymphatic filariasis is reported in 83 countries and infects over 120 million people. This results in disfigurement and incapacitation of about 40 million people (Bockarie and Rebollo, 2016, Netto *et al.*, 2016, Kushwaha *et al.*, 2017, Ndeffo-Mbah and Galvani, 2017).

Zika is a viral disease transmitted to humans mainly by female *Aedes* mosquitoes. It was discovered in 1947 in Uganda. The nature of the infection changes with the geographic range expansion. There are reports of possible transmission of Zika virus from mothers to unborn children, resulting in microcephaly. Such cases make the Zika virus another huge public health problem. Among 39 countries with active transmission of the Zika virus, Brazil has the largest number of reported cases ranging from about 500 000 to 1500 000 (Fauci and Morens, 2016, Kindhauser *et al.*, 2016, Riou *et al.*, 2017, Beltrán-Silva *et al.*, 2018).

The diseases outlined above are examples of some infectious tropical diseases caused by mosquitoes that afflict many people in tropical and sub-tropical regions in the world. However, their impact is most intense in Africa, causing serious economic and social consequences in human productivity, education and development. In the following paragraphs, mosquito-borne disease control will be described.

2.2 Control of mosquito-borne disease

Millions of people die each year from diseases caused by mosquito bites. Among all the members of the genera *Aedes, Anopheles* and *Culex* are the most important carriers of the parasites or viruses to human. Each of mosquito species has different ecological niches, breeding in different places (some in small shaded pools of water such as in tree-holes, on moist soil, leaf-axils, footprint pools; others at the edges of rivers; others on surface stagnant water, others in salty water; others only freshwater) and they bite at different times of the day. Some prefer forest regions, some open savannah, some prefer to come indoors to bite, while others only bite outdoors. Therefore, it has been difficult to find one single strategy to control these different types of mosquitoes. However, some strategies can be based on the mosquito's life cycle (Miller, 2001, Reiter, 2001, Norris, 2004, Benelli, 2016).

Relatively little effort by health institutions has gone into directed control towards mapping and reducing breeding areas near domestic dwellings (e.g. ensuring no empty tins lying around that contain water, eliminating or treating pails or tubs of standing water, ensuring no standing water in plant pots, no surface rain-water pools, etc.).

The use of insecticide-impregnated clothes and topically applied repellent substances on exposed body areas are the only strategies for reducing mosquito bites outdoors. The repellents that are currently in use are either synthetic or from natural sources like EOs. Topical formulations containing N,N-Diethyl-m-toluamide (DEET) are used in most cases, owed to its high efficacy and long-lasting protection. However, protection time depends on the concentration and can only last for few hours. The other available synthetic repellents, such as IR3535, proved to have inferior residual efficacy compared to DEET - even in low concentrations. The necessity of applying expensive repellents over and over and at elevated concentration means that the formulations are entirely directed at wealthier urban components and of little use to rural people in poor tropical areas. The natural repellents (e.g. citriodiol and citronellal) extracted from plants are another possibility to reduce mosquito bites. In addition, they have limited application in formulation due to high evaporation rates (Fradin and Day, 2002, Cisak *et al.*, 2012, Debboun and Strickman, 2013, Van Zyl, 2016).

Malaria control efforts rely almost exclusively on parasite control by way of detection and treatment of infected people, intermittent preventive therapy in pregnant women, biological control and vector control. What is perturbing, however, is the fact that malaria parasites show increasing resistance to the current generation of first-line drugs based on Chloroquine, Primaquine, Quinine and Artemisinin. This drug resistance is spreading to different countries. It seems that the resistance to drugs makes malaria treatment inactive even faster than new alternative drugs can be discovered. This is the pattern that has been observed repeatedly over the past half-century, where every generation of new anti-malaria drug initially creates great hope but soon fails. Although

some scant examples of new and effective drugs can be found, they are not affordable to rural people in impoverished tropical countries, especially in Africa. Currently, there is no obvious new and inexpensive drug identified for mass production to replace the Artemisinin-based treatment drugs. It simply means that this leg of the malaria control strategy is being compromised and will become sub-optimal (Winstanley, 2001). A malaria vaccine remains the Holy Grail, the "Magic Bullet" that will hopefully achieve malaria control, but despite well-funded international research on the subject for several decades, an effective vaccine remains elusive.

Biological control consists of the use of genetically modified species of mosquitoes and larvicides in the breeding sites. Although this is environmentally clean, its use on a large scale is inconvenient. It needs constant mediation and can be expensive in urban areas (Miller, 2001, Sumroiphon *et al.*, 2006, Atkinson *et al.*, 2007, Tiwary *et al.*, 2007, Chowdhury *et al.*, 2008, Alphey *et al.*, 2010, Iturbe-Ormaetxe *et al.*, 2011, Ricci *et al.*, 2011, Maciel-de-Freitas *et al.*, 2012, Ricci *et al.*, 2012, Gabrieli *et al.*, 2014).

Vector control is the single biggest method for controlling malaria but relies entirely on indoor residual spraying (IRS) of insecticides and use of LLINs. They both completely rely on the malaria-transmitting mosquitoes to venture indoors to come into contact with the insecticides. In addition, environmental concerns are increasing, and widespread resistance is being reported (Figure 2.2). Furthermore, no new insecticides are on the horizon (McCarroll *et al.*, 2000, Hemingway *et al.*, 2006, David *et al.*, 2013, Debboun and Strickman, 2013, Ranson and Lissenden, 2016).

Figure 2.2: Reported insecticide resistance status as a percentage of sites for which monitoring was conducted by WHO region, 2010–2017 (WHO, 2019). AFR, WHO African Region; AMR, WHO Region of the Americas; EMR, WHO Eastern Mediterranean Region; EUR, WHO European Region; SEAR, WHO South-East Asia Region; WPR, WHO Pacific Region.

2.3 Introduction to polymers

2.3.1 Origin and history

Polymers represent the uppermost promising materials ever discovered for present and prospective applications. This results from their low cost and special properties, including low densities, good barrier properties, mechanical and chemical resistance, high specific strength and flexibility (Chalmers and Meier, 2008, Osswald and Menges, 2012, Muralisrinivasan, 2014, Padeste and Neuhaus, 2015). Since life began, polymers have been found in natural form. Natural polymers

like ribonucleic acid (RNA), deoxyribonucleic acid (DNA), proteins and carbohydrates are crucial to plants and animals. Natural polymers as materials have been used by man for many different purposes such as construction, beauty, health, garments, ornaments and armament. Nevertheless, the nineteenth century is generally agreed to be the beginning of the polymer industry because of important discoveries regarding the modifications of natural polymers. The polymer industry is well-established, but its development and progress have been limited or restrained by a noticeable misunderstanding of the nature of polymers. The industrial production of polymers is considered a major activity of the chemical industry throughout the world, marking the *Age of Plastics* (Chalmers and Meier, 2008, Pethrick, 2010). Certainly, polymer science is now a fully developed subject and its importance and width continue growing (Osswald and Menges, 2012, Peng *et al.*, 2017).

2.3.2 Definitions and classification

The term *polymer*, first proposed by Berzelius in 1833, derives etymologically from two ancient Greek terms: *poly* that means many and *mer*, which is an abbreviation of the word *monomer* or *part* which is the building block of the polymer (Batten *et al.*, 2012, Hrnjak-Murgić *et al.*, 2015).

Alternatively, a polymer can be named *macromolecule*, indicating that it is a high molar mass substance with a repeating unit. The words *polymer* and *macromolecule* are used interchangeably. The latter strictly describe the molecules of which the former is composed (Young and Lovell, 2011, Callister and Rethwisch, 2013). Macromolecules can be subdivided into two main categories according to their structure. Some macromolecules are multiples of a repeating unit (monomer),

they are called polymers (*polymerised molecules*) and some of them cannot be divided into small units (*non-polymerised molecules*)**.** However, the term macromolecule is used to imply that all the elements along the backbone of the molecule are not necessarily the same (Chalmers and Meier, 2008). A polymer is made by many molecules (usually called monomer) linked by covalent bonds to form a large molecule or long chains. These formed molecules can be cyclic, linear, slightly branched or highly interconnected. The latter structure develops into a large three-dimensional network.

The polymers can be classified in many ways because of the diversity of function and structure found in the field of macromolecules. The most common classifications being **(a)** based on source (natural and synthetic); **(b)** based on structure (linear, branched-chain, crosslinked and network); **(c)** based on thermal behaviour (elastomers, thermoplastic and thermosetting); **(d)** based on elementary composition **(**organic, semi-organic and mineral, sometimes called inorganic); **(e)** based on polymerisation mode - first suggested by Carothers in 1929 (addition and condensation polymers, which are currently referred to as chain-growth polymers and step-growth polymers, respectively) (Akovali, 2005, Nicholson, 2006, Young and Lovell, 2011). A way of classifying polymers is outlined in Figure 2.3.

```
                        ┌─────────────┐
                        │   Polymers  │
                        └──────┬──────┘
              ┌────────────────┴─────────────────┐
        ┌──────────┐                        ┌──────────┐
        │ Natural  │────────────────────────│Synthetic │
        └──────────┘                        └──────────┘
                    ┌────────────┐      (based on thermal behaviour)
                    │ Elastomers │
                    └────────────┘
                        ┌────────────────┬──────────────┐
                 ┌──────────────┐                 ┌──────────────┐
                 │Thermoplastics│                 │  Thermosets  │
                 └──────────────┘                 └──────────────┘
                   ┌──────┴───────┐
            ┌──────────────┐ ┌──────────────┐
            │  Crystalline │ │   Amorphous  │
            └──────────────┘ └──────────────┘
```
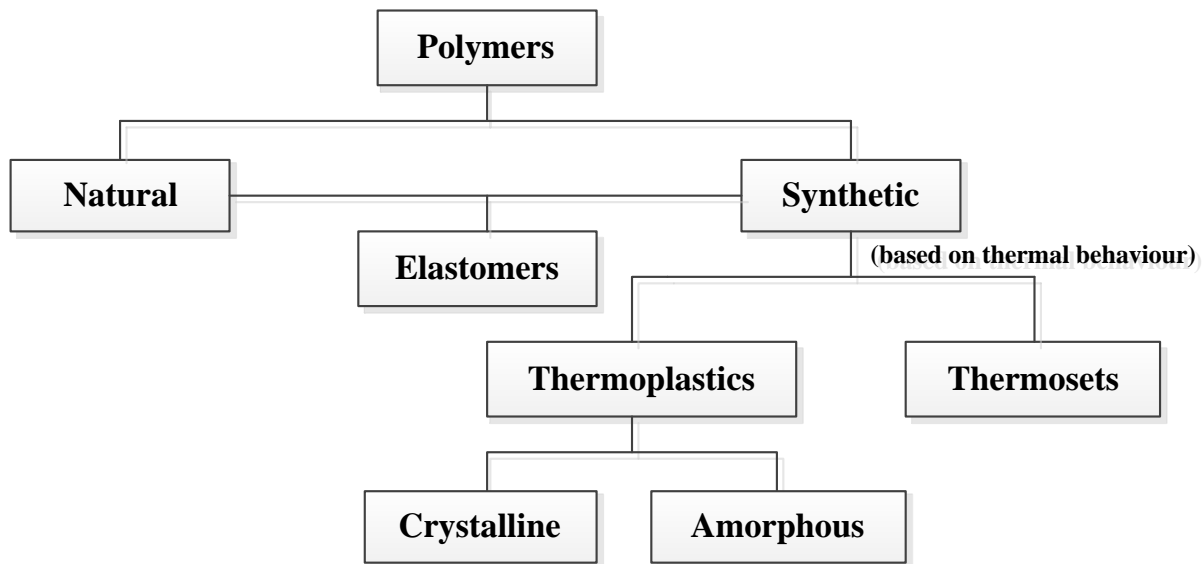
Figure 2.3: Classification of polymers

The classification of polymers based on their thermal response is the most important. By adopting this approach, polymers can be divided into three main groups: thermoplastics, thermosets and elastomers. Thermoplastic is then split into those which are semi-crystalline and those which are amorphous. According to Young and Lovell (2011), this method of classification has an advantage in comparison to others since it is based essentially upon the underlying morphological structure of the polymers.

Thermoplastics, often referred to just as plastics, are linear or slightly branched polymers which become liquid upon the applicability of heat. Thermoplastics can be repeatedly softened and re-solidified by adding or removing heat, allowing materials to be processed in extrusion, injection moulding, and other melt processing equipment numerous times. Thermoplastics' polymeric materials have traditionally been the workhorse of the industry because of their ease of processing. They now constitute by far the largest proportion of the polymers in commercial production. No

chemical reaction takes place during this heating. Reprocessing of such materials is possible (Callister and Rethwisch, 2013, Muralisrinivasan, 2014, Ghosh, 2015).

In terms of microstructures, thermoplastics can be amorphous glassy or a semi-crystalline solid. The amorphous thermoplastics are glassy up to a specific temperature (the T_g), above which they transform into a rubbery structure without a distinct melting point. In an amorphous thermoplastic, chains exist as random coils. Semi-crystalline thermoplastics are two-phase materials comprising an amorphous phase with a certain T_g and a crystalline phase with a specific melting temperature (T_m). In semi-crystalline thermoplastics, a part of the polymeric chain forms a crystalline structure, thereby being arranged in an ordered fashion (Young and Lovell, 2011, Akovali, 2012, Izdebska and Thomas, 2015).

Thermoset materials are made by chemical reaction (crosslink reactions) between different components to produce a crosslinked matrix that cannot be re-melted. They are normally rigid materials. Typically, they are three-dimensional network polymers in which chain motion is greatly restricted by a high degree of crosslinking. Crosslinking causes an irreversible change in the material. Thermosetting materials cannot be recycled as thermoplastic materials can. However, different processes are in use nowadays, providing mechanisms to recycle the material as filler or to reclaim the raw materials (Peacock and Calhoun, 2012, Giles *et al.*, 2013).

Elastomers or rubbers are crosslinked rubbery materials capable of very large deformations with the material behaving in a largely elastic manner. This means that when the deforming force is removed, the material completely, or almost completely, recovers. Elastomers can be either

thermoplastic or thermoset polymers, depending on their chemistry and the processing mechanism. The sulphur-crosslinking process in elastomers is called vulcanisation, which is achieved by a non-reversible chemical reaction, ordinarily carried out at an elevated temperature. As for thermosets, they are intractable once formed and degrade rather than become fluid upon the application of heat. Therefore, their processing into artefacts is often done using processes, such as compression moulding, that require minimum amounts of flow (Young and Lovell, 2011, Callister and Rethwisch, 2013, Giles *et al.*, 2013).

2.3.3 Macromolecule polymer chains

The properties of the final polymer formed by putting together a series of small molecular species into very long chain will be determined by the chemical characteristics of the starting low molecular weight species. When a macromolecule is derived by linking together identical monomers, it forms a homopolymer. However, the word *homopolymer* often is used more broadly to describe polymers whose structure can be represented by multiple repetitions of a single type of repeat unit. This unit may contain one or more species of monomer unit, sometimes called a structural unit (Carter and Paul, 1991, Young and Lovell, 2011, Izdebska and Thomas, 2015, Selke and Culter, 2016).

Very clear differences in morphology and properties occur between amorphous homopolymer, semi-crystalline homopolymer and fully crystalline homopolymer. However, the ability of a polymer to form a crystal depends on the regularity, symmetry and chirality of the monomer units forming the homopolymer chain (Bittrich *et al.*, 2014).

If more than one type of monomer is combined into each chain of the polymer, then the polymer is referred to as a copolymer. If exactly three monomers are used, it is called a terpolymer. They are also known as *heteropolymers*. However, in accordance with the use of the word *homopolymer*, it is common practice to use a structure-based definition. Thus, the word *copolymer* is used more often to describe polymers whose molecules contain two or more different types of the repeat unit (Young and Lovell, 2011, Callister and Rethwisch, 2013, McKeen, 2017).

Copolymers can be classified in several categories, each characterised by a particular arrangement of the repeat units along the polymer chain (Young and Lovell, 2011, Callister and Rethwisch, 2013, Bittrich *et al.*, 2014, Izdebska and Thomas, 2015). Therefore, based on the arrangements of the repeating units in the structure of the copolymers, these polymers can be sub-classified as shown in **Table 2.1.**

Table 2.1: Types and principles of IUPAC Nomenclature of Copolymers (Jones *et al.*, 2009, Young and Lovell, 2011)

Copolymer Type	Arrangement of Monomeric Units	Nomenclature	Example
Unspecified	unknown or unspecified	Poly(A-*co*-B)	Poly(styrene-*co*-methyl methacrylate)
Statistical	obeys known statistical laws	Poly(A-*stat*-B-*stat*-C)	Poly(styrene-*stat*-acrylonitrile-*stat*-butadiene)
Random	obeys Bernoullian statistics	Poly(A-*ran*-B)	Poly[ethylene-*ran*-(vinyl acetate)]
Alternating	alternating	Poly(A-*alt*-B)	Poly[(ethylene glycol)-*alt*-(terephthalic acid)]
Periodic	periodic with respect to at least three monomeric units	Poly(ABC-*per*-ABB-*per*-AABB)	Poly[formaldehyde-*per*-(ethene oxide)-*per*-(ethene oxide)]
Block	the linear arrangement of blocks	PolyA-*block*-PolyB	Polystyrene-*block*-Polybutadiene
Graft	Polymeric side-chain different from main chain	PolyA-*graft*-PolyB[1]	Polybutadiene-*graft*-Polystyrene

Within *unspecified copolymer*, the arrangement of monomeric units is unknown or unspecified. *Statistical copolymers* are copolymers in which the sequential distribution of the repeat units obeys known statistical laws. *Random copolymer* is a special type of statistical copolymer in which two or more numbers of repeating units are arranged randomly in the chain. *Alternating copolymers*

---

[1] Main chain (backbone) is specified first in the name

have only two types of repeat units that are alternately arranged in the chain. *Block copolymers* are linear copolymers in which the repeat units are only arranged in long sequences or blocks within the chain. *Graft copolymers* are branched polymers in which the branches have a different chemical structure to that of the main chain.

Statistical, random and alternating copolymers generally have properties which are intermediate to those of the corresponding homopolymers and block and graft copolymers. They usually show properties characteristic of the constituent homopolymer. From the point of view of morphology, statistical, random, branched, and star copolymers are usually amorphous because their irregular molecular structure prevents crystallisation. Alternating copolymers can be both amorphous and semi-crystalline, depending on the symmetry and regularity of their chains. Block copolymers, composed of immiscible blocks, exhibit microphase separation and a wide range of morphologies (Bittrich *et al.*, 2014).

2.3.4 Skeletal structure of polymers

The physical characteristics of a polymer depend not only on its molecular weight and shape but also on differences in the structure of the molecular chains. The definition of macromolecules presented up to this point implies that they have a linear skeletal structure in which the repeat units are joined together end-to-end in single chains. Whilst this is true for ***polymerised molecules***, there are also many with non-linear skeletal structures (***non-polymerised molecules***, see Figure 2.4) (Young and Lovell, 2011, Callister and Rethwisch, 2013).

Cyclic polymers (*ring polymers*) have no chain ends and show properties that are quite different from their linear counterparts. *Branched polymers* have side chains, or branches, of significant length which are bonded to the main chain at branch points (also known as junction points) and are characterised in terms of the number and size of the branches. *Network polymers* have three-dimensional structures in which each chain is connected to all others by a sequence of junction points and other chains. Such polymers are said to be crosslinked and are called network polymers. Branched and network polymers may be formed by polymerisation or can be prepared by linking together (i.e. crosslinking) pre-existing chains. The importance of crosslink density or degree of crosslinking has already been described in terms of vulcanisation (i.e. sulphur-crosslinking) of natural rubber (Young and Lovell, 2011, Callister and Rethwisch, 2013).

(a)   *(b)*

(c)   *(d)*
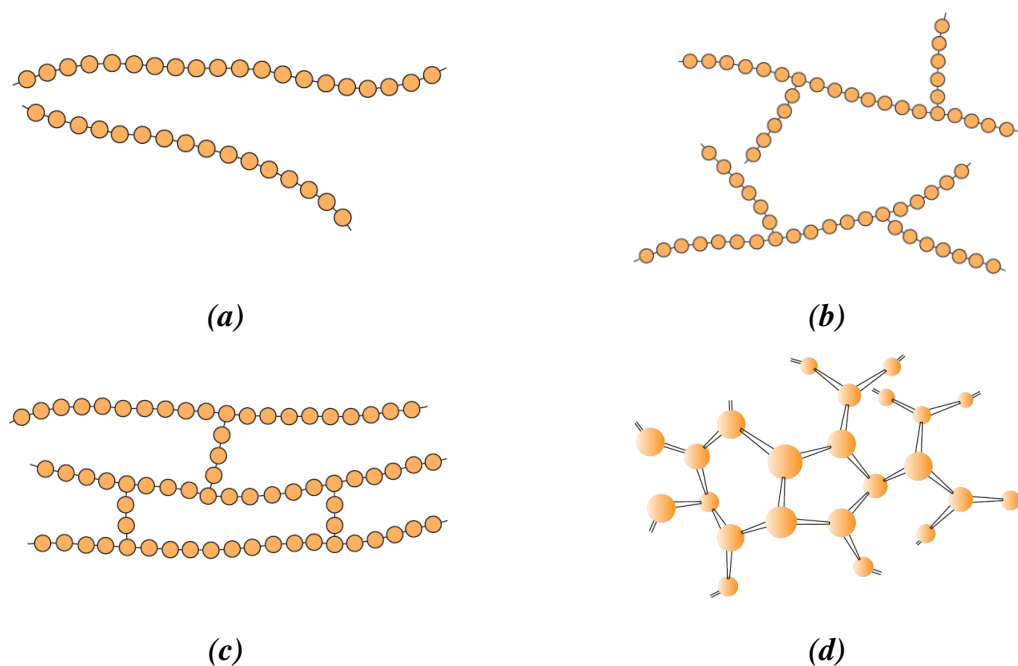
Figure 2.4: Skeletal structures representative of (*a*) linear, (*b*) branched, (*c*) crosslinked, and (*d*) network (three-dimensional) molecular structures. Circles designate individual repeat units.

In addition to these more conventional skeletal structures, there has been growing interest in more elaborate skeletal forms of macromolecules. Of particular interest are dendrimers, which are highly branched polymers of well-defined structure and molar mass; and hyperbranched polymers, which are similar to dendrimers but have a much less well-defined structure and molar mass. Research into these types of polymers intensified during the 1990s and they are now beginning to find applications which take advantage of their unusual properties.

2.3.5 Polymer nanocomposites

Composites, as the term suggests, are composed of at least two types of constituents in order to achieve enhanced properties. The constituents retain their identities, i.e., they do not dissolve or merge completely into one another although they act in concert. Normally, the components can be physically identified and exhibit an interface between one another. The need for materials with a specific combination of properties beyond the obtainable from a single material drove the development of composites. The specific aspect that characterises composite materials is that they are made up of distinct phases with very different physical properties. They are commonly, but not often exclusively, found to consist of a relatively soft flexible matrix reinforced by a stiffer, often fibrous component. However, a softer phase is used to improve properties, such as when rubber particles are added to a rigid polymer (Young and Lovell, 2011, Tiwari and Srivastava, 2012, Tewary and Zhang, 2015).

Many materials can be classified as being composites. Nature provides a number of celebrated examples. Wood consists of strong and flexible cellulose fibres surrounded and held together by a

stiffer material called lignin. Bone is also a composite of the strong yet soft protein collagen and the hard, brittle mineral hydroxyapatite. The most widely studied synthetic composites are based upon polymers reinforced with stiff fibres. Historically, the first type of synthetic polymer composites developed were formaldehyde-based resins filled with mineral particles or sawdust (Young and Lovell, 2011, Callister and Rethwisch, 2013).

The need for property improvement is not the only reason for the development of composite materials. For example, polymers often are employed in low-cost high-volume applications where the addition of a cheap inert mineral filler may reduce the quantity of relatively expensive polymer used, with no sacrifice in mechanical properties.

Nanocomposites can be defined as a composite where at least one of the phases has dimensions in the nanoscale range. The market production of nanocomposites is increasing drastically in order to support their demands. There are a number of reasons why they are of interest: **(a)** as the dimensions of materials decreases the size of flaws diminishes and they become stronger, offering better prospects for reinforcement; **(b)** as the reinforcement becomes smaller in size, the surface-to-volume ratio increases and so the area of the interface between the reinforcement and the matrix is much larger in a nanocomposite, leading to potentially better stress transfer. Nanocomposites have attracted considerable attention in both industry and academia because they usually inherit advantages of the component materials or even produce multifunctional materials with unexpected superior properties (Young and Lovell, 2011, Tiwari and Srivastava, 2012, Callister and Rethwisch, 2013, Huang and Cheng, 2017, Zhao *et al.*, 2017, Kumar *et al.*, 2018, Qi *et al.*, 2018).

PNC are a relatively new class of materials that usually contain an organic matrix (called continuous phase) in which an inorganic nanomaterial (or also called a reinforcement filler or additive) (discontinuous phase) is dispersed. The inorganic components normally include nanoparticles, nanotubes, nanosheets, nanowires, nanoclay and nanoplatelets, while an organic matrix mainly refers to polymer or biomacromolecules (Mittal, 2015, Tewary and Zhang, 2015, Fakirov, 2017, Huang and Cheng, 2017, Zhao *et al.*, 2017, Qi *et al.*, 2018).

The use of nanocomposites dates to 1990 when clay/nylon-6 nanocomposites were used by Toyota for belt covers. The most regularly used inorganic components are clay, silica, alkaline earth metal compounds, alumina and carbon nanotubes, with less than 5% by weight ((Tewary and Zhang, 2015, Fakirov, 2017, Kumar *et al.*, 2018, Vijayashakthivel *et al.*, 2018). According to Kumar *et al.* (2018), PNC have also attracted the interest of numerous researchers in the health care sector because of their significant potential to advance engineering applications.

The properties of PNC are derived from the type of nanomaterials that are dispersed into the polymer matrix, including the concentration, processing methods, sintering techniques, size, shape and interaction of nanomaterials with the polymer matrix (Giovino *et al.*, 2017, Huang and Cheng, 2017, Zhao *et al.*, 2017, Kumar *et al.*, 2018). The PNC will display enhanced optical, thermal, mechanical, magnetic and optoelectronic properties because of the synergism of the characteristics of the inorganic components. These components include large surface area, high surface reactivity, excellent thermal stability, high mechanical strength, and they can be combined with those components of organic polymer including low weight, flexibility and good processability. As a

result, the PNC have found wide use in diversified fields, such as sensing, solar cell, catalysis, oil recovery, electronics, food processing, biomedicine, and biotechnology (Tiwari and Srivastava, 2012, Izdebska and Thomas, 2015, Mittal, 2015, Fakirov, 2017, Giovino *et al.*, 2017, Huang and Cheng, 2017, Shamilov *et al.*, 2017, Zhao *et al.*, 2017, Kumar *et al.*, 2018, Qi *et al.*, 2018).

2.4 Thermodynamics of solutions

2.4.1 Thermodynamics of ideal solutions

A solution can be defined as a homogeneous mixture of two or more substances, i.e. the mixing is on a molecular scale. Under the usual conditions of constant temperature T and pressure P, the thermodynamic requirement for the formation of the two-component solution is that the Gibbs free energy G_{12} of the mixture must be less than the sum of the Gibbs free energy G_1 (for solvent) and G_2 (for solute) of the pure components in isolation. This requirement is defined in terms of the Gibbs free energy of mixing, which must be negative for a solution to form.

$$\Delta G_m < \Delta G_{12} - (\Delta G_1 + \Delta G_2) \qquad (2.1)$$

Since Gibbs free energy is related to enthalpy and entropy, it is expressed as

$$\Delta G_m = \Delta H_m - T\Delta S_m \qquad (2.2)$$

where

ΔH_m is the enthalpy (or heat) of mixing; and

ΔS_m is the entropy of mixing.

Ideal solutions are mixtures of molecules of identical size with equal molecular interactions energies of solvent-solvent, solute-solute and solvent-solute. As a result, the ideal solution

formation leads to a thermal mixing with no change in the enthalpy of the system (athermal mixing or $\Delta H_m = 0$), which means that there are no changes in the rotational, vibrational and translational entropies of the components. The entropy of mixing (ΔS_m) depends only upon the configurational or combinatorial entropy change (ΔS_m^{comb}), which can be defined as the number of ways you can arrange a different molecule, so the combinatorial entropy change is positive; the number of distinguishable spatial arrangements of molecules increases when they are mixed. Therefore, ΔG_m is negative and the formation of an ideal solution is always spontaneous or favourable. Assuming the lattice model for the ideal solution, where each cell contains a molecule placed arbitrarily, an equation for ΔS_m^{comb} can be derived using statistical mechanics or statistical thermodynamics (Figure 2.5).
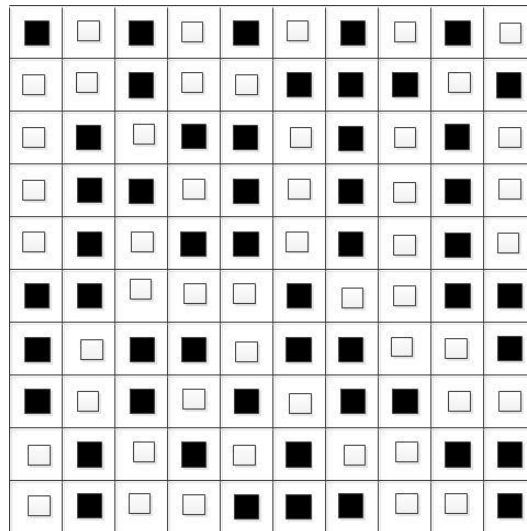
Figure 2.5: Schematic representation of a lattice model of a mixture of solute and solvent molecules with the same size (ideal solution).

The Boltzmann equation gives the fundamental relation between the entropy (*S*) and the number of possible distinguishable degenerate arrangements of the molecules (*W*):

$$S = k \ln W \tag{2.3}$$

where k is the Boltzmann constant. Using this equation for the formation of an ideal solution yields

$$\Delta S_m^{comb} = k[\ln W_{12} - (\ln W_1 + \ln W_2)] \tag{2.4}$$

where W_1, W_2 and W_{12} are the total numbers of distinguishable spatial arrangements of the molecules in the pure solvent, the pure solute and the ideal mixture, respectively. As all molecules of pure substances are identical, if one replaces or change the solvent molecules with another solvent molecule, only one distinguishable spatial arrangement is found for solvent and solute. So, $W_1 = 1$ and $W_2 = 1$, Equation (2.4) can be reduced to

$$\Delta S_m^{comb} = k \ln W_{12} \tag{2.5}$$

For ideal mixing of N_1 molecules of a solvent with N_2 molecules of a solute in a lattice with $(N_1 + N_2)$ cells, the total number of distinguishable spatial arrangements of the molecules is equal to the number of permutations of $(N_1 + N_2)$ objects. These objects fall into two classes containing N_1 identical objects of type 1 and N_2 identical objects of type 2, consequently,

$$W_{12} = \frac{(N_1 + N_2)!}{N_1! \, N_2!} \tag{2.6}$$

So, Equation (2.5) becomes

$$\Delta S_m^{comb} = k \ln \left[\frac{(N_1 + N_2)!}{N_1! \, N_2!} \right] \tag{2.7}$$

and for a large value of N, Stirling's approximation gives $\ln N! = N \ln N - N$, resulting in

$$\Delta S_m^{comb} = -k\left\{N_1 \ln\left[\frac{N_1}{(N_1 + N_2)}\right] + N_2 \ln\left[\frac{N_2}{(N_1 + N_2)}\right]\right\} \qquad (2.8)$$

The thermodynamic equations are most usually written in terms of numbers of moles n: ($n_1 = $

N_1/N_A and $n_2 = N_2/N_A$) and mole fraction X: $X_1 = n_1/(n_1 + n_2)$ and $X_2 = n_2/(n_1 + n_2)$, where

N_A is the Avogadro constant and is related to a universal gas constant by $R = kN_A$ and this allows

Equation (2.8) to be written as

$$\Delta S_m^{comb} = -R(n_1 \ln X_1 + n_2 \ln X_2) \qquad (2.9)$$

Hence, the Gibbs free energy of mixing of an ideal solution becomes

$$\Delta G_m = RT(n_1 \ln X_1 + n_2 \ln X_2) \qquad (2.10)$$

Relatively few solutions of small molecules behave ideally and the non-ideality is invariably

caused by non-athermal mixing ($\Delta H_m \neq 0$). Three types of non-ideality are possible: **1)**

athermal $\Delta H_m = 0$, but ΔS_m is not the same as an ideal solution; **2)** regular ΔS_m is the same as an

ideal solution but $\Delta H_m \neq 0$; and **3)** irregular $\Delta H_m \neq 0$ and ΔS_m are not the same as the ideal

solution.

2.4.2 Thermodynamic of polymer solutions

The polymer solution exhibits considerable deviations from ideal solution behaviour, even

when $\Delta H_m = 0$. The simple lattice theory needs some modifications to be applicable for polymer

solutions since it assumes that the solvent and solutes molecules have the same size. As a result, it

fails to give an accurate estimate of the thermodynamic properties of the polymer solution. Paul

Flory and Maurice Huggins, working independently, suggested a modified lattice theory, which is

generally mentioned as Flory-Huggins (F-H) mean-field theory, where the enormous differences in molecular size between the components (solvent and polymer) and intermolecular interactions are considered (Flory, 1941, Huggins, 1941).

The Flory-Huggins theory considers the polymer molecules as chains of segments (monomer) in the formation of the polymer solution where each segment and solvent molecule is considered to have the same size. The size of the polymer molecule is defined by the total number of segments (monomers) in the chain and may be the ratio of polymer molar volume and solvent molar volume.

The theory uses a two-dimensional lattice model to place the polymer chains segments and solvent molecules. The lattice model has identical cells with the same size as a solvent molecule. Each cell can be occupied by either a segment (monomer) of the polymer or a solvent molecule. The linear polymer chain is laid one by one into empty cells before additional placement of the solvent molecule so that its chain segment is in a continuous sequence of x cells, then the unoccupied cells are filled with solvent molecules. Figure 2.6 shows polymer molecules (N_2), with x chain segments and solvent molecules (N_1) in a lattice with ($N_1 + xN_2$) total cells.
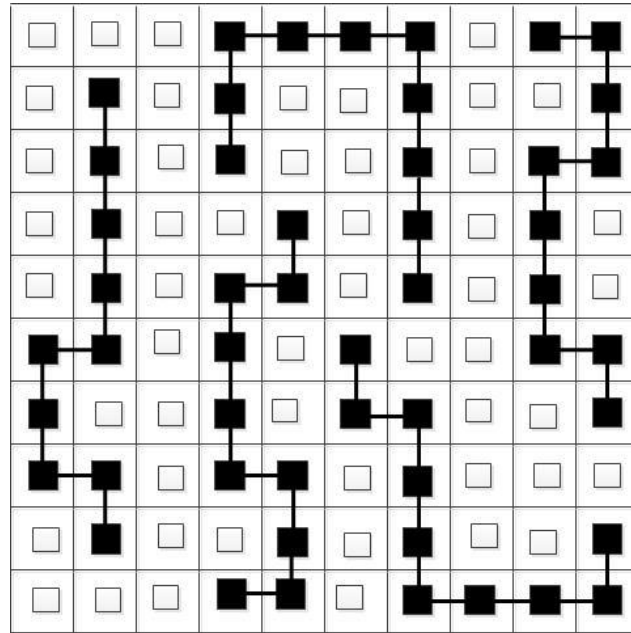
Figure 2.6: Schematic representation of a lattice model of a mixture of solvent molecules with polymer molecules showing connectivity of polymer segments (polymer solution).

As each polymer molecule adopts so many different distinguishable spatial arrangements of the chain segments, the expression for combinatorial entropy for polymer solutions can be given by

$$\Delta S_m^{comb} = -\boldsymbol{k}(N_1 \ln \phi_1 + N_2 \ln \phi_2) \tag{2.11}$$

where ϕ_1 and ϕ_2 are the volume fractions of solvent and polymer, respectively. Knowing that

$\phi_1 = {N_1}/{(N_1 + xN_2)}$ and $\phi_2 = {xN_2}/{(N_1 + xN_2)}$, Equation (2.11) can be written in terms of the

number of moles, which gives

$$\Delta S_m^{comb} = -R(n_1 \ln \phi_1 + n_2 \ln \phi_2) \tag{2.12}$$

If it is assumed that the entire lattice is equal to one mole $[(n_1 + n_2) = 1]$, writing Equation (2.12) per mole of lattice sites gives

$$\Delta S_m^{comb} = -R\left(\phi_1 \ln \phi_1 + \frac{\phi_2}{x} \ln \phi_2\right) \quad (2.13)$$

Considering the effect of intramolecular interaction, Flory-Huggins derived the equation for enthalpy of mixing:

$$\Delta H_m = RT\phi_1\phi_2\chi = RT\chi\phi_2(1 - \phi_2) \quad (2.14)$$

where χ is the Flory-Huggins polymer-solvent interaction parameter. Dissolution of high molar weight polymer in a solvent is only possible for $\chi \leq 0.5$ and molecular mixing of low molar weight liquids for $\chi \leq 2$.

This parameter is the temperature-dependent dimensionless quantity and characterises polymer-solvent interactions. It can be expressed in a simple equation such as

$$\chi = a + \frac{b}{T} \quad (2.15)$$

where a and b are temperature-independent quantities.

Negative χ promotes mixing of polymer with the solvent (single-phase mixture is favourable), whereas positive χ promotes demixing (phase separation). The interaction parameter contains both enthalpy and entropy contribution. It is generally given as

$$\chi = \chi_H + \chi_S \quad (2.16)$$

It can simply be shown that $\chi_H = {}^b/_T$ and $\chi_S = a$.

Therefore, combining ΔS_m^{comb} [Equation (2.12)] and ΔH_m [Equation (2.14)] yields the Flory-Huggins equation for the Gibbs free energy of polymer solution:

$$\Delta G_m = RT(n_1 \ln \phi_1 + n_2 \ln \phi_2 + n_1\phi_2\chi) \tag{2.17}$$

Or Gibbs free energy of polymer solution per mole of lattice sites:

$$\Delta G_m = RT \left(\phi_1 \ln \phi_1 + \frac{\phi_2}{x} \ln \phi_2 + \phi_1\phi_2\chi \right) \text{ or}$$

$$\Delta G_m = RT \left[(1 - \phi_2) \ln(1 - \phi_2) + \frac{\phi_2}{x} \ln \phi_2 + \phi_2\chi(1 - \phi_2) \right] \tag{2.18}$$

The Flory-Huggins can predict general trends of thermodynamic properties of a polymer solution, although the precise agreement with experimental data is not achieved due to unrealistic assumptions (e.g. no volume change on mixing) and model limitations.

2.4.3. Solubility parameters

Usually, when preparing a polymer solution, the solubility parameter approach is used, which is the most useful guide to the miscibility of specific polymer-solvent systems. This approach was first developed by Hildebrand employing this equation:

$$\Delta H_m = V_m \phi_1 \phi_2 (\delta_1 - \delta_2)^2 \tag{2.19}$$

where

V_m is the molar volume of the mixture; and

δ_1 and δ_2 are the solubility parameters of components 1 and 2, respectively.

A separate qualitative judgement must be made to predict the effect of ΔH_m upon miscibility using Equation (2.19) because it yields only zero or positive value, whilst it can be negative as a result of a specific effect, such as hydrogen bonding and charge-transfer interactions.

Hildebrand (1916) pointed out that the order of solubility of a given solute in a series of solvents is determined by the internal pressure of the solvents. In 1931, Scatchard introduced the concept of 'cohesive energy density' into Hildebrand's theories, identifying this quantity with the cohesive energy per unit volume. Finally, Hildebrand (1936) gave a comprehensive treatment of this concept and proposed the square root of the cohesive energy density as a parameter identifying the behaviour of specific solvents. In 1949, he proposed the term 'solubility parameter' and the symbol δ (Belmares *et al.*, 2004, van Krevelen and te Nijenhuis, 2009, Kitak *et al.*, 2015, Gårdebjer *et al.*, 2016, Gaikwad *et al.*, 2017, Huth *et al.*, 2018).

The origin of the solubility parameter was an attempt to formulate an expression for the partial molar energy of mixing. Alternatively, in the special case of zero volume change, for the heat of mixing of two liquids (Fedors, 1974). The solubility parameter δ of liquid is given by

$$\delta = \left[\frac{(\Delta H_V - RT)}{V}\right]^{1/2}$$

(2.20)

where

ΔH_V is its molar enthalpy of vaporization; and

V is its molar volume. Quantity δ^2 is called the cohesive energy density ($\delta^2 = CED$).

Later, Hildebrand and Scott proposed that materials with similar δ values would be miscible and which help to quantify the statements "like dissolves like" or "like seeks like" (Stefanis and Panayiotou, 2012, Hossin *et al.*, 2016, Gaikwad *et al.*, 2017).

Hansen proposed an extension of the Hildebrand parameter method to estimate the relative miscibility of polar and hydrogen bonding systems. The Hansen solubility parameter (HSP) model of 1967 (which was developed later), is based on the concept of dividing the total cohesive energy into individual components, i.e. dispersion, polar, and hydrogen bonding; thus the name 3D solubility parameters (Hansen, 2002, Lindvig *et al.*, 2002, Belmares *et al.*, 2004, Hansen and Smith, 2004, van Krevelen and te Nijenhuis, 2009, Elidrissi *et al.*, 2012, Tang *et al.*, 2015, Hossin *et al.*, 2016, Gaikwad *et al.*, 2017).

Hansen assumed that total cohesive energy is the sum of dispersion E_D, polar E_P, and hydrogen bond energy E_H:

$$E_T = E_D + E_P + E_H \tag{2.21}$$

By dividing both sides of Equation (2.21) by molar volume V, we get the total Hansen solubility parameter or Hansen solubility parameters δ_T:

$$\delta_T^2 = \delta_D^2 + \delta_P^2 + \delta_H^2 \tag{2.22}$$

where,

δ_T = total solubility parameter;

δ_D = dispersion interactive (London) force or energy;

δ_P = permanent dipoles in interacting molecules, called dipole-dipole interactive forces solubility parameter; and

δ_H = hydrogen bonding force.

The commonly used units for δ are $(J/m^3)^{1/2}$, $MPa^{1/2}$, or $(cal/cm^3)^{1/2}$, where 1 $(cal/cm^3)^{1/2}$ is equivalent to 2.0421 $MPa^{1/2}$ or $(J/m^3)^{1/2}$.

The extension of the solubility parameter approach to the prediction of polymer-solvent miscibility requires knowledge of δ values for polymers. However, their values must be obtained indirectly (e.g. theoretical estimates using group contribution methods) because polymers are not volatile.

The Small and Fedors methods yield values for the overall parameter, δ_T, directly. Other group contribution methods such as Hoy and Hoftyzer & Van Krevelen give the values of partial solubility parameters (Savova *et al.*, 2007, van Krevelen and te Nijenhuis, 2009, Mohammad *et al.*, 2011, Vay *et al.*, 2011, Kitak *et al.*, 2015, Saiz *et al.*, 2018). The total solubility parameter, δ_T, can be calculated, if needed.

2.4.3.1 Small's method (van Krevelen and te Nijenhuis, 2009)

Small has demonstrated that the combination $(E_{coh}/V)^{1/2} = F$, the molar attraction constant, is a useful additive quantity for low-molecular as well as for high-molecular substances. Accordingly, the corresponding solubility parameter is given by Equation (2.23):

$$\delta_{Small} = \frac{\sum F}{V} \tag{2.23}$$

Table I.1 in Appendix I gives values of group contribution to **F** in Small's method.

2.4.3.2 Fedors' method (Fedors, 1974, van Krevelen and te Nijenhuis, 2009)

According to Fedors' method, the solubility parameter for a substance is calculated as the square

root of the ratio of the summation of all energy contributions to the summation of all group volume.

Group contributions to E_{coh} and V according to Fedors are shown in Table I.2 in Appendix I.

$$\delta_{Fedors} = \left(\frac{\sum (\Delta E_{coh})_i}{\sum (\Delta V)_i} \right)^{\frac{1}{2}} \tag{2.24}$$

According to de Castro *et al.* (1994), values estimated by Fedors' method are consistent with those

obtained from other sources. On the other hand, van Krevelen and te Nijenhuis (2009) suggest that

the systems of group contributions published by Fedors give a less accurate prediction of E_{coh}.

2.4.3.3 Hoftyzer and Van Krevelen methods (van Krevelen and te Nijenhuis, 2009, Saiz *et al.*,

2018)

The solubility parameters components may be predicted from group contribution, using the

following equations:

$$\delta_D = \frac{\sum F_{Di}}{V} \tag{2.25}$$

$$\delta_P = \frac{\sqrt{\sum (F_{Pi})^2}}{V} \tag{2.26}$$

$$\delta_H = \sqrt{\frac{\sum E_{Hi}}{V}} \tag{2.27}$$

The prediction of δ_D is of the same type of formula proposed by Small for the prediction of total

solubility parameter. The group contributions F_{Di}, F_{Pi} and E_{Hi} for a number of structured groups

are presented in Table I.3 in Appendix I.

2.4.3.4 Hoy's method (van Krevelen and te Nijenhuis, 2009)

Hoy's method is, in many respects, different from that of others. Table 2.2 gives a survey of the system of equations to be used. It contains four additive molar functions, a number of auxiliary equations and the final expressions for δ_T and their components.

Table 2.2: The equations to be used in Hoy's system for estimation of the solubility parameter and its components

Formulae	Low-molecular liquids (solvents)	Amorphous polymers
Additive molar functions	$F_t = \sum N_i F_{t,i}$	$F_t = \sum N_i F_{t,i}$
	$F_P = \sum N_i F_{P,i}$	$F_P = \sum N_i F_{P,i}$
	$V = \sum N_i V_i$	$V = \sum N_i V_i$
	$\triangle_T = \sum N_i \triangle_{T,i}$	$\triangle_t{}^{(P)} = \sum N_i \triangle_{T,i}{}^{(P)}$
Auxiliary equations	$\log \alpha = 3.39(T_b/T_{cr}) - 0.1585 - \log V$	$\alpha(P) = 777\left(\triangle_T{}^{(P)}/V\right)$
	$(T_b/T_{cr}) = 0.567 + \Delta_T - (\Delta_T)^2$	$n = 0.5/\Delta_T{}^{(P)}$
	(Lyderson equation)	
Expressions for δ and δ-components	$\delta_T = (F_i + B)/V; \ B = 277$	$\delta_T = (F_i + B/\tilde{n})/V$
	$\delta_P = \delta_T \left(\dfrac{1}{\alpha}\dfrac{F_P}{F_t + B}\right)^{\frac{1}{2}}$	$\delta_P = \delta_T \left(\dfrac{1}{\alpha^{(P)}}\dfrac{F_P}{F_t + B/\tilde{n}}\right)^{\frac{1}{2}}$
	$\delta = \delta_T[(\alpha - 1)/\alpha]^{\frac{1}{2}}$	$\delta_H = \delta_T[(\alpha^{(P)} - 1)/\alpha^{(P)}]^{\frac{1}{2}}$
	$\delta_D = \left(\delta_T{}^2 - \delta_P{}^2 - \delta{}^2\right)^{\frac{1}{2}}$	$\delta_D = \left(\delta_T{}^2 - \delta_P{}^2 - \delta_H{}^2\right)^{\frac{1}{2}}$

Where F_t is the molar attraction function, F_P its polar component; V is the molar volume of the solvent or the structural unit of the polymer. Δ_T is the Lyderson correction for non-ideality, used in the auxiliary equations. α is the molecular aggregation number, describing the association of the molecules and n is the number of repeating units per effective chain segment of the polymer. Table I.4 in Appendix I lists values of increments in Hoy's system for the molar attraction function.

By uniting Equation (2.19) with Equations (2.16) and (2.14), it is possible to obtain the expression χ_H for in terms of solubility parameters:

$$\chi_H = \frac{V_1(\delta_1 - \delta_2)^2}{RT} \tag{2.28}$$

where, V_1 is the molar volume of the solvent or volume per cell.

The entropic contribution, χ_S, is usually taken to be a constant of the order 0.35 ± 0.1 and for non-polar systems, $\chi_S = 0.35$ is generally used

$$\chi = 0.34 + \frac{V_1(\delta_1 - \delta_2)^2}{RT} \tag{2.29}$$

For estimation of Flory-Huggins interaction parameter, Hansen has used the following equation with $\alpha = 1$, particularly for systems where dispersion forces dominate over polar and hydrogen bonding ones:

$$\chi = \alpha \frac{V_1}{RT}\left[\left(\delta_{1,D} - \delta_{2,D}\right)^2 + 0.25\left(\delta_{1,P} - \delta_{2,P}\right)^2 + 0.25\left(\delta_{1,H} - \delta_{2,H}\right)^2\right] \tag{2.30}$$

2.4.4 Equilibrium and stability of polymer solutions

Theoretically, phase separation can be dealt with based on the Flory-Huggins theory since the change of Gibbs free energy of mixing can simply be induced by a change of the composition or temperature in the polymer solution. In this research, it will be considered the effect of temperature upon demixing, as it is easier to analyse.

In the Flory-Huggins equation for the Gibbs free energy of polymer solution, the first two terms have an entropic origin and always act to promote mixing while the last term has an energetic origin. It can be positive (opposing mixing), zero (ideal solution) or negative (promoting mixing) depending on the sign of the interaction parameter which acts as a balance. Additionally, it can be said that the balance of the enthalpy of mixing and entropy of mixing contribution depends upon temperature and whether a polymer solution will phase separately or not.

Using Equation (2.18), a series of curves for the variation of the Gibbs free energy with the composition (volume fraction of the polymer) can be constructed at different temperatures (T_1, T_2, T_3, T_4, and T_5), as illustrated in Figure 2.7.
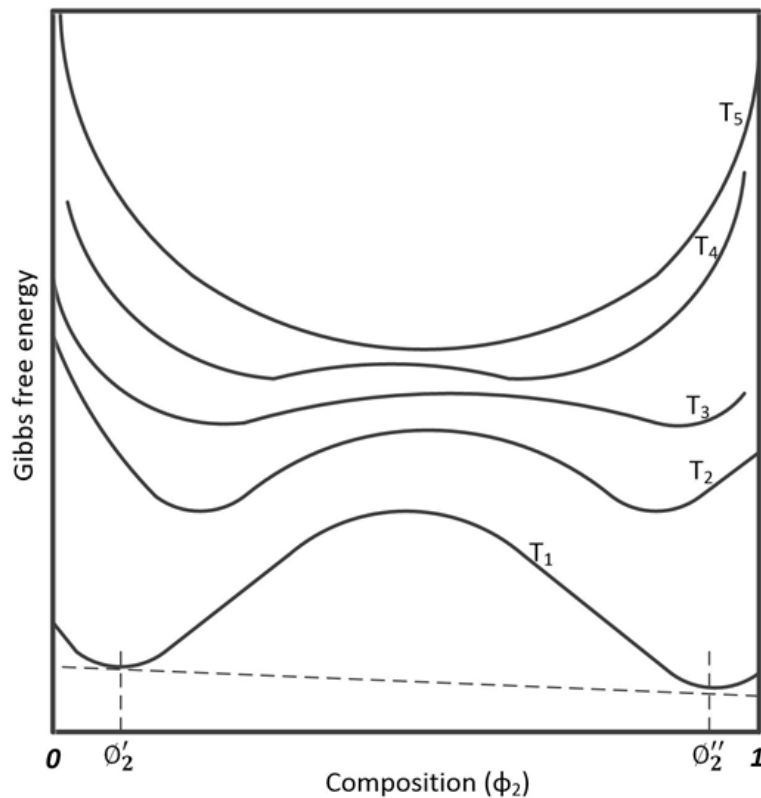
Figure 2.7: Schematic illustration of the Gibbs free energy-composition phase diagram of the polymer solution at different temperatures. On cooling (from T_5 to T_1) the Gibbs free energy shows two minima, which shows that the polymer solution transforms from a one-phase to a two-phase structure.

The Gibbs free energy curve shows only one minimum point at T_5, it means that the system remains as one phase or homogeneous at all composition. By decreasing the temperature from T_5 to T_1, the curves rapidly turn asymmetric and the Gibbs free energy curves show two minima, the minimum at low values of ϕ_2 (ϕ_2') and minimum at high values of $\phi_2(\phi_2'')$. Here, the situation is more complex as the system can be stable, metastable or unstable depending on the composition position. The criterion for local stability is written in terms of the second derivative of the Gibbs free energy:

$$\frac{\partial^2 \Delta G_m}{\partial \phi_2^2} < 0 \qquad \text{unstable} \tag{2.31}$$

$$\frac{\partial^2 \Delta G_m}{\partial \phi_2^2} > 0 \qquad \text{locally stable} \tag{2.32}$$

As the polymer solutions have both energetic and entropic contributions to their Gibbs free energy of mixing, so the local stability of the polymer solution is determined by the sign of the second derivative of the Gibbs free energy with respect to composition:

$$\frac{\partial^2 \Delta G_m}{\partial \phi_2^2} = \frac{\partial^2 \Delta H_m}{\partial \phi_2^2} - T \frac{\partial^2 \Delta S_m}{\partial \phi_2^2}$$

$$\frac{\partial^2 \Delta G_m}{\partial \phi_2^2} = RT \left(\frac{1}{x\phi_2} + \frac{1}{1 - \phi_2} \right) - 2\chi RT \tag{2.33}$$

At finite temperatures, ΔG_m is convex at both ends of the composition range because its second derivative is positive due to the diverging slope of the entropy of mixing.

The two equilibrium compositions ϕ_2' and ϕ_2'' at T_1 correspond to a common tangent line in Figure 2.7. For any overall composition in the miscibility gap between ϕ_2' and ϕ_2'', the system can minimise its Gibbs free energy by phase separating into two phases of composition ϕ_2' and ϕ_2''. The amounts of each phase are determined by the lever rule.

The composition ranges $0 < \phi_2 < \phi_2'$ and $\phi_2'' < \phi_2 < 1$ are outside the miscibility gap and the homogeneously mixed state is the stable equilibrium state for this composition of the polymer solution.

Within the miscibility gap, there are metastable and unstable regions, separated by inflection points at which the second derivative of the Gibbs free energy is zero ($\partial^2 \Delta G_m / \partial \phi_2^2 = 0$). Between the inflection points, the second derivative of the Gibbs free energy is negative, and the homogeneously mixed state is unstable. Even the smallest fluctuations in composition lower the Gibbs free energy, leading to spontaneous phase separation called SD.

Between the inflection points and equilibrium phase-separated composition, there are two regions that have a positive second derivative of Gibbs free energy of mixing. The mixed state is locally stable to small composition fluctuations. Such states are metastable because large fluctuations are required for the system to reach thermodynamic equilibrium. Phase separation in this metastable region occurs by nucleation and growth and requires exceeding an energy barrier.

2.4.5 Phase separation of polymer solutions

Bearing in mind the temperature dependence of the Gibbs free energy of mixing, a phase diagram can be built, sum up, the phase behaviour of the polymer solution, where the regions of stability, metastability, and instability can be shown. Recall the Gibbs free energy of polymer solutions [Equation (2.18)]

$$\Delta G_m = RT \left[(1 - \phi_2) \ln(1 - \phi_2) + \frac{\phi_2}{x} \ln \phi_2 + \phi_2 \chi (1 - \phi_2) \right] \qquad (2.18)$$

The phase boundary is determined by the common tangent of the Gibbs free energy at the composition ϕ_2' and ϕ_2'' corresponding to two equilibrium phases (see the top part of Figure 2.8).

$$\left(\frac{\partial \Delta G_m}{\partial \phi_2}\right)_{\phi_2 = \phi_2'} = \left(\frac{\partial \Delta G_m}{\partial \phi_2}\right)_{\phi_2 = \phi_2''} \tag{2.34}$$

By setting the first derivative of the Gibbs free energy to zero can be obtained the phase boundary – the bimodal (the dashed line in the bottom part of Figure 2.8).

$$\frac{\partial \Delta G_m}{\partial \phi_2} = RT \left[\frac{\ln \phi_2}{x} - \ln(1 - \phi_2) + \frac{1}{x} - 1 + \chi(1 - 2\phi_2)\right] = 0 \tag{2.35}$$

The spinodal compositions boundary occurs at the inflection points and can be found by equating the second derivative of Gibbs free energy to zero

$$\frac{\partial^2 \Delta G_m}{\partial \phi_2^2} = RT \left[\frac{1}{x\phi_2} + \frac{1}{1 - \phi_2} - 2\chi\right] = 0 \tag{2.36}$$

The curve corresponding to the inflection points is the boundary between unstable and metastable regions and is called the spinodal (solid line in the bottom part of Figure 2.8). By assuming that χ is independent of ϕ_2, a theoretical spinodal curve can be constructed if the variation of χ with temperature is known.
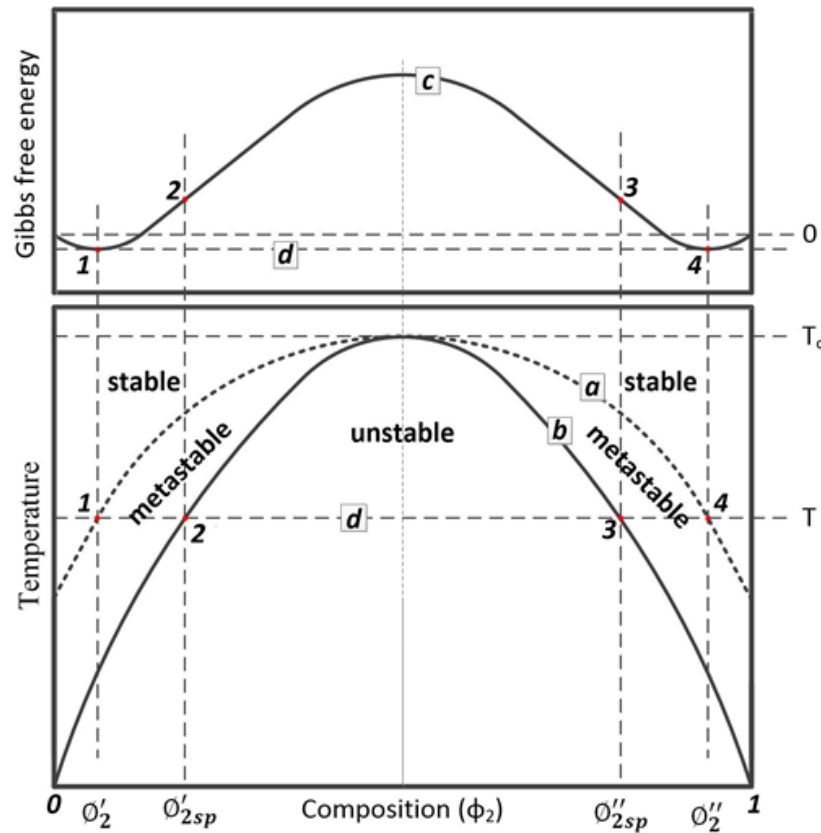
Figure 2.8: Schematic illustrations of the composition dependence of the Gibbs free energy of mixing for polymer solution (top figure) and the corresponding phase diagram with a miscibility gap (bottom figure). Line (*a*) is the phase boundary. Above this line, the system is homogeneous and stable. Below this line, there is a metastable region. Line (*b*) is the spinodal. Below this line the system is unstable. The metastable and unstable regions constitute the miscibility gap. Within that gap is more favourable for the system to separate rather than in one phase. Temperature (T$_c$) is the upper critical solution temperature. At a given temperature (T) the tie line (*d*) cuts the phase boundary and the spinodal at points (*1* and *4*) and (*2* and *3*), respectively. In the top figure, line (*c*) shows the change in Gibbs free energy of mixing at a given temperature in respect to composition. Segments (*12*) and (*34*) correspond to a positive second derivative of Gibbs free energy, $\partial^2 \Delta G_m / \partial \phi_2^2 > 0$ while segment (*23*) to a negative one, $\partial^2 \Delta G_m / \partial \phi_2^2 < 0$. At points (*2*) and (*3*) the second derivative of Gibbs free energy is zero, $\partial^2 \Delta G_m / \partial \phi_2^2 = 0$.

In the top part of Figure 2.8 one can see where the Gibbs free energy shows two minima where the first derivative is zero and at the inflection points the second derivative is zero too. The phase boundary is defined by a projection of the points of the Gibbs free energy minima on a temperature-composition phase diagram and the spinodal by the inflection points (the bottom part of Figure 2.8). The curves defined by spinodal points and bimodal points have the common maximum known as the upper critical solution temperature (UCST), above which the polymer and solvent are miscible in all proportions. This is common for most polymer solutions, where χ reduces as temperature increases. However, in some polymers solutions the χ increases as temperature increases, showing a common minimum known as the lower critical solution temperature (LCST).

The regions outside bimodal (dashed line in the bottom part of Figure 2.8) correspond to a stable homogeneous solution, whereas the regions within the spinodal (solid line in the bottom part of Figure 2.8) correspond to unstable solutions which will spontaneously phase separate. The regions between the bimodal and spinodal correspond to metastable solutions which only phase separate if an energy barrier can be overcome.

For both UCST and LCST behaviour, T_c coincides with the turning point in the spinodal and so can be located by application of the condition

$$\frac{\partial^2 \Delta G_m}{\partial \phi_2^2} = \frac{\partial^3 \Delta G_m}{\partial \phi_2^3} \tag{2.37}$$

and the application of the condition ($\partial^3 \Delta G_m / \partial \phi_2^3 = 0$) gives the critical composition as

$$\frac{\partial^3 \Delta G_m}{\partial \phi_2^3} = \frac{1}{(1-\phi_2)^2} - \frac{1}{x\phi_2^2} = 0$$

$$\phi_{2c} = \frac{1}{1-\sqrt{x}} \cong \frac{1}{\sqrt{x}} \tag{2.38}$$

Hence, ϕ_{2c} is very small for polymer (x is large). The critical value χ_c of the interaction parameter of the Flory-Huggins is obtained by substituting Equation (2.38) into (2.37)

$$\chi_c = \frac{1}{2} + \frac{1}{\sqrt{x}} + \frac{1}{2x} \cong \frac{1}{2} + \frac{1}{\sqrt{x}} \tag{2.39}$$

Notice that as $x \to \infty$, $\phi_{2c} \to 0$ and $\chi_c \to 1/2$.

2.5 Microporous polymer preparation

Currently, there are several ways to prepare microporous polymers and these different strategies can be found in the literature, such as: melt processing, sintering, and phase separation process. These include polymerisation of emulsions, phase inversion, TIPS, diffusion induced phase separation (DIPS), thermally assisted evaporative phase separation (TAEPS), supercritical induced phase separation or pressure-induced phase separation (PIPS), nonsolvent induced phase separation (NIPS), solvent-induced phase separation (SIPS), etc (Wijmans *et al.*, 1983, Mehta *et al.*, 1995, van de Witte *et al.*, 1996, Liu and Kiran, 1999, Matsuyama *et al.*, 1999, Zhang *et al.*, 2000, Matsuyama *et al.*, 2002, Chandavasu *et al.*, 2003, Hellman, 2004, Hong *et al.*, 2005, Gu *et al.*, 2006, Li *et al.*, 2006, Reverchon and Cardea, 2007, Li *et al.*, 2008, Rasouli and Rey, 2014, Tang *et al.*, 2015, Wang *et al.*, 2015, Jung *et al.*, 2016, Wang *et al.*, 2016, Kim *et al.*, 2017).

Diverse kind of structures with different properties (e.g. selectivity, thermal, electrical and mechanical stability) can be produced. Therefore, they are becoming an appealing choice in the industry for several applications, such as separation technology in hydrogen separation, therefore reducing the costs. However, it is difficult to manage and optimise the morphology. Even a small change in the process parameters (raw material, quantities, cooling rate, diluents, temperature, etc.) can lead to significant changes in the distribution of pore size, porosity and some other properties (Mehta *et al.*, 1995, van de Witte *et al.*, 1996, Staiger *et al.*, 2004, Wang *et al.*, 2015, Jung *et al.*, 2016, Wang *et al.*, 2016, Kim *et al.*, 2017).

2.5.1 Thermally induced phase separation

Numerous microporous structures are obtained by controlled phase separation of polymer solutions according to many different procedures. Contrary to other phase separation processes that are induced by diffusion, change of solvent/pressure or composition, the TIPS is driven by heat change (Song and Torkelson, 1995, Matsuyama *et al.*, 2002, Li *et al.*, 2006). TIPS was invented in 1981 by Anthony Castro and is widely used to produce microporous structures due in part to its flexibility, simplicity, reproducibility, versatility, applicability for several polymers and production of different structures, as well as high porosity with different sizes (Castro, 1981, Lloyd *et al.*, 1990, Li *et al.*, 1995, Song and Torkelson, 1995, Li *et al.*, 2006, Chen *et al.*, 2007, Kim *et al.*, 2016, Liu *et al.*, 2016).

Usually, TIPS involves basic steps: **1)** a homogeneous polymer solution is obtained at high temperatures by mixing a polymer and liquid or solid diluent with a high-boiling point and low

molecular weight (i.e. the diluent does not dissolve or swell the polymer at room temperature); **2)** to induce phase separation the homogeneous solution is quickly cooled or quenched in the desired shape; **3)** the diluent trapped during phase separation is typically extracted from the polymer matrix by a solvent extractor and a microporous structure is obtained (Lloyd *et al.*, 1990, Li *et al.*, 1995, Li *et al.*, 2006, Tang *et al.*, 2015, Kim *et al.*, 2016, Liu *et al.*, 2016).

The phase separation can be either solid-liquid (S-L), where it occurs via the crystallisation of the polymer; gelation and/or vitrification of the polymer solution, or liquid-liquid (L-L). The latter plays a significant role in most TIPS. Two phases are formed from the solution, a polymer-rich continuous phase, and a polymer-poor droplet phase. However, a combination of these processes is possible if a crystalline polymer is used. It is of singular relevance in inducing microporous structures (Lloyd *et al.*, 1991, van de Witte *et al.*, 1996, Matsuyama *et al.*, 1999, Matsuyama *et al.*, 2001, Gu *et al.*, 2006, Kim *et al.*, 2016, Liu *et al.*, 2016).

In the case of L-L phase separation, nucleation-and-growth and SD mechanism must be considered. The phase separation by nucleation and growth mechanism takes place in the metastable region, which is located below the phase boundary in the phase diagram. The nuclei of the more stable phase must be larger than some critical size in order to grow in the metastable region due to the surface tension between phases. The new phase can grow only when a sufficiently large fluctuation creates a domain larger than the critical size. In the thermodynamically unstable region located bellow the spinodal line, the phase separation mechanism is SD. This process was first studied in metallurgical systems by Cahn and Hilliard (Cahn, 1961, Huston *et al.*, 1966, Cahn

and Hilliard, 1971). In this region, the phase separation is induced without an energy barrier to be overcome so consequently the phase demixing is spontaneous. It is possible to enter directly into the spinodal region if the cooling is started at the critical point while in other situations the metastable region must first be passed. However, cooling the system at highly elevated rates can be applied to avoid demixing in the metastable region (Siggia, 1979, van de Witte *et al.*, 1996, Liu and Kiran, 1999, Gu *et al.*, 2006, Favvas and Mitropoulos, 2008, Rasouli and Rey, 2014).

Comparing the two mechanisms of phase separation, it can be said that the spinodal is small in degree and large in extent while nucleation and growth are large in degree and small in extent. The membranes formed by these mechanisms are different in porosity, morphology and structure. The SD results in a highly interconnected structure with uniform pore sizes and have mechanical strength whilst the nucleation and growth process form either a weakly interconnected, fibrous and/or spherical structure which is not mechanically strong for solution with polymer-poor phase (below the critical composition) or an interconnected structure but with different pore sizes in the case of a solution with a polymer-rich continuous phase (above the critical composition) (Song and Torkelson, 1995, van de Witte *et al.*, 1996, Favvas and Mitropoulos, 2008, Kim *et al.*, 2016).

2.6 Controlled-release system from swellable EVA polymer strands

For the past few centuries, the major focus of drug-related research has been the synthesis or discovery of potent drugs with new kinds of biological activity. Increasing attention is being devoted to the manner in which these drugs are delivered. The first approaches for incorporating drugs into solid polymers dates to the 1950s and began with the development of agricultural

products, which then extended to medicine (Langer and Peppas, 1981). The use of polymers as carriers has the advantage of releasing the active ingredient continuously for very long periods of time (over a year in some cases) and widely varying the rate of release by using different polymeric systems (Langer and Peppas, 1981, van Laarhoven *et al.*, 2002, Fu and Kao, 2009, Dash *et al.*, 2010). According to Langer and Peppas (1981), ethylene-vinyl acetate copolymer and various hydrogels were most successful in this regard. Schneider *et al.* (2017) state that ethylene-vinyl acetate copolymers gained prominence due to their broad applicability, long sustained release time scales and highly favourably inflammatory characteristics. Ethylene-vinyl acetate copolymer as polymeric carrier proved to be suitable material for drug release for different purposes (Rhine *et al.*, 1980, van Laarhoven *et al.*, 2002, Fu and Kao, 2010, Almeida *et al.*, 2011, Genina *et al.*, 2016, Schneider *et al.*, 2017).

Controlled-release polymeric systems can be classified based on the mechanism controlling the release of the active ingredient. The rate-limiting step of the release process may be diffusion, according to Fick's law, i.e. diffusion-controlled systems; chemical reaction at the continuously depleted interface between the polymer and the dissolution medium, i.e. chemically-controlled systems; countercurrent diffusion of dissolution medium at constant penetration velocity in the polymer, swelling-controlled systems. Externally imposed controls may also be responsible for release, e.g. magnetically-controlled systems (Langer and Peppas, 1981, Siepmann and Peppas, 2011).

In an amorphous polymer, dynamic swelling controls the solute diffusion in most cases. The mechanism involves diffusional release from the continuously swelling or shrinking system (Peppas and Franson, 1983, Cunha *et al.*, 1998a, Cunha *et al.*, 1998b, Marabi *et al.*, 2003).

2.6.1 Modelling release from swellable EVA polymeric systems

In swelling controlled-release systems, the release of a solute is controlled by one or more of the following processes: namely, the transport of the solvent into the polymer matrix, swelling of the associated polymer, diffusion of the solute through the swollen polymer, erosion of the swollen polymer, etc. Controlled release from swellable polymeric systems has been studied and models proposed. They have been reviewed from time to time by several researchers (Hopfenberg and Hsu, 1978, Davidson and Peppas, 1986a, Davidson and Peppas, 1986b, Korsmeyer *et al.*, 1986a, Korsmeyer *et al.*, 1986b, Harland and Peppas, 1987, Lustig and Peppas, 1987, Klier and Peppas, 1988, Rao and Devi, 1988, Brannon-Peppas and Peppas, 1989, Harland and Peppas, 1989, Walker and Peppas, 1990, Hariharan *et al.*, 1994, Brazel and Peppas, 2000). However, there is no single model that successfully predicts all possible experimental conditions. Nevertheless, collectively they can contribute towards the elucidation of the mechanism involved. Modelling of release from swellable polymeric systems belongs to a category of diffusion problems known as moving-boundary or Stefan- Neumann problems (Ritger and Peppas, 1987b).

Figure 2.9 serves, for the present purposes, as a simple model for the repellent-release characteristics. It represents a long cylindrical microporous strand covered by a thin membrane-like outer skin layer.
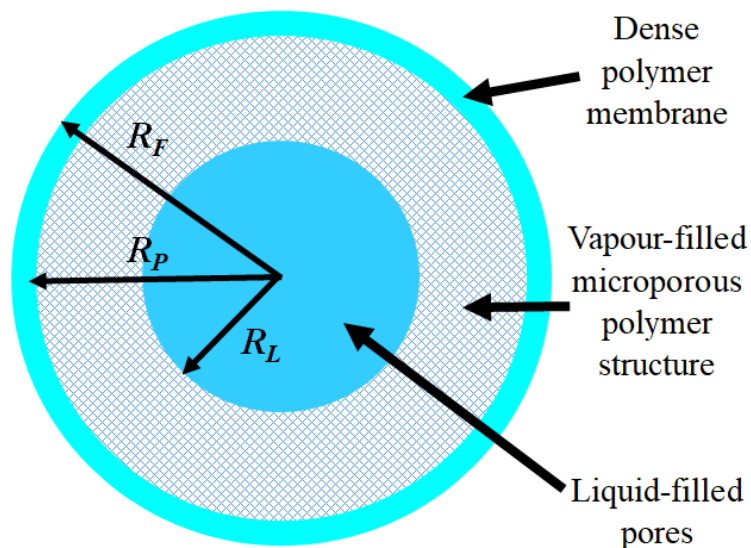
Figure 2.9: Model of the microporous strand showing the liquid core location, the vapour-filled microporous region and the outer skin layer that functions as a membrane that limits the rate at which the repellent is released.

The cross-section is assumed to be circular, and the structure of the inner polymer section is assumed to be microporous. Conceptually, it corresponds to an open-cell polymer foam, which is initially filled with the liquid repellent. As the repellent is gradually released into the atmosphere, it is assumed that the outer pores are progressively emptied, and the lost liquid is replaced by air and repellent vapour. In a first approximation, it is assumed that the location of the liquid-vapour boundary is concentric with the outer wall.

For the active compound to be released from the strand, a portion of the liquid evaporates and diffuses through the porous matrix towards the outer membrane. The matrix polymer forms both the microporous structure and the outer membrane. The permeability of the repellent through this

membrane is defined by the product of its solubility in the membrane and the diffusion coefficient inside the membrane. The implication is that the active ingredient is also dissolved in the rest of the microporous polymer structure. This has several implications, including the fact that the polymer structure could change shape (e.g. shrink) and that it can contribute to the rate of mass transport. The fact that the active ingredient must diffuse through a porous polymer may also affect the release rate. Therefore, it is necessary to consider the transport mechanisms of the active ingredient in the porous region, in addition to the permeation through the membrane and the deswelling of the polymer scaffold. The surface tension will affect the shape of the liquid meniscus inside partially filled pores. This has implications for the rate at which the liquid transforms into vapour, i.e. the evaporation rate. Finally, it is assumed that once the repellent molecules reach the outside surface of the strand, they are rapidly removed by convection air currents so that it can be assumed that the concentration on the outside surface of the strand is negligible.

EVA is a random copolymer of ethylene and vinyl acetate (VA) as the repeating unit. The ethylene unit is nonpolar and crystallisable while vinyl acetate is polar and non-crystallisable; consequently, the incorporation of the vinyl acetate unit into polyethylene produces a wide range of properties depending on the content of vinyl acetate units incorporated (Allen *et al.*, 2000, Hull *et al.*, 2003, Wang *et al.*, 2007, Chen *et al.*, 2014, Martín-Alfonso and Franco, 2014, Genina *et al.*, 2016, Suárez and Coto, 2016). As EVA is rubberier compared to LLDPE, this allows for a high degree of swelling and shrinkage; it is for this reason that empirical models were proposed for EVA microporous strands.

2.6.1.1 Peppas Model

A simple semi-empirical equation can be introduced to express general drug release behaviour from polymers. Equation (2.40) expresses a Fickian diffusion (Case I) in a thin film and indicates that the first 60% of the fractional release at any time can be characterised by some constant multiplied by the square root of time. The distribution function $X(t) = \frac{M_t}{M_\infty}$ is the time-dependent release equation that describes the temporal release of the repellent from a microporous polymer strand. This is the classical Higuchi equation written in the more general form:

$$X(t) = \sqrt{\frac{t}{\tau}} \tag{2.40}$$

where, $\tau = 1/k$ is a dimensionless time constant and k is a kinetic rate constant incorporating characteristics of the macromolecular network system and the active ingredient to release.

A limiting case is one where the drug release rate is independent of time, i.e., the kinetics is of zero-order (also called a non-Fickian mechanism or Case II transport mechanism). Such a situation is described by a general equation of the form:

$$X(t) = \frac{t}{\tau} \tag{2.41}$$

Transport from swellable systems may often lead to release under conditions that do not agree with Higuchi's or the Fickian behaviour. Most transport processes in glassy polymers fall between these two limiting cases; as such, they can be represented by a coupling of the Fickian and non-Fickian mechanism or Case II transport mechanisms. Therefore, a simple expression of this observation

can be heuristically written by adding the two expressions of Equation (2.40) (representing the diffusion-controlled) and Equation (2.41) (which represents the relaxation-controlled):

$$X(t) = \sqrt{\frac{t}{\tau_1}} + \frac{t}{\tau_2} \tag{2.42}$$

where τ_1 and τ_2 are dimensionless time constants.

Another generalised expression can be written as

$$X(t) = \left(\frac{t}{\tau}\right)^n \tag{2.43}$$

where $\tau = 1/k$ is a dimensionless time constant and k is a kinetic rate constant incorporating characteristics of the macromolecular network system and the active ingredient to release, and $\boldsymbol{n}$ is the diffusional exponent which is indicative of the transport mechanism. This power-law has first been introduced in the pharmaceutical field in 1985 and has become known as the 'Peppas equation' (Siepmann and Peppas, 2011).

The exponential dependence of the amount of drug released on time, as described by Equation (2.43), can still be used for the analysis of swelling-controlled release systems as long as these systems swell only moderately in the solute. The first estimate of applicability of this equation in swellable systems is that the system does not swell more than 25% of its original volume (Ritger and Peppas, 1987b). The equation is usually valid for the first 60% of the normalised drug release. In the case of thin films with negligible edge effects, Fickian drug diffusion and relaxational drug transport are defined by $\boldsymbol{n}$ equal to 0.5 and $\boldsymbol{n}$ equal to 1, respectively. Anomalous drug transport behaviour is intermediate between Fickian and Case II; this is reflected by the fact that anomalous

behaviour is defined by values of **n** between 0.5 and 1. For other geometries, different **n**-values are indicative of diffusion or polymer relaxation-controlled drug release, as shown in Table 2.3.

Table 2.3: Diffusional exponent and mechanism of diffusional release from non-swellable controlled release systems for different geometries (Siepmann and Peppas, 2011)

Thin Film	Cylinder Exponent, n	Sphere	Drug Release Mechanism
0.5	0.45	0.43	Fickian diffusion (Case I)
$0.5 < n < 1.0$	$0.5 < n < 0.89$	$0.43 < n < 0.85$	Anomalous (non-Fickian) transport
1.0	0.89	0.85	Case-II transport
> 1	> 0.89	> 0.85	Super Case-II transport

An ideal kinetic profile of drug release from a prolonged release carrier is a zero-order curve. A value of $n = 1$ means that the drug release rate is independent of time, regardless of the geometry. Thus, zero-order release can exist for any geometry (Ritger and Peppas, 1987a, Balcerzak and Mucha, 2010).

Additional structural parameters influencing the transport mechanism include the molecular weight, degree of crosslinking and degree of branching of the polymer and its thermal and solvent expansion coefficients. Non-Fickian and Case II transports are indicative of the coupling of diffusion and relaxation mechanisms. Relaxation is related to a transition from a rubbery to a glassy state. Major relaxation mechanisms are indicative of stresses formed in the polymer during swelling (Marabi *et al.*, 2003).

2.6.1.2 Hill Model

In the context of chemical reaction kinetics, the logistic rate equation is defined as

$$\frac{d\alpha}{dt} = k\alpha(1 - \alpha) \tag{2.44}$$

where k is a kinetic rate constant, α is the degree of conversion but for this case is the amount of repellent probable to be released. Equation (2.44) is also referred to as the Prout-Tompkins rate equation.

The Hill equation was originally derived on the basis of equilibrium principles applied to the cooperative binding of ligands to a macromolecule. Here, the Hill equation provides a rate expression that governs the release of the repellent from the microporous polymer strand:

$$\frac{d\alpha}{dt} = k\alpha^{1-1/n}(1 - \alpha)^{1+1/n} \tag{2.45}$$

where the constant n is a shape parameter. Note that this differential equation provides a parametric interpolation formula between the predictions of the logistic equation ($n \to \infty$) and second-order kinetics ($n = 1$). The general solution is

$$[\alpha/(1 - \alpha)]^{1/n} = 1 + \frac{[k(t - t_0)]}{n} \tag{2.46}$$

It can be cast in the following explicit form:

$$1 - \alpha = 1/\{1 + [1 + k(t - t_0)/n]^n\} \tag{2.47}$$

For $n \to \infty$, Equation (2.45) reduces to Equation (2.44), for $0 < 1/\theta < \infty$ it is possible to force $\alpha = 0$ at $t = 0$ by setting $t_0 = 0$. With this condition, the equation reduces to the simpler form:

$$1 - \alpha = 1/[1 + (t/\tau)^n]\,\pi r^2 \tag{2.48}$$

66

Where, the time constant, defined by $\tau = n/k$, is a scale parameter. Defining the distribution function $X(t) = \alpha(t)$ yields the general Hill time-release equation for describing the temporal release of the repellent from microporous polymer strand:

$$(t) = \frac{(t/\tau)^n}{1 + (t/\tau)^n} \tag{2.49}$$

2.6.1.3 Weibull model

The Weibull distribution describes the process as a sequence of probabilistic events. It is a flexible empirical model and yields good results (Cunha *et al.*, 1998a, Cunha *et al.*, 1998b, Marabi *et al.*, 2003). Utilisation of the Weibull distribution can show an excellent fit for the description of the release of the repellent from microporous polymer strands and adequately describes the release rate controlled by different mechanisms. The Weibull distribution is described as

$$X(t) = 1 - e^{-(t/\tau)^n} \tag{2.50}$$

This model has two parameters: the scale parameter τ, which represents the process rate constant (s^{-1}), and the shape parameter n (dimensionless). The scale parameter, τ, defines the rate and represents the time needed to accomplish approximately 63% of the process. The higher τ is, the faster the process is at the beginning of the release. If $n = 1$, Weibull's model reduces to classical first-order kinetics (Cunha *et al.*, 1998a, Fernández *et al.*, 2002, Marabi *et al.*, 2003, Oms-Oliu *et al.*, 2009). When $n > 1$, the sigmoid shape of the Weibull function indicates that a complex mechanism governs the release process (Mateus *et al.*, 2007, Dash *et al.*, 2010).

Utilisation of the Weibull distribution showed excellent fit for the description of rehydration of a variety of dried foods and adequately described rehydration processes controlled by different

mechanisms, which included internal diffusion, external convection and relaxation (Cunha *et al.*, 1998a, Marabi *et al.*, 2003).

CHAPTER THREE

EXPERIMENTAL

3.1 Materials

3.1.1 Chemicals

In this study, the following chemicals were used: the alkanes, Hexadecane [CAS No. 544-76-3], Eicosane [CAS No. 112-95-8], Tetracontane [CAS No. 4181-95-7]; the insect repellents, 1-(1-methylpropoxycarbonyl)-2-(2-hydroxyethyl)piperidine (Icaridin) [CAS No. 119515-38-7] and N,N-diethyl-3-methylbenzamide (DEET) [CAS No. 134-62-3]; Dichloromethane [CAS No. 75-09-2]. The molecular mass, purity, the melting and boiling points, density at 20°C, and suppliers of the chemicals are listed in Table 3.1. All the chemicals were used without further purification.

Table 3.1: List of chemicals, their properties and suppliers

Chemical	$M_w/(\text{g·mol}^{-1})$	Purity (%)	$\rho/(\text{g·cm}^{-3})$	$T_b/(°C)$	$T_m/(°C)$	Supplier
Hexadecane	226345	≥ 99	0.773	286.8	18.2	Sigma-Aldrich
Eicosane	282.55	99	0.790	342.7	36.7	Sigma-Aldrich
Tetracontane	563.08	≥ 98	0.810	523.7	84.0	Sigma-Aldrich
Icaridin	229.30	97	#	296	#	Endura S.pA
DEET	191.27	≥ 97	0.998	288	-	Sigma-Aldrich
Dichloromethane	84.93	99.9	1.33	40	-95	Merck-KGaA

No information available.

3.1.2 Polymers

Poly(ethylene-co-vinyl acetate) grade Elvax 760A ex DuPont pellets were pulverised by Dreamweaver. The vinyl acetate (VA) content was 9%, the density 0.930g cm^{-1} and the melt flow index (MFI) 2.0 g/10 min at 190°C. LLDPE (Sasol HR411) was obtained from Sasol. The number average molar mass and weight-average molar mass were 57889 and 214009, respectively. The density was 0.939g cm^{-3} and MFI was 3.5 g/10 min (190°C/2.16 kg). The number average molar mass and weight-average molar mass of LLDPE was determined on a PL-GPC 220 High-Temperature Chromatograph [Polymer Laboratories, (now Agilent) UK] equipped with a differential refractive index (RI) detector. The samples (4 mg) were dissolved in 2mL of 1,2,4-trichlorobenzene (TCB) for at least 3 hours together with 0.025% butylated hydroxytoluene (BHT), which acted as a stabiliser to prevent sample decomposition/degradation. TCB with 0.0125% BHT was used as the mobile phase at a flow rate of 1mLmin^{-1}. Three $300 \times$ 7.5mm^2 PLgel Olexis columns (Agilent Technologies, UK) were used together with a $50 \times$ 7.5mm^2 PLgel Olexis guard column and 200 μL of each sample was injected. All experiments in High-Temperature Size Exclusion Chromatography (HT-SEC) were carried out at 150°C. The instrument was calibrated using narrowly distributed polystyrene standards (Agilent Technologies, UK).

3.1.3 Nanofillers

Dellite 43B organoclay was supplied by Laviosa Chimica Mineraria S.pA. According to the supplier, the moisture content was 3% (max). The approximate medium particle size (dry basis)

was 7–9 µm and the bulk density was 0.40g cm^{-3}. The clay was organo-modified with dimethyl benzyl hydrogenated tallow ammonium.

Fumed silica (HDK$^{®}$ N20 pyrogenic silica) was supplied by Wacker silicones. The SiO$_2$ content (based on the substance heated at 1 000°C for 2 h) was > 99.8%; the density at 20°C (SiO$_2$) was approximately 2,2 g·cm^{-3}; the RI at 20°C was reportedly 1.46; the BET (Brunauer–Emmett–Teller) surface was around 170–230 m^2·g^{-1} and the pH value of a 4% aqueous dispersion was around 3.8–4.3.

3.2 Preparation of the samples

The objective of this study was to produce polymer strands impregnated with mosquito repellent (Icaridin and DEET). The concept was to trap the insect repellents inside the polymer matrix. The two Nanofillers (fumed silica and Dellite 43B) were added to assist the compounding into the polymer. It was also thought that, if properly exfoliated and dispersed in the polymer matrix, the presence of the clays could reduce the rate at which the mosquito repellents are released from the expected microporous polymer strands.

3.2.1 Preparation of mosquito repellent polymer strands without nanofiller

The compounding and extrusion of polymer strands without nanofiller was done on a Nanjing Only Extrusion Machinery Co., Ltd (Model TE-30/600-11-40) co-rotating twin-screw laboratory extruder (diameter = 30mm, L/D = 40:1). Liquid repellent was dosed via a peristaltic pump (Cole-Parmer with Easy-load 11, Masterflex L/S, head using Masterflex platinum-cured silicone tubing 16, Model 77200-60). The temperature profile, from hopper to die, was set

71

at 85/100/1710/170/170/170/170/170°C, and the screw speed was set at 80 revolutions per minute (rpm) for EVA strands and at 85/170/210/210/210/210/210/210°C, and the screw speed was set at 46.65 rpm for LLDPE strands. The extruded strands were quenched in an ice-water bath. Additional information is presented in Appendix III. Before starting the compounding, the feeder and the pump were calibrated in order to ensure the correct mixture ratios were achieved. The calibration results are presented in Appendix II.

3.2.2 Preparation of mosquito repellent polymer strands with nanofiller

All polymer repellent compositions were done on a TX28P 28mm co-rotating twin-screw laboratory extruder with a screw diameter of 28mm and an L/D ratio of 18. The screw design of this machine comprised intermeshing kneader blocks that also impart a forward transport action.

The polymer and nanofiller powders were first mixed together in a plastic container. Then the repellent was added and mixed-in to obtain a semi-dry consistency that could be fed into the compounding extruder. The exiting polymer strands were quench-cooled in an ice-water bath. After compounding, the polymer strands did not show a visible leaking of the incorporated repellent.

Table 3.2 lists typical compounder settings, i.e. temperature profiles from hopper to die and screw speed. They were used to compound a composition comprising EVA (65 wt-%), Dellite 43B (5 wt.%) and DEET (30 wt-%). The conditions used for other EVA- and LLDPE compositions are given in Appendix IV.

Table 3.2: TX28P extrusion conditions used for compounding EVA strands

Conditions	Zone 1 (ºC)	Zone 2 (ºC)	Zone 3 (ºC)	Die (ºC)	Speed screw (rpm)
Set	140	160	160	160	100
Read	143.4	160.2	159.1	160.4	100

A Perkin Elmer Spectrum 100 Fourier Transform Infrared (FTIR) spectrometer was used to study the repellent stability under processing conditions. A sample of the repellent impregnated in the polymer was expressed from the microporous polymer matrix. The sample was placed on the platform of an attenuated total reflectance (ATR) attachment. The spectra represent average values obtained with fifty scans collected at a resolution of 2 cm^{-1}.

3.4 Characterising of polymer strands

Figure 3.1 shows the instrument used to measure the diameter of the polymer's strands. The Mitutoyo Digital Vernier caliper had a measurement range of up to 150mm.

Figure 3.1: Mitutoyo Digital Vernier caliper

3.4.1 Estimation of repellent trapped by polymer matrix

3.4.1.1 Solvent extraction

Polymer strands with trapped repellent were cut to lengths of approximately 50mm, weighed using a Radwag Wagi Elektroniczne scale, PS 360/C/2, Nr 263678/09 (Figure 3.2) and placed in 50mL glass vials. Approximately 45mL dichloromethane was added, and the vials were closed. The extraction solvent was replaced on a daily basis. After the fifth or sixth extraction, the strands were removed and allowed to dry in a fume hood at ambient temperature. The repellent content was estimated from the recorded mass loss of the strands in the dried form. Reported values are the results obtained from triplicate mass loss determinations. The estimated amount of repellent was calculated using Equation (3.1).

$$E(\%) = 100 - \left(\frac{W_f}{W_i} * 100\right) \qquad (3.1)$$

where E is the estimated repellent amount in percent (%) that was in the polymer strand and W_i and W_f are the weights of the strands before and after extraction of the repellent in grams (g).

Figure 3.2: Radwag Wagi Elektroniczne scale

3.4.1.2 Thermogravimetric analysis

TGA was used to estimate the amount of the repellent trapped by the polymer matrix. The TGA was carried out with a TA Instruments SDT-Q600 Simultaneous TGA/DSC (Figure 3.3). Samples weighing approximately 15mg were heated from ambient temperature to 600°C at a rate of 10 K·min^{-1}. The purge gas was nitrogen flowing at 50mL·min^{-1}. The first mass loss step of the polymer strand was associated with the loss of the repellent by volatilisation.
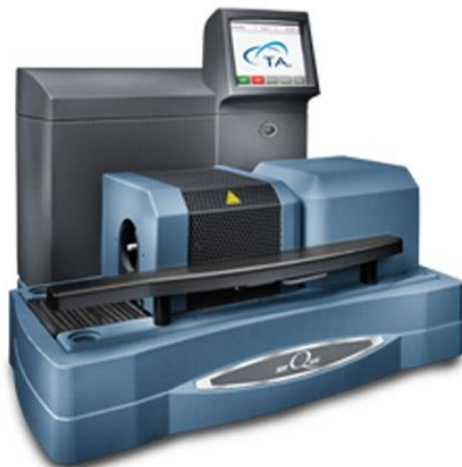
Figure 3.3: TA Instruments SDT-Q600 Simultaneous TGA/DSC

3.4.3 Polymer swelling and shrinkage

Approximately 4.0g of neat EVA and LLDPE pellets were weighed using a Radwag Wagi Elektroniczne scale, PS 360/C/2, Nr 263678/09, and placed in glass vials containing approximately 20mL repellent (DEET or Icaridin). The vials were placed in an EcoTherm-Labcon (Figure 3.4) forced convection oven set at a temperature of 30°C or 50°C. After 72 hours, the pellets were removed, and the excess repellent was removed using a quick rinse with dichloromethane. The pellets were then allowed to dry for a few minutes on paper towels before weighing. After that, the repellent absorption was estimated from the recorded mass gain of the pellets. Reported values represent results obtained from multiple measurements of the mass gain of the pellets.

Figure 3.4: EcoTherm-Labcon forced convection oven

According to Vasenin (1964), the swelling of polymers involves either mutual solution of two completely miscible substances (the solvent and the polymer) or solution of the low-molecular component in the polymer. The percentage of swelling (S) was determined gravimetrically by Equation (3.2) (Kaplan and Güner, 2000, Isik and Kis, 2004, Randová *et al.*, 2009, Krasucka *et al.*, 2018):

$$S(\%) = 100 * \left(\frac{m_t - m_0}{m_0}\right) \qquad (3.2)$$

where S is the estimated percentage of swelling of the polymer matrix by repellents; m_o is the initial weight of dried polymer pellets and m_t is the weight of swollen polymer at time t.

50mm lengths were cut from neat polymer strands and polymer strands containing repellents. The strands were placed in an EcoTherm-Labcon forced convection oven, set at a temperature of 50°C

for one month. The rate of shrinkage of the polymer matrix was determined according to Equation (3.3) proposed by Li *et al.* (2008). The shrinkage rate (S_R) was calculated by the diameter of strand (D_i) before and after (D_f) the shrinkage process occurred after complete loss of repellent:

$$S_R(\%) = 100 * \left(\frac{D_i - D_f}{D_i}\right) \tag{3.3}$$

3.4.4 Scanning electron microscopy

Scanning electron microscopy (SEM) was used to observe the microporous structure of the polymer strands. Repellent-free polymer strands were immersed in liquid nitrogen for approximately 1 hour and then fractured. The fracture surface was coated about six times with carbon using an Emitech K950X sputter coater prior to analysis. The samples were viewed through a Zeiss Ultra 55 Field Emission Scanning Electron Microscope (FESEM) at acceleration voltages of 1kV and 5kV.

3.5 Repellent release rate studies

The time-dependent repellent release of repellent from the strands was determined by ageing at 50°C and 30°C in an EcoTherm-Labcon forced convection oven. The strands were suspended from the inside roof of the ovens in the form of loose coils. They were weighed twice a week. The repellent release kinetics from the microporous polymer strands in various formulations were investigated by fitting the release data into the mathematical models previously developed and described in Chapter Two.

Again, a Perkin Elmer Spectrum 100 FTIR spectrometer was used to study the possible degradation of the repellent under oven-ageing conditions. For this, approximately 4.0g of repellent was poured in an open Polytop glass and placed in a forced convection oven at 50°C for four months.

In this study, the correlation of the release rate of the swellable polymeric system described by different semi-empirical models is presented and discussed. This is done on the basis of the best-fitted model parameter values to obtain important information about the diffusional release mechanism of the active ingredient from a polymeric strand.

3.6 Efficacy studies of the repellent polymer strands

3.6.1 Ethical considerations

As the study included laboratory testing of the product by way of a foot-in-cage test, ethical clearance was required. Before any repellence tests commence, ethical clearance for the study was obtained from the Faculty of Health Sciences' ethics committee of the University of Pretoria (Protocol No. 720/2018).

All repellents used are existing products approved by the WHO and consequently pose no known risk to humans. The mosquitoes used to test the repellents' effects are bred in an insectary at the Faculty of Health Sciences, University of Pretoria, under very strict conditions and have no known pathogens. Therefore, these mosquitoes also pose no threat to human health.

Participants were not asked to give their personal details but signed an informed consent form. No remuneration was offered to volunteers. Test subjects were fellow students volunteering to have one foot treated with repellent and then exposed to mosquitoes.

Three human volunteers participated in the mosquito foot-in-cage test. These individuals had different blood groups (A, B and O, all three Rh^+). No allergic reaction after bioassay was observed.

3.6.2 Efficacy studies using foot-in-cage test

The polymer strands were first aged at 50^oC in forced convection ovens, a model Labcon FSOH 16. Every two weeks, samples were removed for foot-in-cage bioassay tests as described below. The mass loss testing and repellence testing were done for up to 12 weeks. Selected strands with a microporous structure were subjected to repellence testing. The tests for mosquito repellent efficacy was conducted under controlled insectary conditions. Caged mosquitoes were offered dual-choice opportunities for feeding on the treated and untreated body parts of human volunteers (Barnard and Xue, 2004, WHO, 2009). For the purposes of this study, the insectary colony of *Anopheles arabiensis* was derived from stock material maintained by the South African National Institute for Communicable Diseases (NICD). One hundred and fifty mixed-gender mosquitoes were placed in a large (1200mm × 600mm × 600mm) netting cage, which had two entry portals for the insertion of legs, spaced ca. 500mm apart on one side. Every effort was made to ensure minimal disturbance of mosquitoes prior to each test and no blood meals were offered for 72 hours prior to each trial to ensure that mosquitoes would readily try to bite and want to feed. All

mosquitoes were kept, and trials were conducted within the insectary, which was kept at a constant temperature of $25 \pm 2°C$ and relative humidity of $75 \pm 5\%$. The mosquitoes had access to cotton wool soaked with a 10% sugar solution, which was removed 6 hours prior to the commencement of repellent trials.

The test strand, 3.0m long, was wound around the lower limb region of one leg of a volunteer (Figure 3.5), leaving the other leg fully exposed (Figure 3.6). No socks or shoes or any other item of clothing was worn below the knee.

Figure 3.5: A photograph of a treated foot prepared for a foot-in-cage test

Both legs were then inserted into the cage, one leg per entry hole, and the volunteer had to stand still for five minutes (Figure 3.7). At the end of the five minutes, two other volunteers used

flashlights to count the number of mosquitos present on the lower leg of the person conducting the foot test. The number of mosquitoes on the treated and untreated legs were recorded separately.

Figure 3.6: A photograph of an untreated foot during the foot-in-cage test.

As long as a mosquito remained stationary on the foot or lower leg for at least five seconds it was counted. Only mosquitoes below the mid-calf region were counted (halfway between the foot and the knee). To avoid possible build-up of repellent on any ankle due to continuous use, each person alternated ankles on every alternative test day. Tests were conducted at least three days apart, at 15h00, allowing enough time to ensure that the mosquitoes did not become accustomed to any odour that may have lingered after each application.

Figure 3.7: Photo of the foot-in-cage test

3.6.2.1 Determination of degree of protection

The degree of protection (p) was calculated as the proportion of the number of mosquitoes landing on and/or probing the treated leg (N_T) in relation to the number landing on and/or probing the control leg (N_C) of the same individual (Pascual-Villalobos and Robledo, 1998, Salari *et al.*, 2012, Licciardello *et al.*, 2013). The formula is given by Equation (3.4).

$$p\ (\%) = \frac{(N_C - N_T)}{(N_C + N_T)} \times 100 \qquad (3.4)$$

The degree of protection was reported in percentage units.

3.6.2.2 Statistical analysis

Data collected during bioassays of the performance of the polymer strands impregnated with mosquito repellents were subjected to a statistical analysis of variance (ANOVA). The statistical analysis was used to check the reliability of the results obtained from the bioassay, such as the factors that affect the efficiency of a mosquito repellent.

3.7 Modelling phase behaviour of the LLDPE/repellent systems

3.7.1 Differential scanning calorimetry

Perkin Elmer DSC 4000 equipment (Figure 3.8) was used to detect the temperatures of crystallisation/solid-liquid and liquid-liquid phase separation of the system alkane/repellent. Samples of different alkane/repellent ratios of 20:80, 30:70, 40:60, 50:50, 60:40, 70:30, 80:20 and 100:0 were used. All samples were sealed in 50μL aluminium pans. Measurements were performed using a calibrated PerkinElmer DSC 4000 instrument in a nitrogen atmosphere. The experimental protocol was as follows: initial temperature of 5°C; heated to 160°C at a scan rate of 20°C min^{-1}; held at 150°C for 5 min and cooled to 5°C at different cooling rates of 1, 3, 5, 7.5, 10, 12.5, and 15°C min^{-1}, and then held at 5°C for 5 min. This heating cycle was repeated at least twice at a faster heating rate of 40°C min^{-1} before data collection commenced. The samples were used multiples times to ensure the reproducibility of the results. The absence of evaporation of the solvent was checked after each cooling scan, by analysis of the sample mass.

Figure 3.8: Perkin Elmer DSC 4000 instrument

3.7.2 Hot stage optical microscopy

A Leica DM2500M optical microscope fitted with a Leica DFC420 video camera and Linkam CSS 450 hot stage was used to determine the cloud point temperature (T_{cloud}). Leica Materials Workstation (Version V 3.6.1) software was used to analyse samples visually and Linksys32 (Version 1.9.5) software was used for setting up temperature profiles connected to the hot stage. The cloud point was taken as the highest solution temperature, where the onset of turbidity was observed. Samples of different Eicosane/repellent ratios of 20:80, 30:70, 40:60, 50:50, 60:40, 70:30, 80:20 and 100:0 were taken from freshly prepared solutions while heated in the reactor-block at 160°C, using a spatula to transfer a droplet with a mass of 25 – 30mg. Samples were placed between glass slides, using a spacer to reproducibly adjust the sample thickness to about 15μm. The samples were heated to 160°C in the microscope using a Linkam CSS 450 hot stage, to obtain a solution, and then cooled to 20°C at rates of 1 and $5°C\,min^{-1}$ for controlled

crystallisation. All cloud-point measurements were repeated at least two times to ensure the reproducibility of the results. Images were taken with a Leica DFC420 video camera.

CHAPTER FOUR

RESULTS AND DISCUSSION

4.1 Characterising of polymer strands

4.1.1 Chemical composition of Dellite 43B by X-ray fluorescence

Table 4.1 presents the results of chemical composition in the form of the corresponding oxides. Unsurprisingly, these results revealed high Si, Al, Fe and Mg contents consistent with the fact that montmorillonite is a phyllosilicate. Related to the organic modifier (dimethyl benzyl hydrogenated tallow ammonium) of the Dellite 43B clay, the results revealed much organic material. It is shown by the high content of Loss on Ignition (LOI).

Table 4.1: Chemical composition in (% oxides) of Dellite 43B organoclay

SiO_2	Al_2O_3	Fe_2O_3	MgO	CaO	P_2O_5	Na_2O	TiO_2	K_2O	ZrO_2	LOI	Total
43.54	14.29	3.26	1.57	0.47	0.37	0.11	0.08	0.01	0.01	36.22	99.93

4.1.2 Effect of repellent on swelling and shrinkage of the polymers

Table 4.2 lists the amount of repellent absorbed by the two polymers at 30°C and 50°C determined by Equation (3.2). The results are in agreement with those observed by Charara *et al.* (1992) studying the absorption of EOs in various polymeric packaging materials. They reported that the highest absorption was found in materials with low crystallinity. The semi-crystalline and nonpolar LLDPE absorbed less polar repellent compared to the amorphous and polar EVA matrix. The polar repellents interacted more weakly with the nonpolar LLDPE matrix compared to EVA that

contained the polar group (containing 9% VA). The results show that the solubility of Icaridin was less compared to DEET, this can suggest that Icaridin had less compatibility with the polymers.

Table 4.2: Polymer swelling by repellents expressed in wt.% evaluated at 30°C and 50°C

Temperature (°C)	30		50	
Polymer	DEET	Icaridin	DEET	Icaridin
LLDPE	0.29±0.02	0.18±0.03	0.79±0.02	0.44±0.04
EVA	1.65±0.14	0.99±0.10	5.14±0.10	3.18±0.11

The polymer matrix strands produced could be used for controlled release applications. There is a possibility of shrinkage of the swelled polymer matrix as the repellent will be released over time by evaporation. Such shrinkage could become uncomfortable to the wearer if it caused constriction. Therefore, it was important to estimate the degree of shrinkage of the polymer matrix strands containing repellents. According to Akhtar and Focke (2015), this dimensional instability is undesirable in products, such as insect repellent bracelets and anklets.

Table 4.3 shows the shrinkage of neat polymer strands and polymer strands impregnated with DEET and Icaridin determined by Equation (3.3). The sample dimensions were measured after ageing for one month at 50°C in a convection oven. As expected, looking at the swelling results, the EVA strands showed more extensive shrinkage than LLDPE strands. In addition, DEET-containing strands showed a higher shrinkage than Icaridin-filled polymers irrespective of the matrix polymer (EVA and LLDPE). This could be due to the higher solubility and diffusibility of DEET, compared to Icaridin, in the polymers. The neat polymer strands showed a degree of

shrinkage less than that of the repellent-filled samples. However, the LLDPE matrix showed better dimensional stability than the EVA matrix due to its crystallinity and polarity.

Table 4.3: Shrinkage of polymer strands expressed in wt.% evaluated at 50°C

Polymer strand	Sample No.	Diameter before shrinkage (mm)	Diameter after shrinkage (mm)	Shrinkage (%)
Neat LLDPE	BM00	3.28±0.07	3.25±0.04	0.78
Neat EVA	AS00	3.58±0.05	3.49±0.12	2.64
LLDPE-Icaridin (20)	BM400	3.43±0.07	3.31±0.06	3.59
LLDPE-Icaridin (30)	BM401	4.29±0.05	4.19±0.03	2.31
LLDPE-DEET (20)	BM402	4.24±0.13	4.08±0.19	3.73
LLDPE-DEET (30)	BM403	4.16±0.05	3.96±0.04	4.76
EVA-Icaridin (20)	AS400	3.53±0.25	3.38±0.10	4.43
EVA-Icaridin (30)	AS401	3.65±0.26	3.48±0.06	4.66
EVA-DEET (20)	AS402	3.40±0.12	3.22±0.10	5.23
EVA-DEET (30)	AS403	3.55±0.06	3.20±0.07	9.77

4.1.2 Repellent content of the extruded strands by TGA and solvent extraction

Figure 4.1 and 4.2 show TGA traces of the repellent, neat polymer and trapped repellent through the polymer-clay nanocomposite matrix. The first mass loss is assigned to the loss of the volatile repellent component in polymer-based strands in all samples analysed. The mass loss of the neat Icaridin by vaporisation commenced just above 125°C and was complete by 293°C, while the

evaporative mass loss of the neat DEET commenced earlier, just above 104°C and was complete by 267°C. However, the DEET and Icaridin mass loss were complete before the polymer started to lose mass in earnest above 400°C. Therefore, the volatility of the repellents was suppressed when they were trapped in the polymer filaments. Similar trends were observed for the DEET-filled EVA and the Icaridin-filled EVA. However, the DEET mass loss by evaporation overlapped with the first mass-loss event for the EVA, while this behaviour was not observed for Icaridin and the mass loss by evaporation commenced just above 111°C.
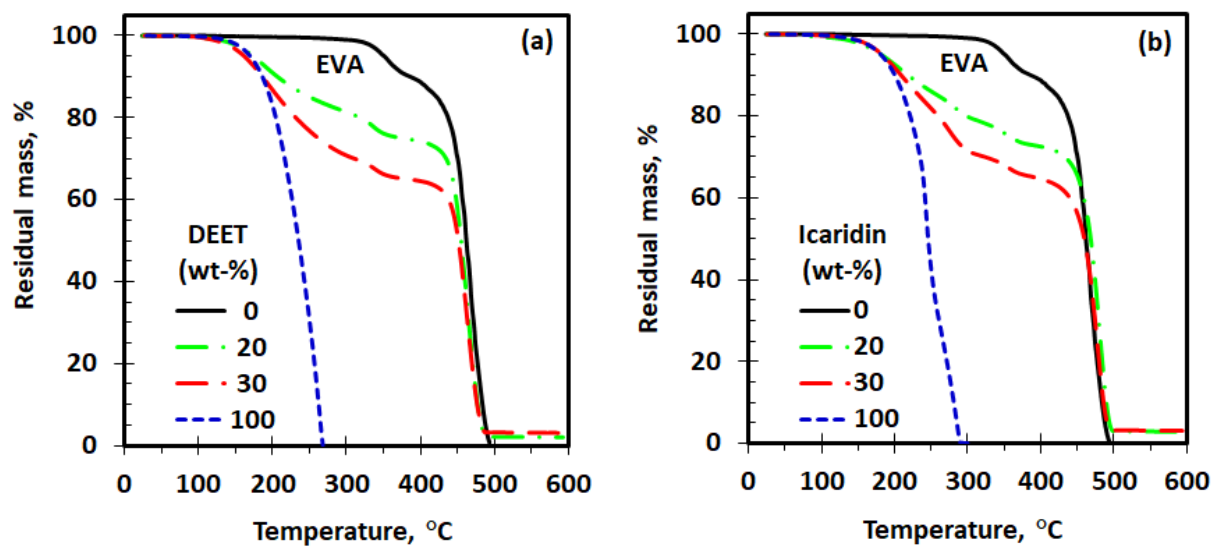
Figure 4.1: TGA mass loss traces for DEET, Icaridin, neat polymers and EVA polymer-based strands containing 5 wt-% Dellite 43B clay and either 20 or 30 wt-% DEET (a) and 20 or 30 wt-% Icaridin (b)
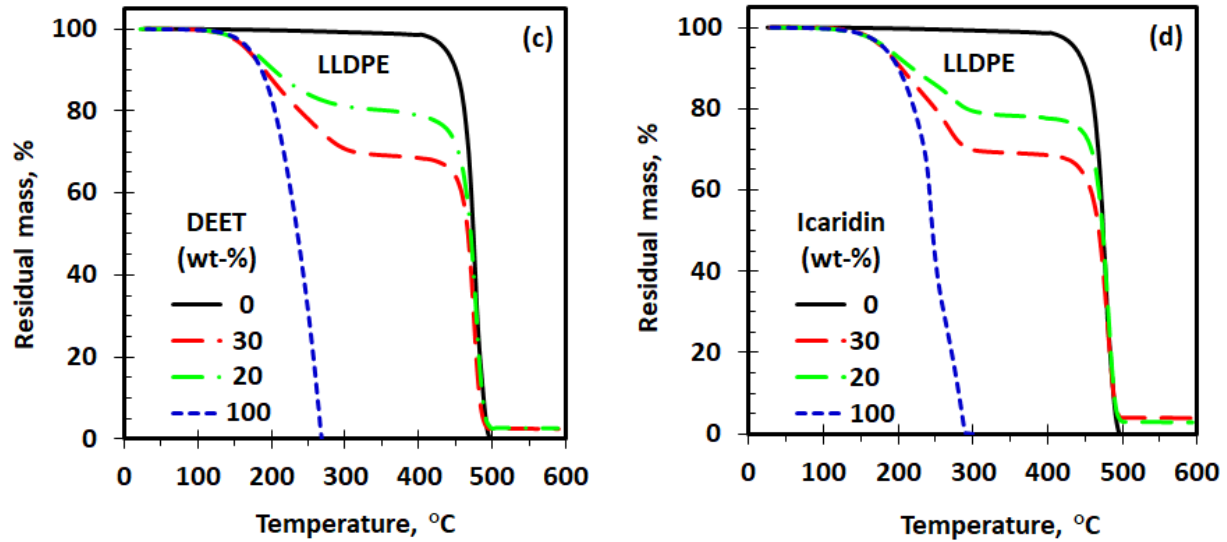
Figure 4.2: TGA mass loss traces for DEET, Icaridin, neat polymers and LLDPE polymer-based strands containing 5 wt-% Dellite 43B clay and either 20 or 30 wt-% DEET (c) and 20 or 30 wt-% Icaridin (d).

Table 4.4 shows the estimated amount of repellent determined by TGA and solvent extraction, calculated using Equation (3.1). It is notable that there was an agreement with the amount of repellent initially loaded in the compounding process and the TGA analysis as well as the solvent extraction results. This shows that very little repellent mass was lost by evaporation during the compounding process (see Appendix VI for other compositions).

Table 4.4: Nominal repellent content (in wt-%) and values estimated using solvent extraction and TGA

Polymer strand	Nominal	TGA	Solvent extraction	Sample code
LLDPE-DEET	20	19.8	19.3±0.6	BM402
LLDPE-DEET	30	30.2	30.0±0.9	BM403
LLDPE-Icaridin	20	20.1	20.2±0.6	BM400
LLDPE-Icaridin	30	30.3	29.0±0.2	BM401
EVA-DEET	20	19.7	18.7±0.5	AS402
EVA-DEET	30	29.9	29.0±0.2	AS403
EVA-Icaridin	20	20.3	19.6±0.2	AS400
EVA-Icaridin	30	28.47	30.1±0.5	AS401

Figure 4.3 shows an example of TGA curves for the polymer-repellent and polymer-repellent-clay strands. The mass loss proceeded stepwise in all samples. There was not much difference in the mass loss for the nanocomposite strand compared to that of the polymer strand without clay.
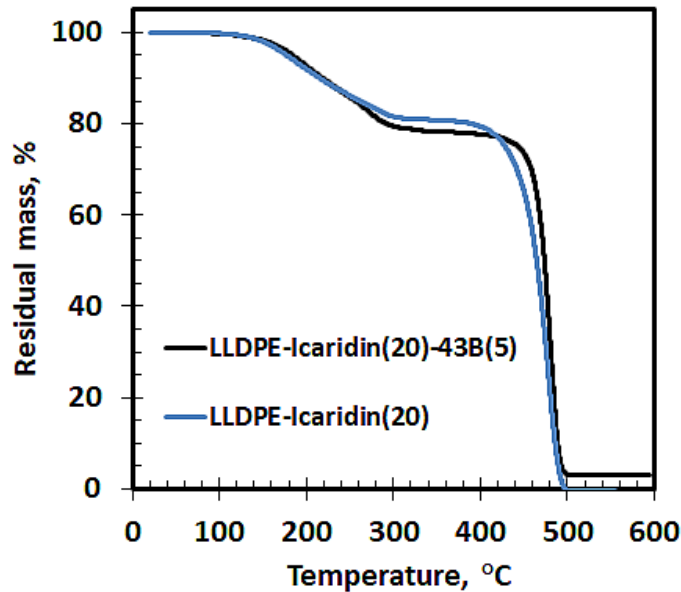
Figure 4.3: TGA curves of LLDPE strands initially containing: (▬) 20 wt-% Icaridin and loaded with 5 wt-% Dellite 43B organoclay; and (▬) 20 wt-% Icaridin with the absence of nanofillers.

4.1.3 Scanning electron microscopy

Figures 4.4 and Figure 4.5 show SEM micrographs of EVA and LLDPE strands prepared in the absence of the nanofillers. The open-cell foam structure of the polymer scaffold comprising the strands is clearly visible in these Figures. Different repellents gave rise to different microporous structures in the interior of the strands and it is clearly visible that the type of repellent and polymer did affect the morphology.
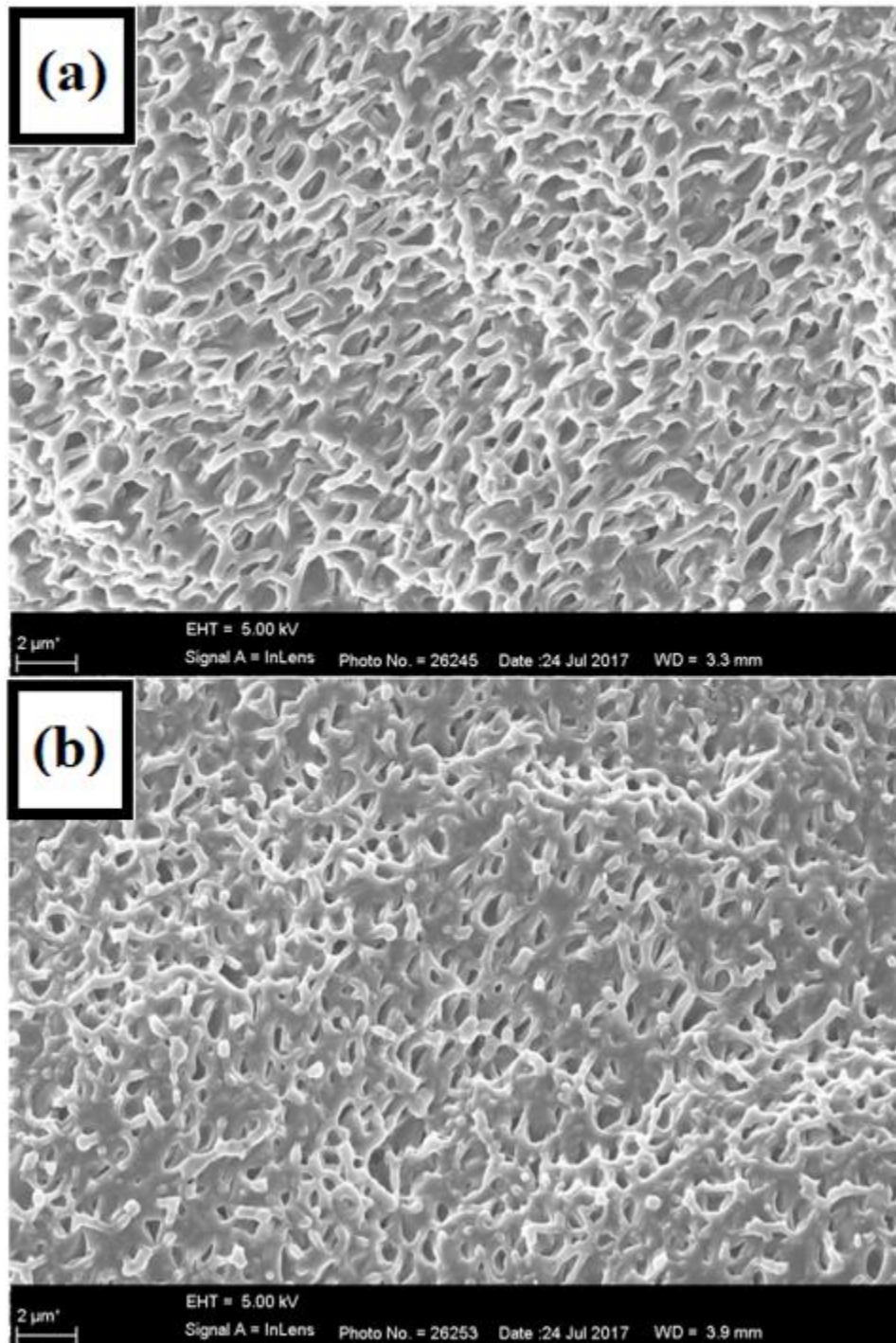
Figure 4.4: SEM micrographs of EVA strands impregnated with: (a) 40 wt-% of DEET; and (b) 40 wt-% of Icaridin. No fillers were added.
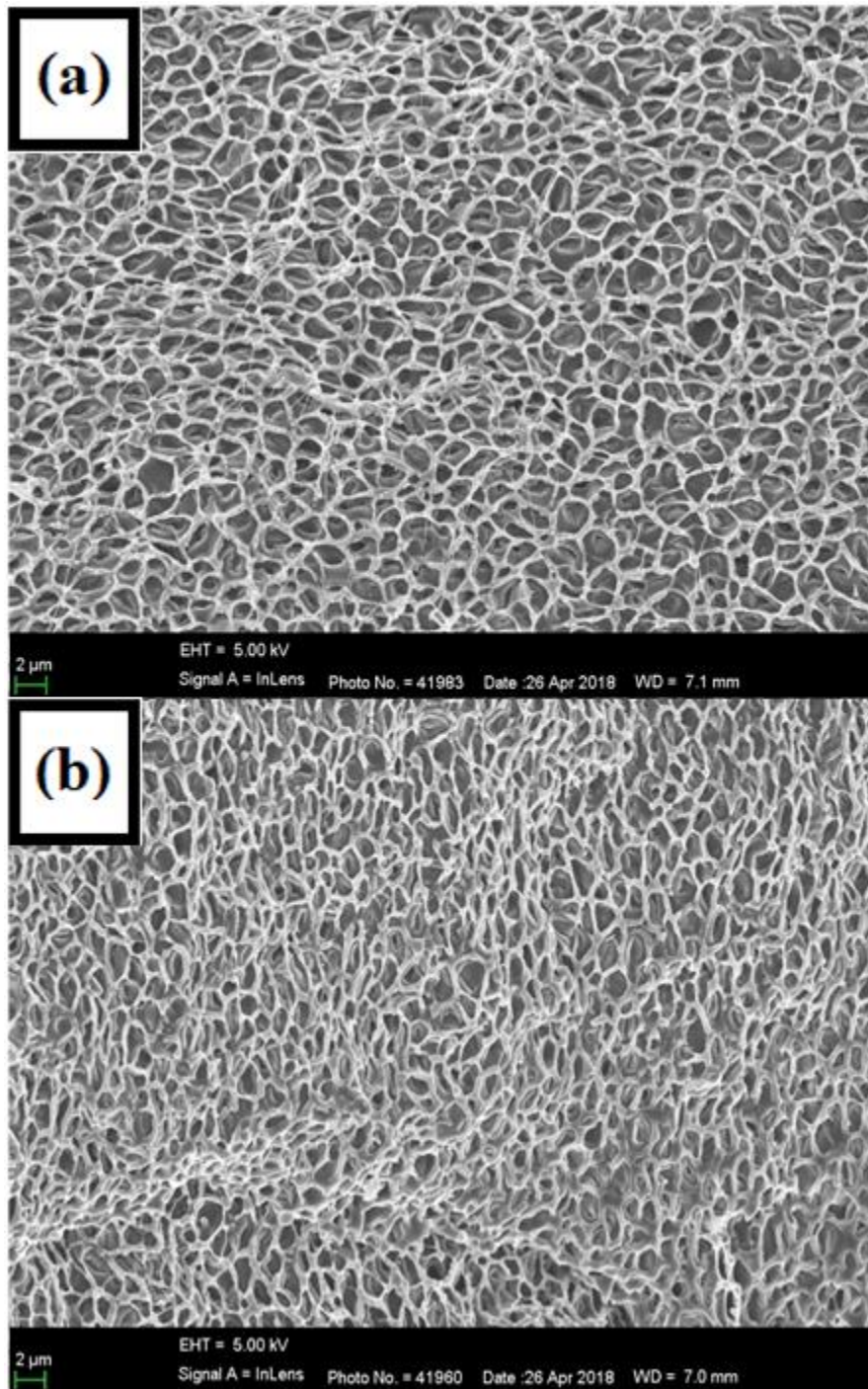
Figure 4.5: SEM micrographs of LLDPE strands impregnated with: (a) 41 wt-% of DEET; and (b) 42 wt-% of Icaridin. No fillers were added.

Figure 4.6 and Figure 4.7 show the effect of fumed silica and insect repellent type on the structure of the internal microporous region of extruded polymer strands. The micrographs revealed the presence of agglomerated fumed silica particles inside the cavities, suggesting that the fumed silica was primarily present in the repellent-rich phase after phase separation was complete. The morphology of polymer strands did not change with the incorporation of fumed silica into the microporous polymer strand.
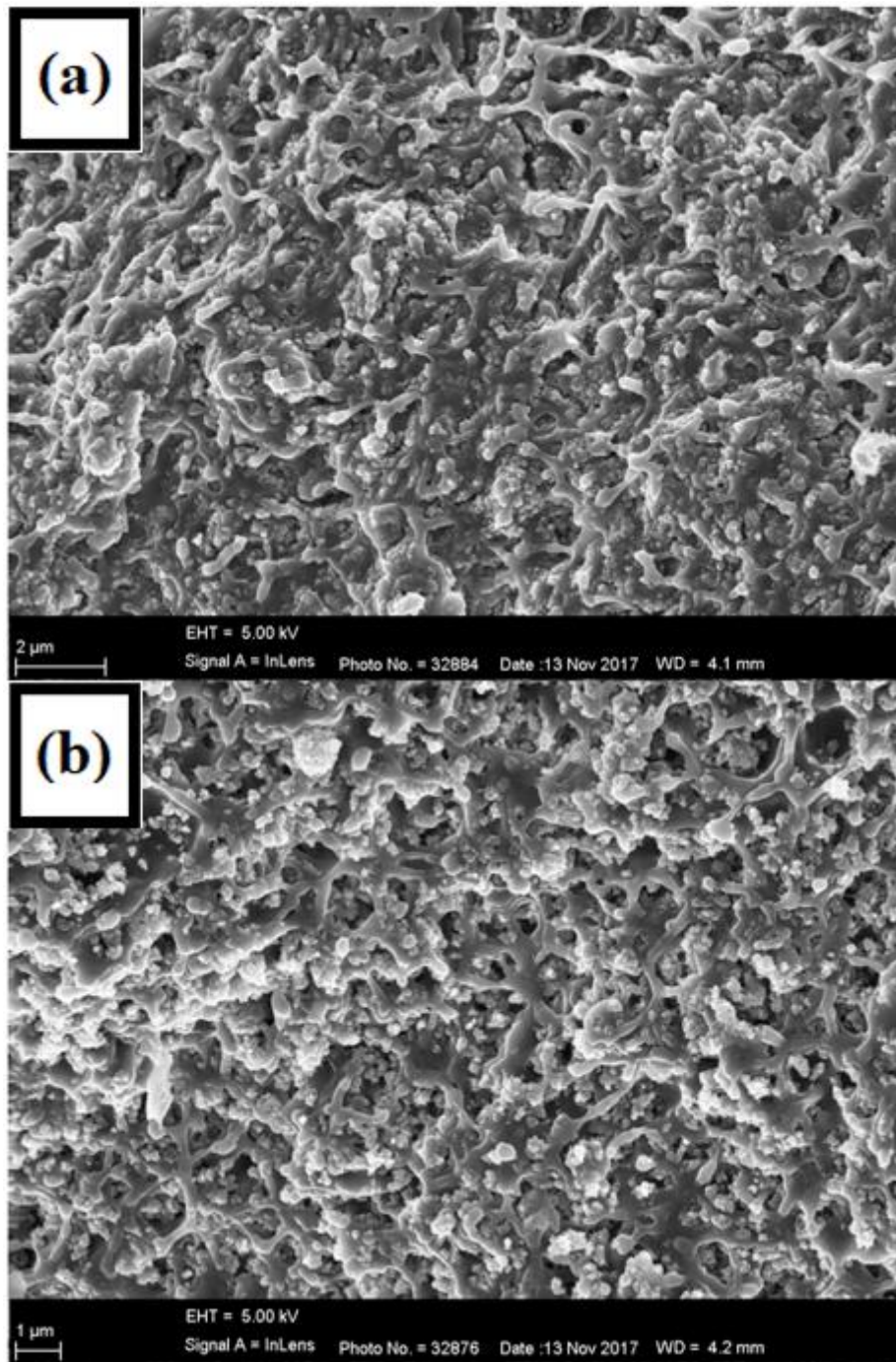
Figure 4.6: SEM micrographs showing the effect of silica and insect repellent type on the structure of the internal microporous region of extruded EVA strands. (a) 30 wt-% Icaridin; and (b) 30 wt-% DEET. All strands contained 5 wt-% fumed silica.
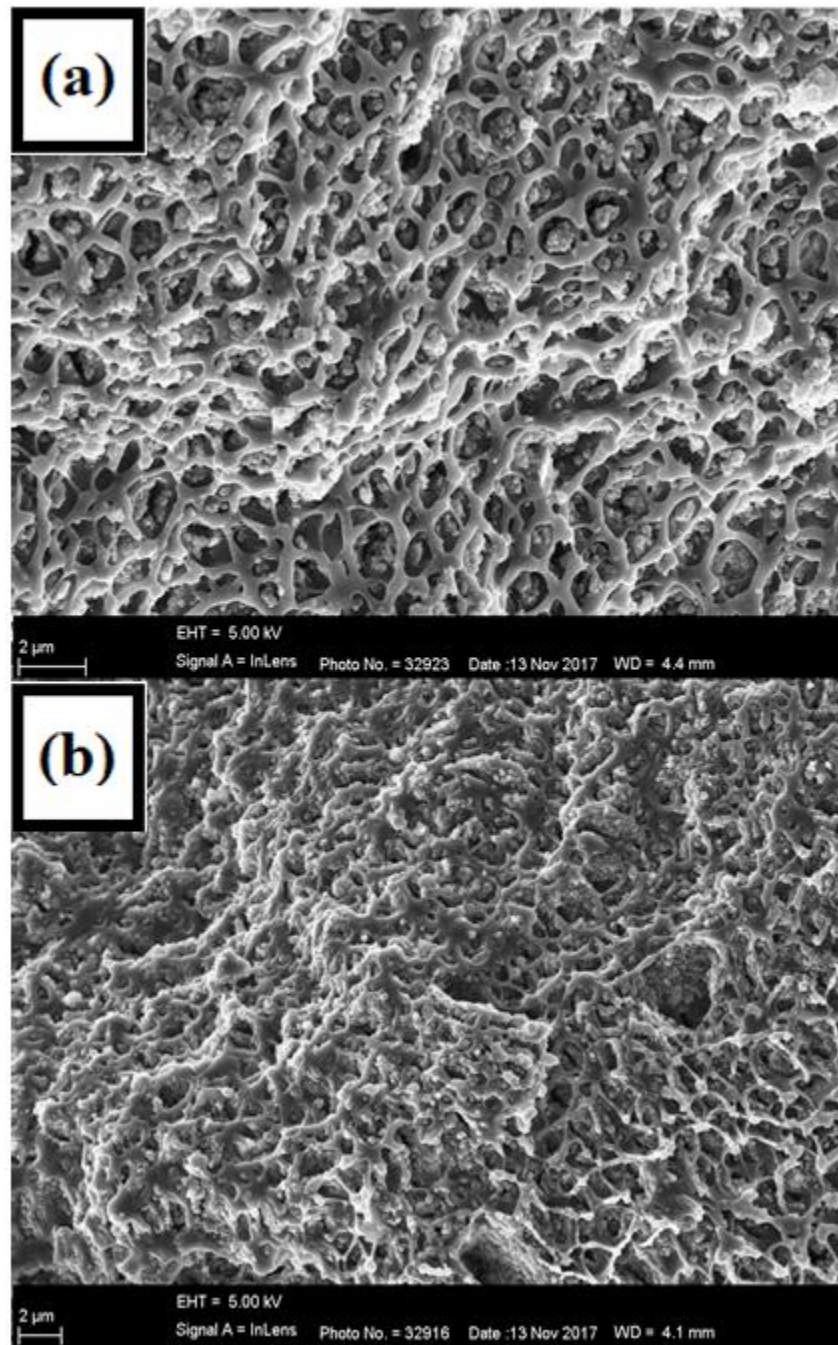
Figure 4.7: SEM micrographs showing the effect of silica and insect repellent type on the structure of the internal microporous region of extruded LLDPE strands. (a) 30 wt-% Icaridin; and (b) 30 wt-% DEET. All strands contained 5 wt-% fumed silica.

Figure 4.8, Figure 4.9 and Figure 4.10 show the effect of the polymer type (EVA and LLDPE) and their concentration on the LLDPE clay phase morphology. The interconnectivity of the pores is clearly visible. However, it is clear from the micrographs that the nature of the polymer, repellent, as well as the concentration that was used, did affect the final microstructure. In all cases, the scale of the pores was in the order of a few microns. No clay platelets were observed, suggesting that they were confined to the polymer-rich phase that formed the microporous scaffold. Those experiments showed that the thermally induced SD route can, in fact, lead to a microporous polymer structure.
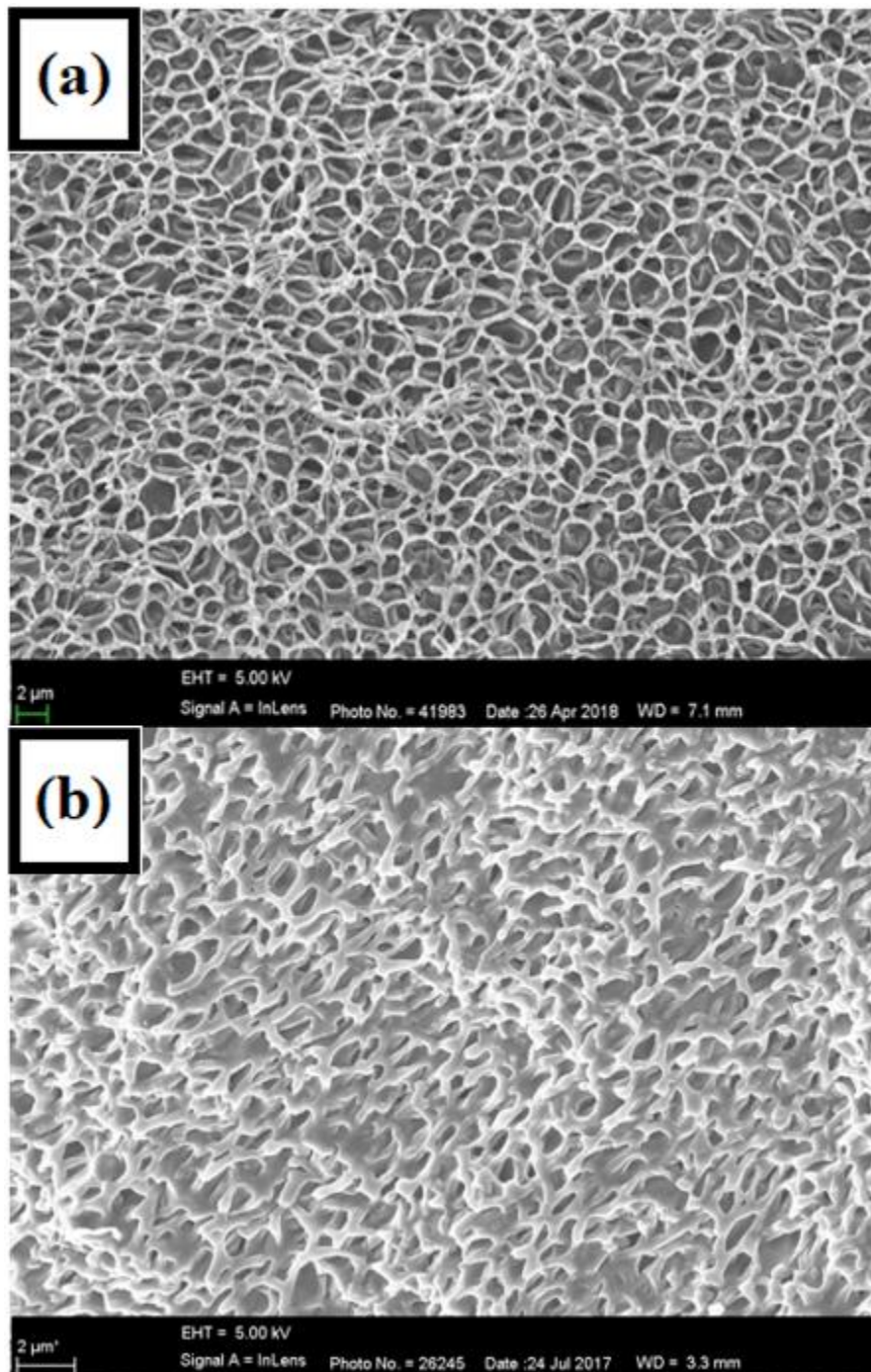
Figure 4.8: SEM micrographs showing the effect of polymer type on the structure of the internal microporous region of extruded strands containing 40 wt-% Icaridin. (a) LLDPE and (b) EVA. No fillers were added.
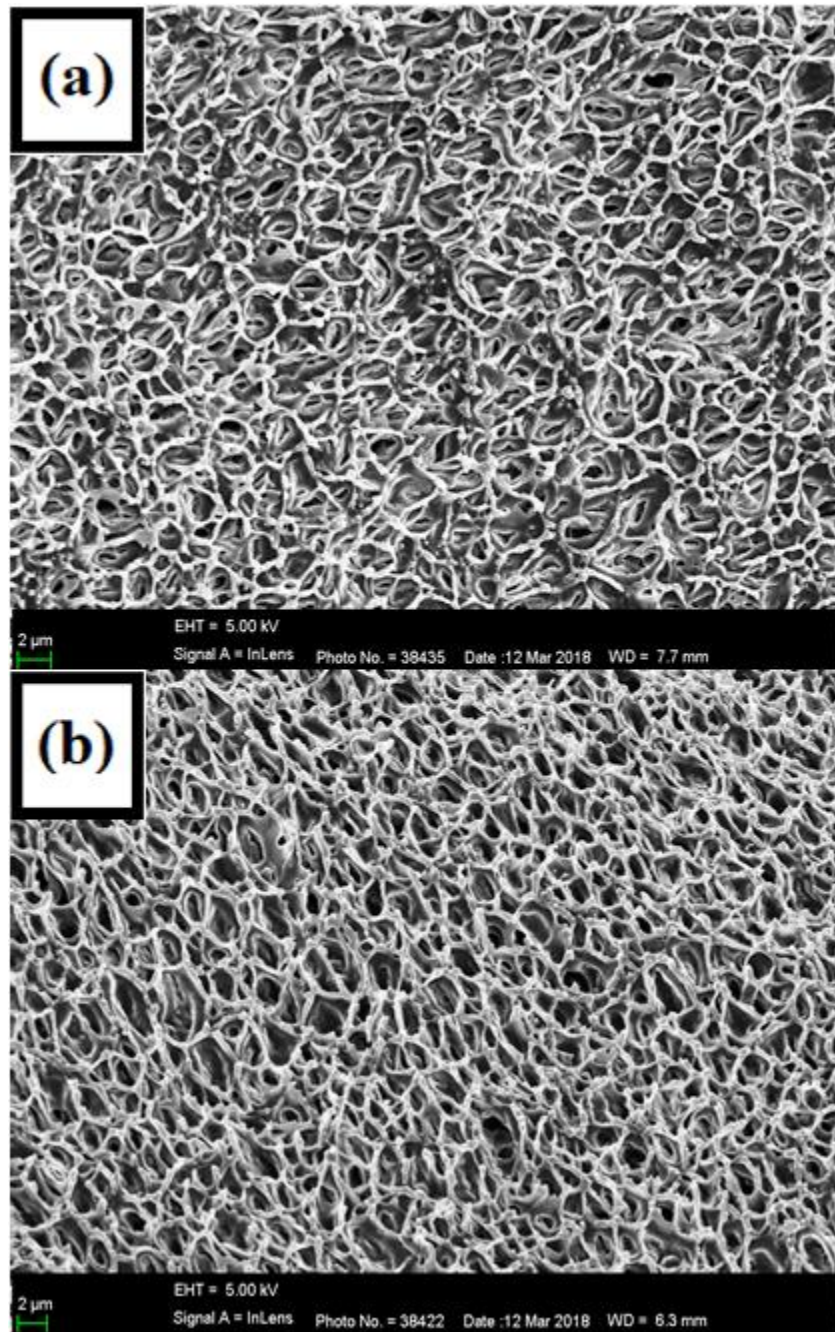
Figure 4.9: SEM micrographs showing the effect of insect repellent type and concentration on the structure of the internal microporous region of extruded LLDPE strands. (a) 20 wt-% DEET; and (b) 30 wt-% DEET. All strands contained 5 wt-% Dellite 43B clay.
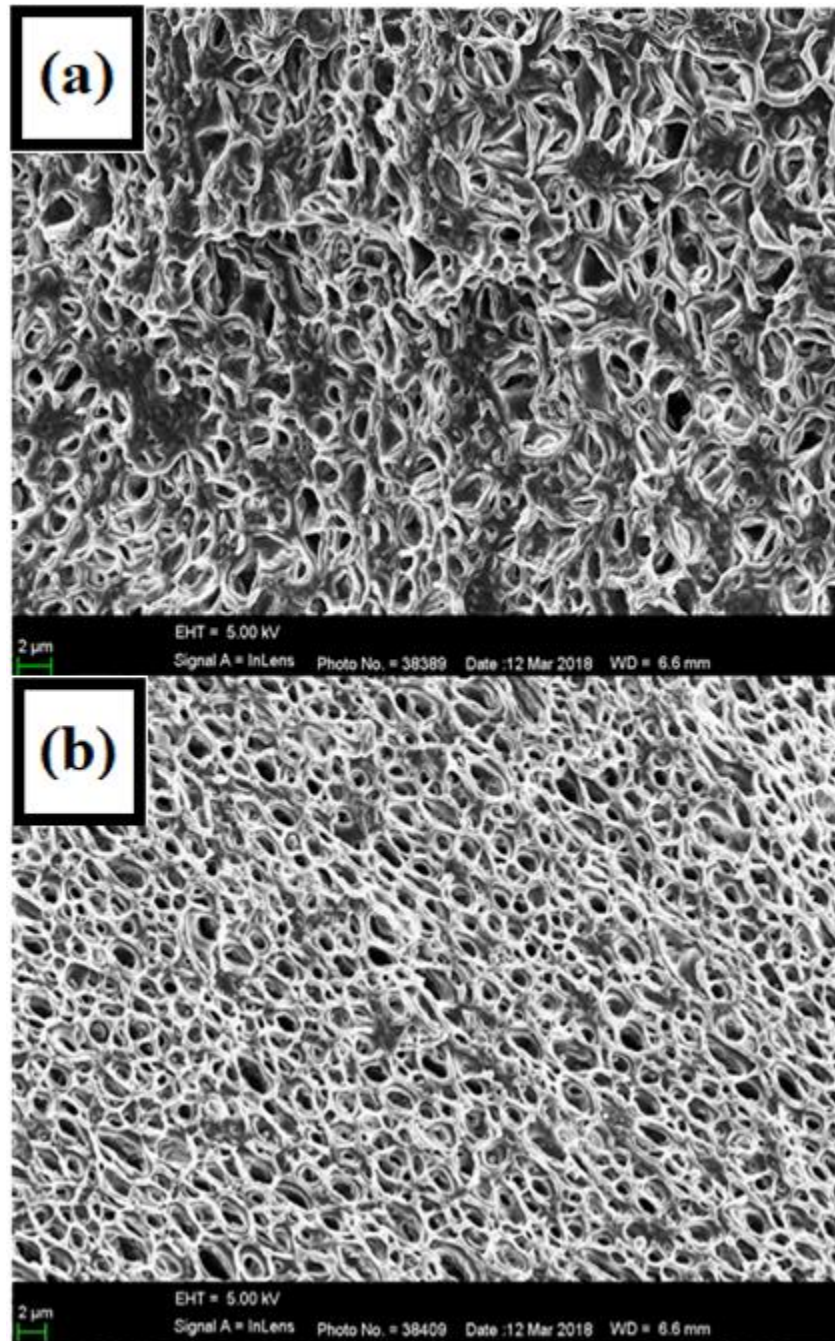
Figure 4.10: SEM micrographs showing the effect of insect repellent type and concentration on the structure of the internal microporous region of extruded LLDPE strands. (a) 20 wt-% Icaridin; and (b) 30 wt-% Icaridin. All strands contained 5 wt-% Dellite 43B clay.

102

4.1.4 Micropore image analysis

For digital processing of SEM images of microporous LLDPE polymer strands, the ImageJ2 (Version: 2.0.0-rc-43/1.50e) program was used. For the processing and analysis of the microporous structure of polymer strands, the following steps were taken in the program ImageJ2:

1. Conversion of the image to an 8-bit format to enhance the contrast and simplify and allow the subsequent analysis;

2. Elimination of noises using the filter function, sharpen and rescale;

3. Segmentation of the image to find the threshold value in order to fully determine the object; and

4. Analysis of selected objects (analyse particles).
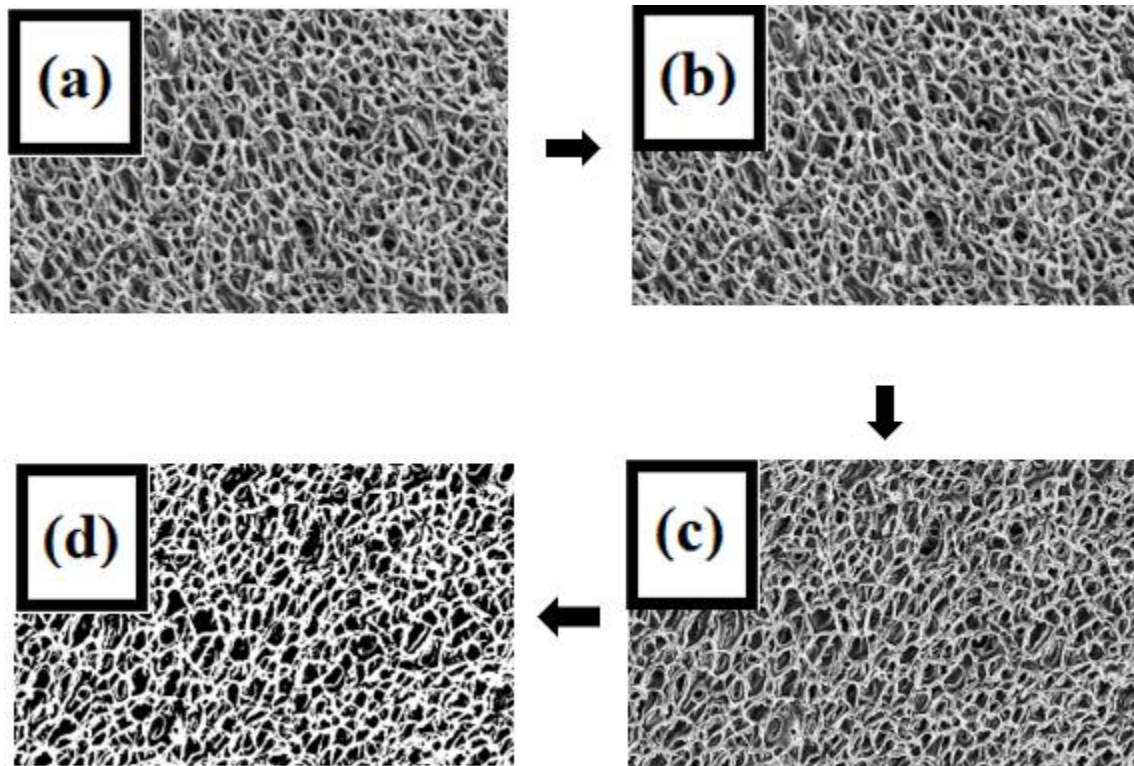
Figure 4.11: The processing scheme of SEM images of microporous polymer strands using ImageJ2 software: **(a)** original SEM image; **(b)** contrast-enhanced image (converted to 8 bits image); **(c)** sharpen, rescaled and random noises eliminated; **(d)** threshold image ready for particle size analysis.

The projected pore areas distribution was calculated from SEM images using the Imagej2 processing software. To visualise the analysis process, graphics of the projected pore area distribution on area fraction and percentage using Microsoft Office Excel package were plotted.
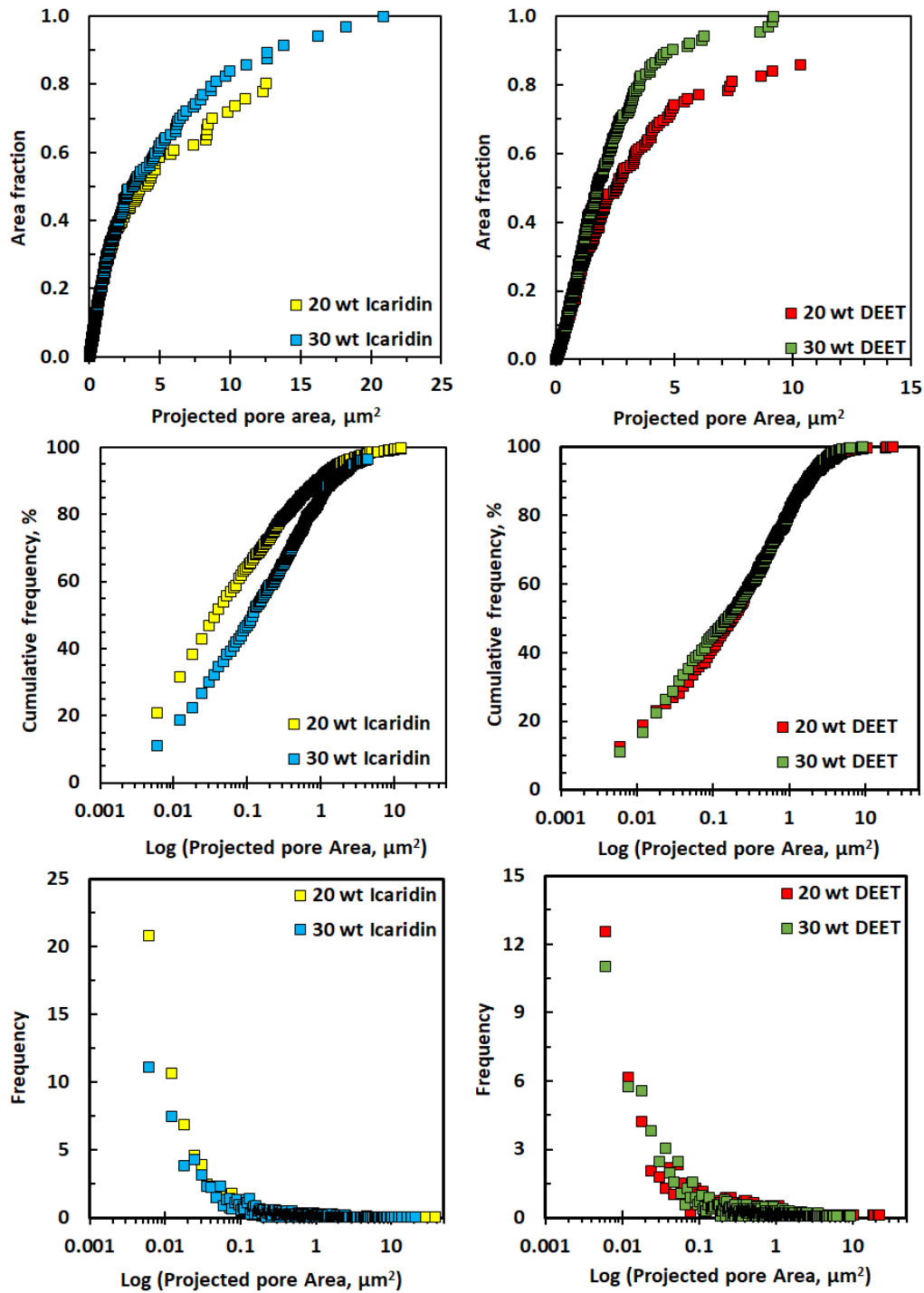
Figure 4.12: Pore area distribution results of microporous micrographs of LLDPE strands impregnated by Icaridin (on the left side) and DEET (on the right side) processed using ImageJ2 software.

The results in Figure 4.12 show that the projected pore area distribution was uniform independently of the repellent and concentration trapped. However, the number of pores increased as the quantity of repellent trapped increased too.

4.2 Factors affecting the repellent release rate

Figure 4.13 shows the release curves of DEET and Icaridin-based polymers strands aged at $50^{\circ}C$ in a convection oven. Both strands contained 5 wt-% clay. DEET was, in general, released faster than Icaridin from the different polymer strands. The repellents were released at an almost constant rate over an extended period of time. The repellent was more rapidly released from a polar matrix compared to nonpolar matrix. This agrees with the results found in the swelling experiments. The polar matrix allowed faster permeation of the polar repellent.
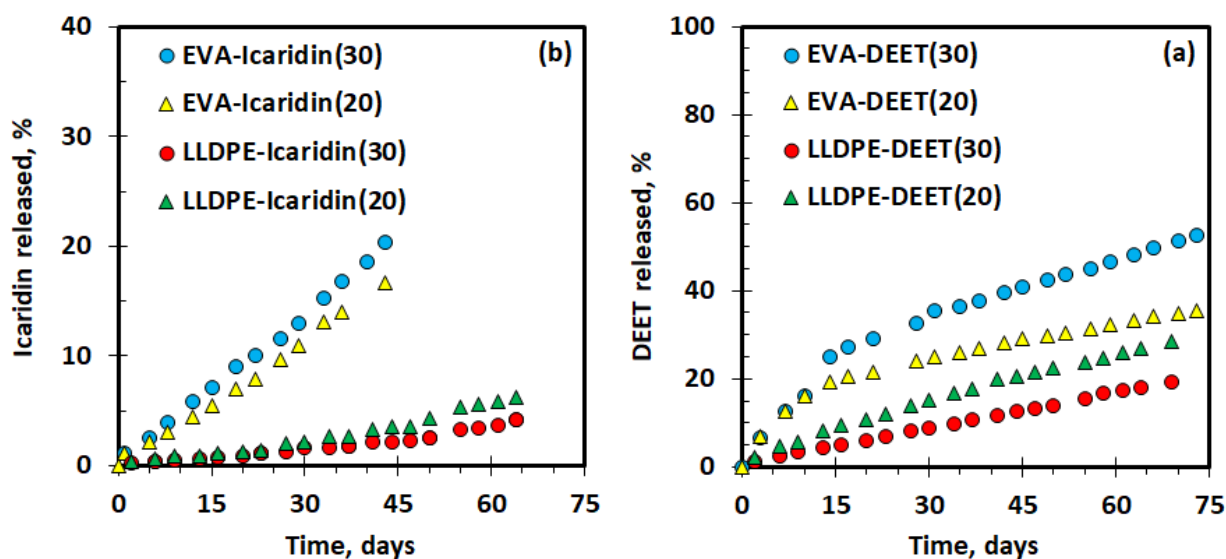
Figure 4.13: Repellent release curves during oven-ageing at 50°C. The LLDPE- and EVA-based strands contained 5 wt-% Dellite 43B clay and either DEET or Icaridin as a repellent.

Figure 4.14 shows the measured DEET (a) and Icaridin (b) release curves for samples aged in a convection oven at 50ºC. The EVA strands contained DEET and Icaridin in two different concentrations of 30 wt-% and 20 wt-% and both strands contained 5 wt-% Dellite 43B. The repellent depletion happened most rapidly for the strand with the higher repellent loading. This difference in behaviour can be attributed to differences in the porosity of the samples, as the results of the ImageJ2 analysis showed that strands with a high level of repellent formed more pores however with the same pore area distribution.
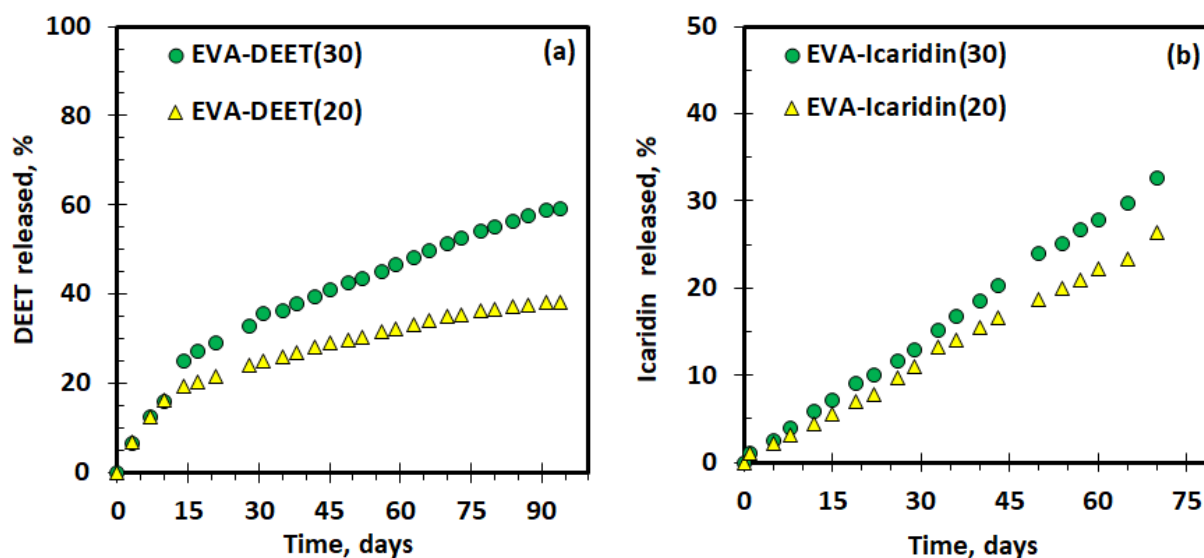
Figure 4.14: Effect of concentration of the repellent on release from the EVA strands: (a) DEET and (b) Icaridin. The amount of repellent initially incorporated into the EVA strands was: (△) 30wt-% and (●) 20wt-%. Both strands contained 5 wt-% clay.

Figure 4.15 shows the effect of nanofiller (silica or Dellite 43B organoclay) on the repellent release from EVA strands aged in a convection oven set at a temperature of 50°C. The release of the repellents was high for strands containing the silica. This can be explained by the polarity of the silica.
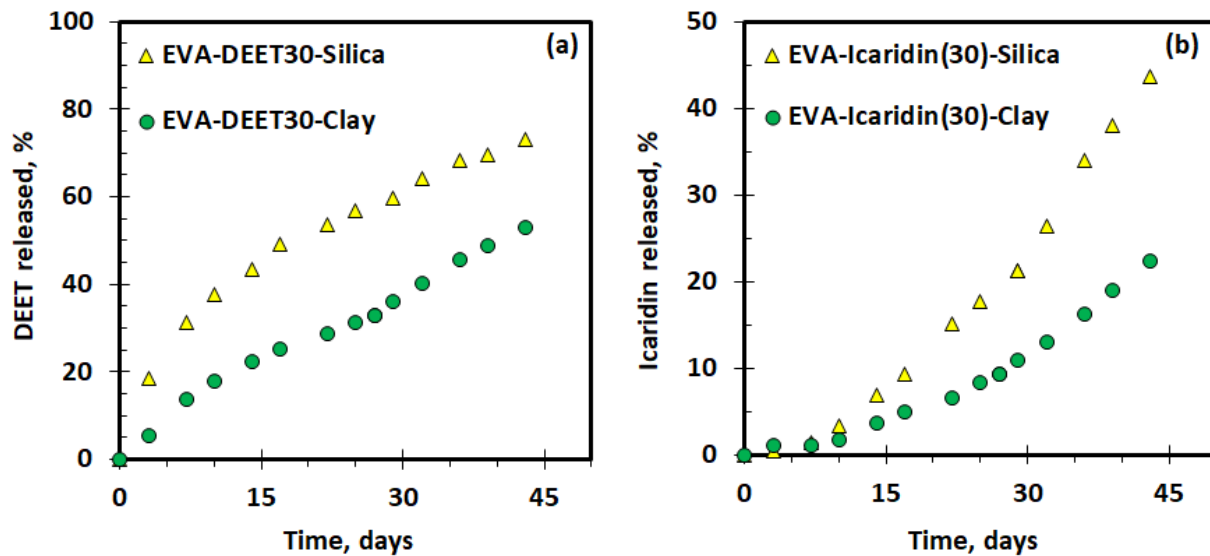
Figure 4.15: Effect of nanofiller on repellent release from EVA strands: (a) DEET and (b) Icaridin. The EVA strands initially containing: (△) 30 wt-% repellent and 5 wt-% fumed silica; and (●) 30 wt-% repellent DEET and 5 wt% Dellite 43B clay.

Figure 4.16 shows the effect of the diameter of the strands on the release of Icaridin and DEET aged in a convection oven at a temperature of 50°C. Strands of different diameter sizes were studied for each repellent-polymer composition (see Appendix V). The release of repellents (DEET and Icaridin) occurred fastest for polymer strands, with a small diameter in contradiction to the theoretical expectations. However, the differences in release rate were likely caused by differences in other geometric parameters than those of the strand diameter, e.g. the thickness of the membrane or the structure of the internal porous regions. This behaviour was observed in all repellent-strand compositions.
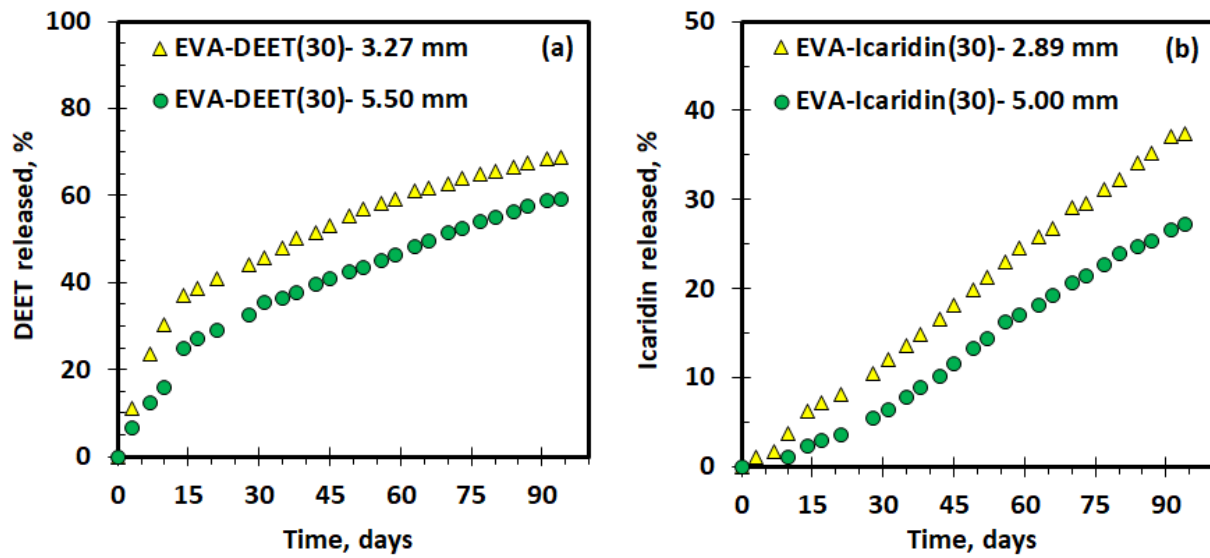
Figure 4.16: Effect of diameter sizes of EVA-strands on the release of the repellent: (a) DEET and (b) Icaridin.

Figure 4.17 shows the effect of temperature on the release of repellent from EVA strands aged in a convection oven at a temperature of 30°C and 50°C, respectively. As expected, the repellents were released at a faster rate at the higher temperature.
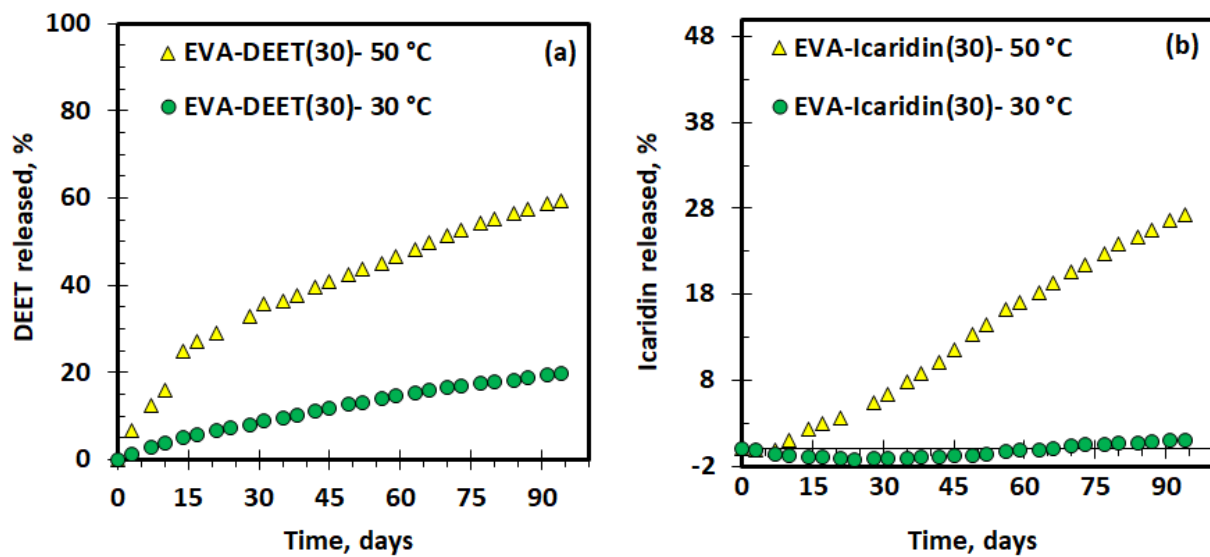
Figure 4.17: Effect of temperature on the release of EVA strands. (a) DEET and (b) Icaridin.

Figure 4.18 shows the effect of the quantity of clay on the release of repellent from EVA strands aged in a convection oven at a temperature of 50°C with a constant concentration of 20% of Icaridin. There was no difference in the release when the clay was added up to 1%. A drop is seen when 2.5% of the clay was added, showing a very big effect on the release rate of Icaridin. There is no substantial change when the quantity of clay was increased to 5%.
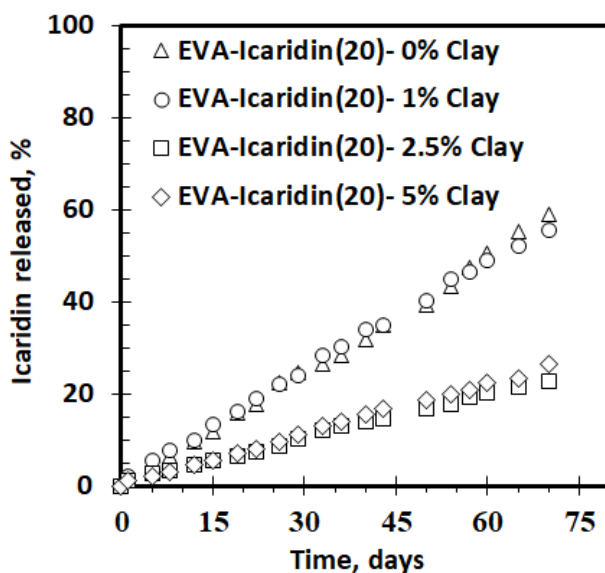
Figure 4.18: Effect of clay quantity on the release of Icaridin from EVA strands.

4.3 Repellent stability under processing and ageing conditions

Figure 4.19 presents the FTIR spectra of DEET and Icaridin before and after compounding the repellent-impregnated EVA strands. All the spectra show a prominent carbonyl ($- C = O$) absorption band, located at approximately 1650 cm^{-1}, present in all the actives. The presence of the alcohol ($-$ OH) functional group is observed at approximately 3500 cm^{-1} for Icaridin and absent in the DEET spectra because the molecular structure of DEET does not contain the $-$ OH

110

group. The FTIR spectra of samples recovered from the polymer after compounding were, for all practical purposes, identical to those of the neat repellents.
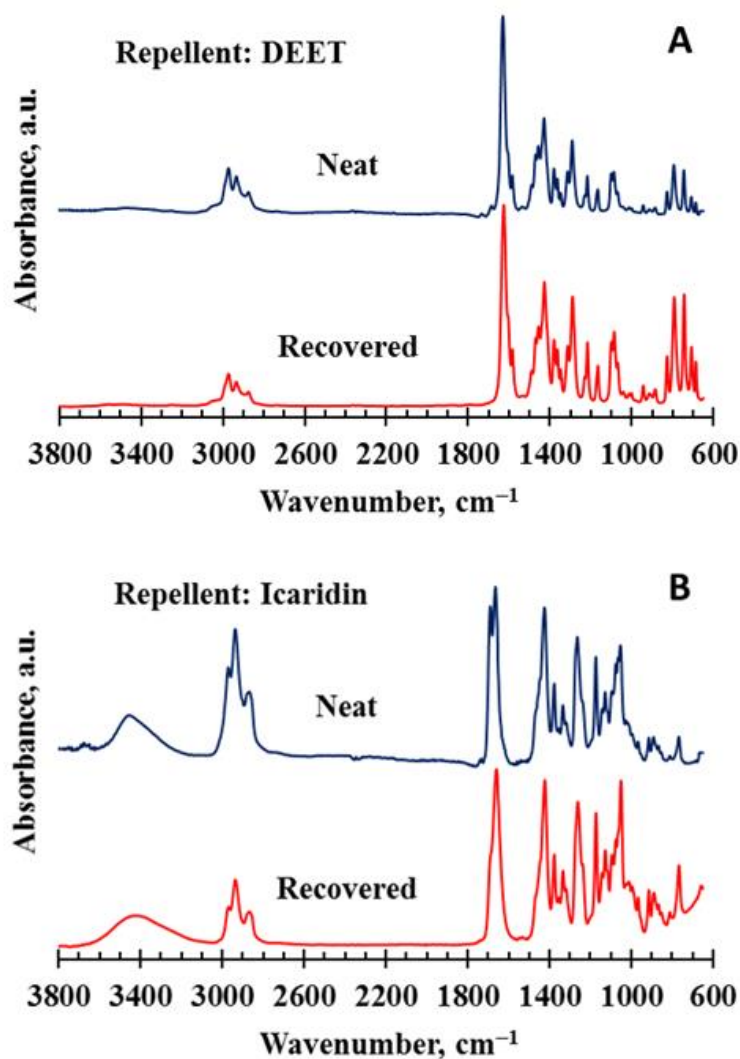
Figure 4.19: FTIR spectrograms of A. DEET and B. Icaridin before and after compounding.

Figure 4.20 shows the FTIR spectra of DEET and Icaridin after four months at 50°C. Once again, it was proven that the repellents continued steadily during the testing time. This means that the

FTIR results are consistent with the absence of thermal degradation during the polymer processing and ageing conditions.
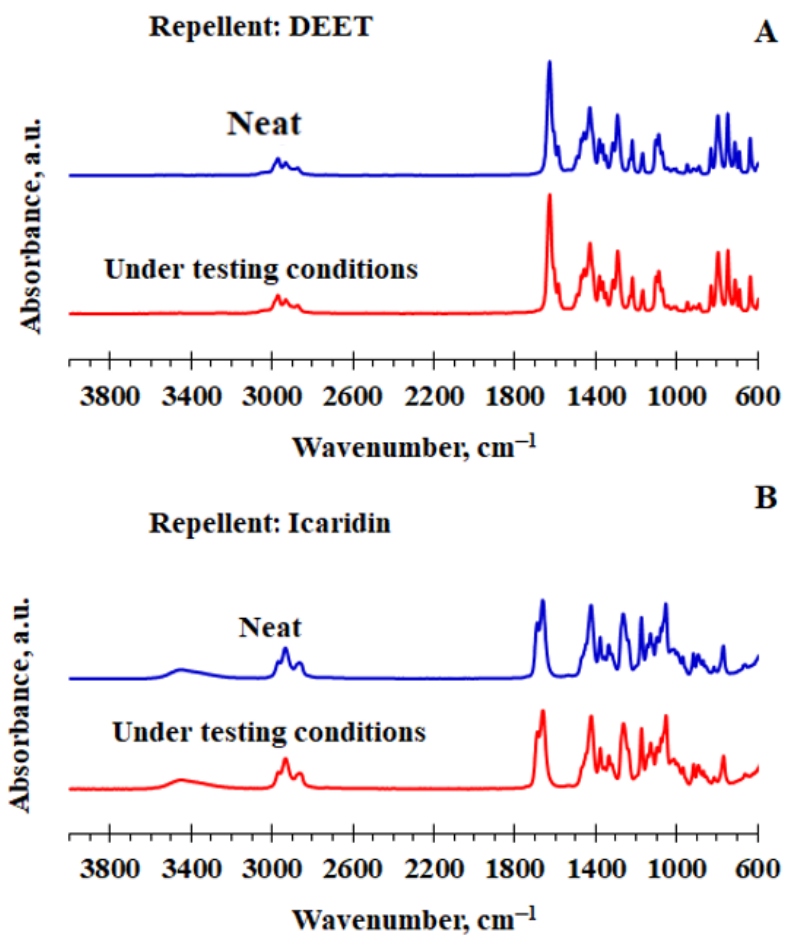
Figure 4.20: FTIR spectrograms of A. DEET and B. Icaridin before and after mimicking the oven-ageing conditions for four months.

4.4 Modelling for repellent release from EVA strands

The correlation of release rate of a swellable polymeric system was described by different models and was discussed on the basis of the best-fitted model parameter values to obtain important information about the diffusional release mechanism of the active ingredient from a polymeric device. The data were fitted to different models and the values of *n* (diffusional exponent for Peppas equation and shape parameter for Hill and Weibull models), as well as the correlation, were calculated. Table 4.5 and 4.6 show the results for repellent release rate studies of DEET and Icaridin, respectively, from EVA polymer samples fitting the models proposed in this study.

Table 4.5: Results of fitting the release of DEET for proposed models at different compositions and temperature

	(°C)	(mm)	wt-%			Hill		Weibull		Peppas	
SAMPLE	Temp.	Dimeter	Dellite 43B	Silica	DEET	*n*	R^2	*n*	R^2	*n*	R^2
AS100	50	3.32	0.00	5.00	0.38	2.33	0.9968	1.52	0.9989	0.72	0.9751
AS200	50	3.84	0.00	5.00	0.30	0.93	0.9944	0.69	0.9980	0.47	0.9981
AS201	50	3.60	0.00	5.00	0.39	0.95	0.9947	0.73	0.9900	0.53	0.9820
AS202	50	3.42	5.00	5.00	0.29	0.97	0.9827	0.69	0.9926	0.44	0.9974
AS203	50	3.22	5.00	5.00	0.36	0.92	0.9899	0.65	0.9815	0.43	0.9674
AS208	50	3.96	5.00	0.00	0.29	1.14	0.9826	0.97	0.9876	0.81	0.9921
AS402	50	6.37	5.00	0.00	0.19	1.14	0.9967	0.87	0.9990	0.63	0.9974
AS403	50	6.22	5.00	0.00	0.29	1.53	0.9963	1.25	0.9983	0.95	0.9976
AS204	30	6.01	5.00	0.00	0.18	0.86	0.9995	0.80	0.9994	0.73	0.9992
AS205	30	3.39	5.00	0.00	0.18	0.85	0.9994	0.75	0.9985	0.66	0.9972
AS206	30	5.50	5.00	0.00	0.29	0.83	0.9994	0.78	0.9993	0.73	0.9990
AS207	30	3.27	5.00	0.00	0.29	0.82	0.9998	0.75	0.9996	0.68	0.9991
AS304	50	6.01	5.00	0.00	0.18	0.55	0.9973	0.48	0.9971	0.41	0.9963
AS305	50	3.39	5.00	0.00	0.18	0.43	0.9982	0.36	0.9969	0.30	0.9949
AS306	50	5.50	5.00	0.00	0.29	0.84	0.9951	0.67	0.9961	0.52	0.9953
AS307	50	3.27	5.00	0.00	0.29	0.75	0.9951	0.55	0.9953	0.39	0.9920

Table 4.6: Results of fitting the release of Icaridin for proposed models at different compositions

	(°C)	(mm)		wt-%		Hill		Weibull		Peppas	
SAMPLE	Temp.	Dimeter	Dellite 43B	silica	Icaridin	n	R^2	n	R^2	n	R^2
AS101	50	3.51	0.00	5.00	0.40	2.59	0.9948	1.89	0.9987	1.25	0.9971
AS204	50	4.84	0.00	5.00	0.30	2.29	0.9966	2.00	0.9978	1.72	0.9983
AS205	50	3.95	0.00	5.00	0.39	2.05	0.9960	1.80	0.9974	1.57	0.9985
AS206	50	3.72	5.00	5.00	0.31	2.12	0.9908	1.85	0.9933	1.59	0.9953
AS207	50	4.15	5.00	5.00	0.38	2.48	0.9931	2.14	0.9949	1.81	0.9959
AS209	50	3.94	5.00	0.00	0.26	2.05	0.9978	1.92	0.9983	1.79	0.9987
AS400	50	6.15	5.00	0.00	0.19	1.91	0.9989	1.72	0.9995	1.53	0.9997
AS401	50	5.82	5.00	0.00	0.27	1.77	0.9985	1.70	0.9983	1.49	0.9980
AS300	50	5.76	5.00	0.00	0.20	1.18	0.9968	1.06	0.9977	0.93	0.9983
AS301	50	3.13	5.00	0.00	0.20	1.30	0.9952	1.03	0.9944	0.79	0.9907
AS302	50	5.00	5.00	0.00	0.30	1.49	0.9985	1.36	0.9978	1.24	0.9969
AS303	50	2.89	5.00	0.00	0.30	1.31	0.9989	1.16	0.9993	1.02	0.9993

In case of release of Icaridin from EVA polymer strands, the release rate is remarkably constant, without exhibition of any significant bust effect. Some Icaridin had diffusional exponent close to unit corresponding to a first-order release behaviour. In all samples studied, the release of DEET samples occurred faster compared to Icaridin ones. Figure 4.21 shows examples of the fit of the models of repellent release as a function of time.
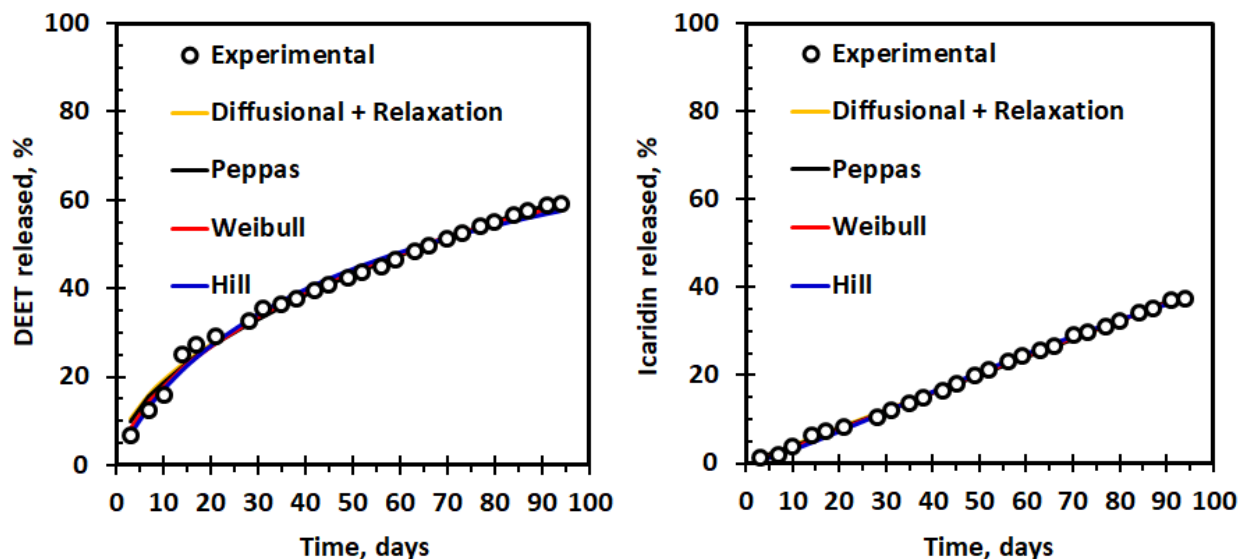
Figure 4.21: Repellent release data from EVA strands fitted with: Hill model; Weibull model; Coupling Diffusion and relaxation and Peppas model.

As can be seen from the results presented in Table 4.5 and 4.6, the diffusional exponents are all lager than 0.45 for Icaridin samples, indicating non-Fickian behaviour where polymer relaxation is an important factor in the repellent release. For DEET samples, the values ranged from 0.3 to 0.95, indicating a Fickian behaviour for some samples and for others a coupling of Fickian diffusion and a relaxation mechanism. Previous studies reported values for the Weibull shape parameter (n): internal diffusion mechanism for 0.6 to 0.7; between $0.9 – 1.0$ indicating an external resistance to mass transfer while values higher than 1.0 correspond to the relaxation-controlled mechanism (Cunha *et al.*, 1998a).

Icaridin samples used for studying the influence of organoclay (see Table 4.7) had values of diffusional exponent (***n***) around 1.0, showing a highly non-Fickian mechanism. This indicates that Case II transport was the rate-limiting step of the release of the repellent during dynamic swelling

of the polymer. In general, it can be said that the release of Icaridin approaches super Case II transport as a result of being controlled by a relaxation mechanism.

Table 4.7: Results of fitting the release of Icaridin for proposed models at different compositions of organoclay

	(°C)	(mm)		wt-%		Weibull		Peppas	
SAMPLE	Temp.	Dimeter	Dellite 43B	silica	Icaridin	n	R^2	n	R^2
AS500	50	2.49	0.00	0.00	0.18	1.27	0.9966	1.03	0.9987
AS501	50	2.99	1.00	0.00	0.22	1.14	0.9988	0.93	0.9995
AS502	50	3.88	2.50	0.00	0.22	0.98	0.9984	0.91	0.9984
AS503	50	4.16	5.00	0.00	0.20	1.05	0.9987	0.97	0.9986
AS504	50	2.86	5.00	0.00	0.30	1.11	0.9992	0.99	0.9994

4.5 Repellence testing

The initial foot-in-cage experiments compared untreated feet with feet covered with neat EVA or LLDPE polymer strands. It was observed that the mosquitoes preferred probing the foot covered by repellent-free strands rather than the fully exposed foot. The degree of protection, averaged over both the neat LLDPE and EVA strands, was estimated at -19 ±8%. This means that the mosquitoes preferred the foot covered by neat, repellent-free strands over the bare foot. The reasons for this behaviour are not currently understood. Therefore, it was decided to use a bare foot as control rather than a foot covered with a repellent-free strand.

EVA with a low content of VA degrades through exposure to UV light, in the presence of air or at elevated temperatures > 200°C. The initial step of degradation involves the loss of acetic acid (Allen *et al.*, 2000, Hull *et al.*, 2003, Patel *et al.*, 2013). It is known that acetic acid can act as a mosquito attractant (Allan *et al.*, 2006). EVA releases acetic acid in small quantities when

processed at elevated temperatures. This can explain the observed behaviour of attracting mosquitoes. On the other hand, processing or degradation of LLDPE does not release acetic acid and the reason for the observed attraction, therefore, remains a mystery. However, the observation that the neat strands acted as attractants informed the decision to conduct all the foot-in-cage tests comparing a covered foot to a bare foot rather than a foot covered by an inert strand.

The results presented in Figure 4.22 showed that EVA strands had a good performance regardless of the repellent used. On the other hand, LLDPE strands suggest that the best repellency performance was obtained with Icaridin, which initially contained 30 wt-%. The repellents were released from LLDPE polymer strands at a two to three times slower rate than from the EVA. Nevertheless, they still offer the same repellence efficacy. In both cases, the repellence efficacy was maintained for the full test period of 12 weeks.
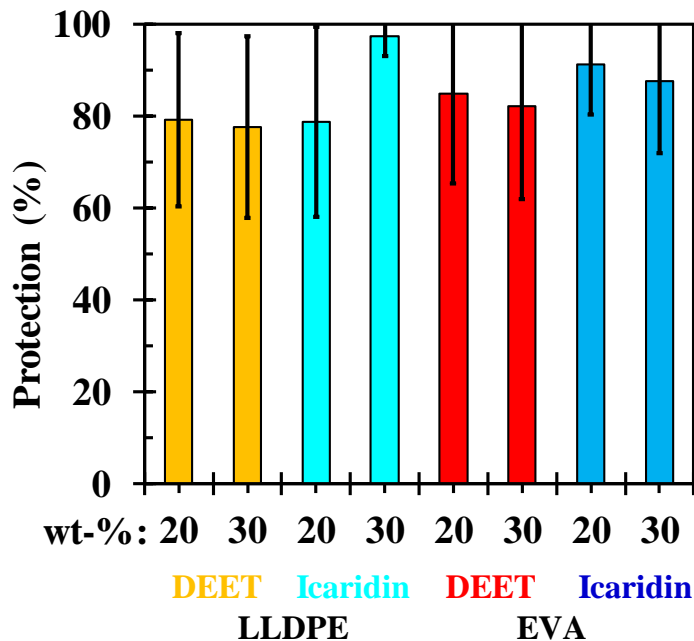
Figure 4.22: Bar plot of results of foot-in-cage repellent tests for polymer strands containing either DEET or Icaridin as repellents. All the compositions utilised Dellite 43B clay as the thickening agent. The strands were aged at 50°C in a convection oven and the bioassay tests were done every two weeks for up to 12 weeks.

4.5.1 Statistical analysis

The data of the foot-in-cage tests and statistical analysis of the results are presented in the supplementary material (see Appendix IX). First, an ANOVA was performed in order to detect significant factors that might have an influence on the protection measurements obtained for the repellents. Following this, a non-parametric ANOVA was performed using the Kruskal-Wallis test, which makes no assumptions of the underlying data structure. In all these tests, the null hypothesis was that no effects were observed. The important conclusions of the statistical analysis were that, at the 95% level of confidence, neither polymer, repellent type, repellent loading level,

test person, treated foot, nor ageing time had a significant effect on the level of protection provided. Although no significant effects could be detected between the different treatments, they all differed significantly from the effects of untreated feet, which indicated that being treated differed significantly from not being treated, i.e. there were significantly fewer mosquito probings. The implication is that all the strands provided a similar level of protection against mosquito bites for up to 12 weeks. The observation that oven-ageing time did not have a statistically significant effect on the degree of protection was expected since the measured mass loss rate of the strands was approximately constant over time. This implies that all the repellence tests conducted over the full oven-ageing time for a given strand represent repeat measurements of the protection performance.

4.6 Modelling phase behaviour of the LLDPE/repellent systems

4.6.1 Differential scanning calorimetry

Figure 4.23 shows a representative DSC cooling curve for Eicosane - DEET mixtures. The DSC curves for all alkanes suggest that liquid-liquid phase separation occurred before alkane crystallisation commenced. In addition, the position of the crystallisation peak shifted as the repellent content was increased.
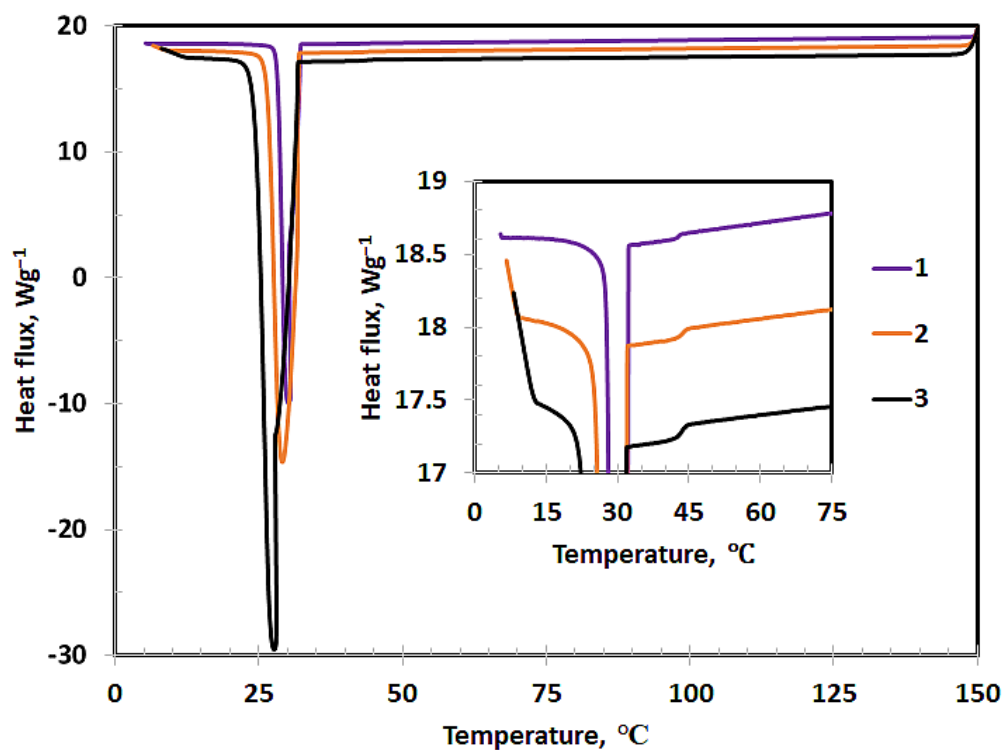
Figure 4.23: Representative DSC crystallisation curves for Eicosane-DEET mixtures obtained at different scan rates (1, 2 and 3°C min^{-1})

4.6.2 Hot stage optical microscopy

The stages of phase change observed for a binary mixture with optical microscopy (OM) are shown in Figure 4.24. In order to determine the cloud point for each composition, hot stage OM was used to obtain optical micrographs of eicosane/repellent mixture. The samples were heated to a temperature well above the melting temperature of eicosane, where the two components were fully miscible. Subsequently, samples were cooled at a constant rate of 1°C min^{-1}. At the cloud point, a sudden appearance of numerous spots was observed and the liquid became cloudy and opaque. Finally, crystallisation occurred in the mixture upon further cooling. At 25°C, it was possible to

see (spots) the repellent trapped by the alkanes. However, qualitative differences regarding the crystal structure were not detected for all sample compositions.

Homogeneous solution	L-L phase separation	S-L phase separation	Crystal formation with different morphology	Crystal trapping liquid-repellent
(150 ºC)	(53 ºC)	(34 ºC)		(25 ºC)
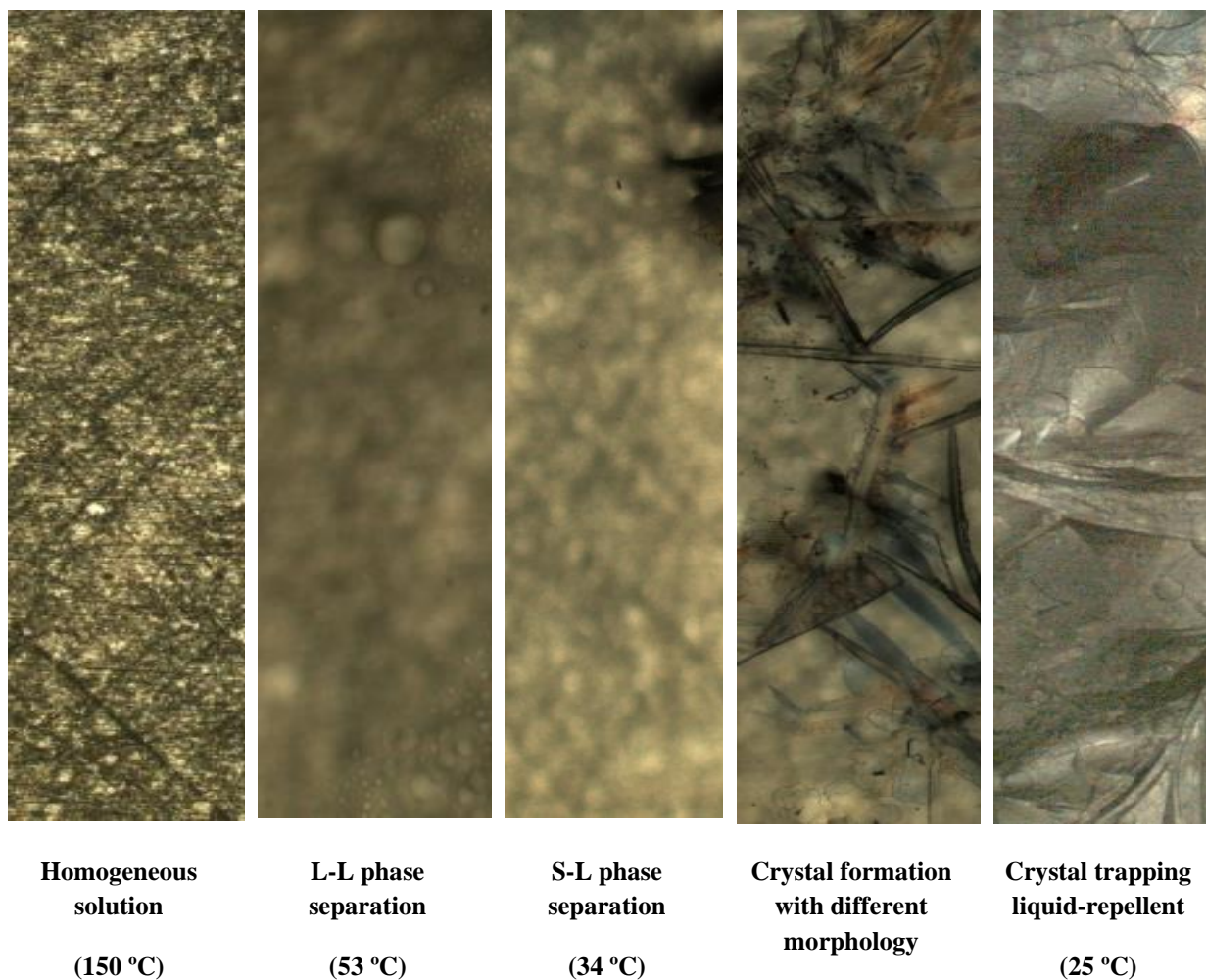
Figure 4.24: Optical micrographs of the phase changes in a binary system containing 30 wt-% Eicosane and 70 wt-% Icaridin. In the leftmost picture, the reflexive metal surface at the bottom of the hot cell can be seen.

4.6.3 Phase diagram

The cloud point was associated with the phase boundaries of the phase diagram. Together with the results from DSC, these data were used to model the repellent/alkane systems. The alkanes represented low molecular mass polymer model compounds.

The Flory-Huggins theory is one of the simplest theories describing the thermodynamics of polymer solutions. It is a lattice model in which it is assumed that each solvent molecule and polymer segment occupies exactly one lattice site (Flory, 1941, Huggins, 1941). As described in Chapter Two, the Flory-Huggins model accounts for the effect of the great dissimilarity in the size of the polymer and solvent molecules on the entropy of mixing:

$$\Delta G_{mix} = RT[n_1 ln\phi_1 + n_2 \ln \phi_2 + n_1\phi_2\chi] \tag{2.17}$$

Upper critical solution temperature (UCST) phase behaviour is well accounted for by the Flory-Huggins theory with the interaction parameter χ exhibiting the following temperature dependence:

$$\chi = a + \frac{b}{T} \tag{2.15}$$

McGuire *et al.* (1994) presented two equations that relate the tie line compositions with the interaction parameter. They provide a simple method for extrapolating the coexistence or binodal curve (liquid-liquid phase boundary):

$$\left[\left(\phi_2^\beta\right)^2 - (\phi_2^\alpha)^2\right]\chi = \ln\left[(1 - \phi_2^\alpha)/\left(1 - \phi_2^\beta\right)\right] + (1 - 1/x)\left(\phi_2^\alpha - \phi_2^\beta\right) \tag{4.1}$$

$$x\left[\left(1 - \phi_2^\beta\right)^2 - (1 - \phi_2^\alpha)^2\right]\chi = \ln\left(\phi_2^\alpha/\phi_2^\beta\right) + (x - 1)\left(\phi_2^\alpha - \phi_2^\beta\right) \tag{4.2}$$

where ϕ_2^α is the polymer's volume fraction in the polymer-poor phase and ϕ_2^β is the polymer volume fraction in the polymer-rich phase.

The experimentally determined cloud points were assumed to be representative of the coexistence curve compositions. The interaction parameter χ corresponding to each cloud point could then be calculated by simultaneously solving Equations (4.1) and (4.2), based on the known ϕ_2^β values. This yielded interaction parameter values as a function of temperature. Thereafter, all the repellent/alkane systems were plotted *vs*. the inverse of the absolute temperature, to check whether the data conform to the linear relationship for all systems suggested by Equation (2.15). Using all the above expressions, the binodal coexistence curves were determined. They are plotted in Figures 4.25 and 4.26 as the experimental and predicted cloud points.
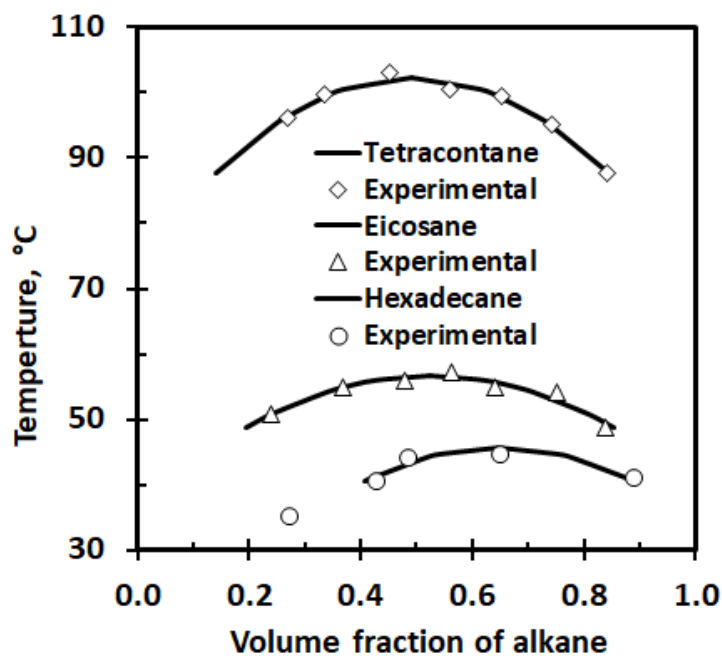
Figure 4.25: Experimental and predicted phase diagrams of alkanes in DEET
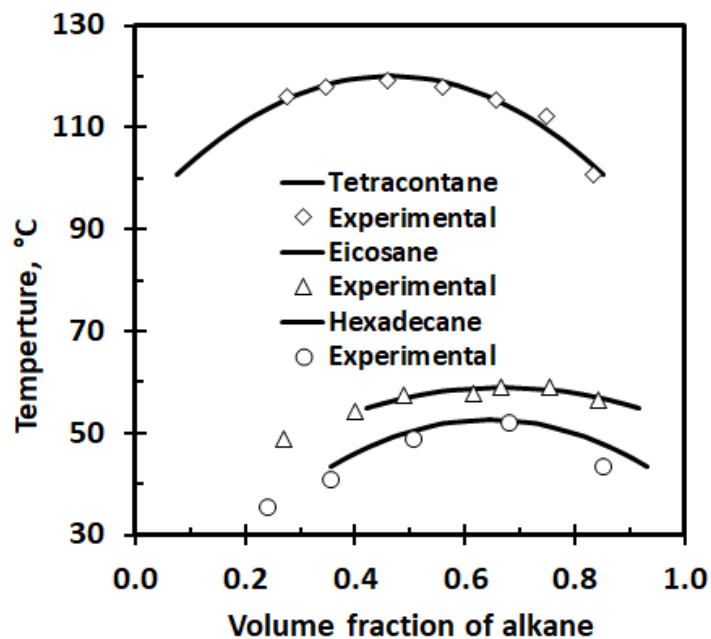
Figure 4.26: Experimental and predicted phase diagrams of alkanes in Icaridin.
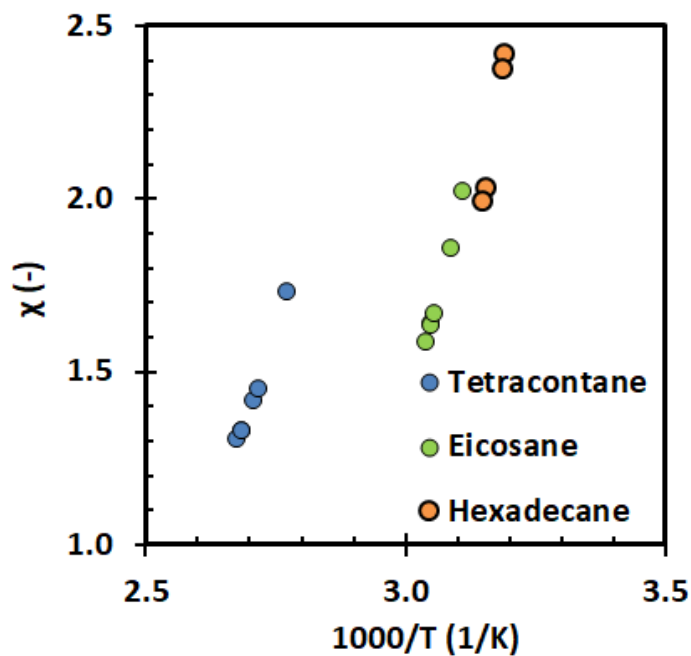
Figure 4.27: Temperature dependence of the Flory-Huggins interaction parameter for the systems alkane-DEET.
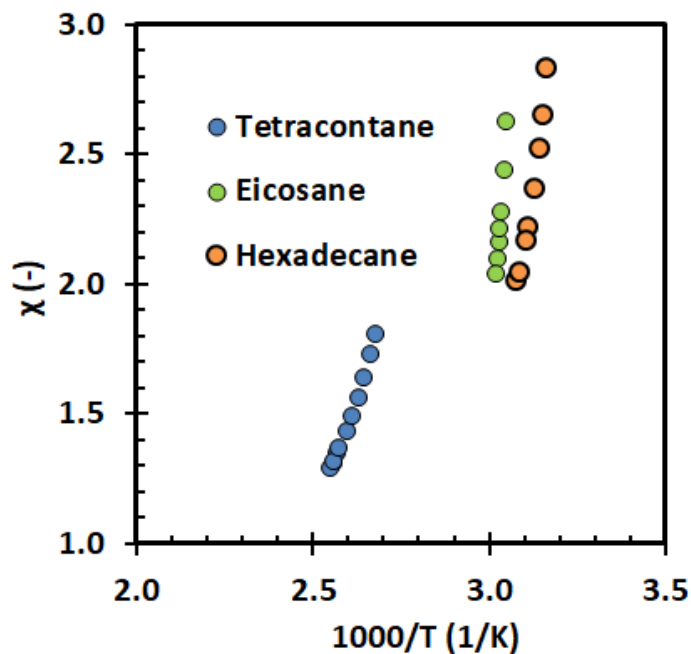
Figure 4.28: Temperature dependence of the Flory-Huggins interaction parameter for the systems alkane-Icaridin.

The results obtained for various repellent/alkane systems with different molar mass did not fit a common linear relationship for all the alkanes (Figures 4.27 and 4.28). According to Sungkapreecha *et al.* (2018), this confirms that the different demixing temperatures are not only due to a decrease in the entropy of mixing with an increase in the alkane molar mass. This means that there are also differences in energetic interactions. Unfortunately, this means that the data cannot be used to predict the phase diagram for repellent/LLDPE systems.

CHAPTER FIVE

CONCLUSIONS AND RECOMMENDATIONS

The aim of this conceptual study was to develop technology for repellent impregnated polymer products (anklets or sandals). The idea was for them to act as reservoirs for active mosquito repellents to be released efficiently and optimally to the environment at a controlled rate. This can help with outdoor protection against mosquito bites. The two polymers employed, i.e. EVA and LLDPE were found viable for incorporating mosquito repellents. The microporous polymer strands were made via a convectional plastic extrusion process. In this process, polymer and liquid repellent formed a homogeneous polymer melt at elevated temperatures (170°C for EVA and 180°C for LLDPE). Phase separation by SD was induced by directly quenching the exiting strands into ice-cold water. In addition to the kind of polymer matrix considered (stiff or flexible), it was possible to trap large quantities of repellent (up to 50 wt-%).

The FTIR spectra, recorded before and after processing as well as before and after oven-ageing, proved the thermal stability of the repellents under processing and testing conditions. They suggest that the repellents are sufficiently stable at polymer processing conditions and for long-term end-use applications. The TGA and solvent extractions confirmed that all the repellent was trapped in the polymer matrices during the processing step.

After checking the thermal stability of the repellents, there was a need to establish the compatibility of the polymer and repellent to evaluate the dimensional stability of the polymers. For this, the swelling and shrinkage of the polymer matrix were estimated. EVA swelled (close

to 5%) more than LLDPE and consequently, it also shrunk significantly more when the repellent was released. Therefore, it was concluded that EVA had poorer dimensional stability compared to LLDPE. However, EVA can still be considered for end-use application because of its high flexibility derived from its rubbery nature.

SEM confirmed the porous co-continuous repellent-polymer microstructure. It was possible to successfully prepare strands containing different repellent compositions (20, 30, 40 and 50 wt-%) via TIPS. The scaffold morphology of the strands was affected by the type and concentration of the repellent, nature of the nanofiller (fumed silica or clay) and polymer matrix (EVA or LLDPE).

The release of the active ingredient in the polymer matrix was followed as a function of oven-ageing temperature (50°C and 30°C) and time (approximately six months). Most of the Icaridin-containing strands retained more than 50% of the repellent trapped in the polymer matrix even after six months of ageing. This was attributed to the microporous structure and outer dense skin layer that provided the necessary diffusion barrier that limited the release of the repellent at effective and constant levels over a considerable period. As a result of different scaffolds, the release studies showed different patterns changing the type and concentration of the repellent, nature of polymer matrix and slight differences caused by the nature of nanofiller.

The kinetics of the release of the repellent from the microporous polymer swellable matrix strands was mathematically modelled using semi-empirical models (Hill model, Weibull model and Peppas model). These models were found to be valuable in providing insights into the

mechanism that the repellent was being released from EVA swellable matrix strand. It was possible to differentiate between diffusion and relaxation mechanisms.

The performance of the repellent-based strands was evaluated using foot-in-cage repellence testing. Here, only strands of EVA and LLDPE containing 20 and 30 wt-% of either DEET or Icaridin were considered. It was found that the repellence efficacy of polymer strands containing DEET or Icaridin with 30 wt-% could be maintained for more than 12 weeks. Those polymer strands gave effective protection against *An. arabiensis* mosquitoes even after ageing the strands for up to 12 weeks in a convection oven at 50°C.

Finally, a partially successful attempt was made to establish the phase diagrams of the LLDPE/repellent system. This attempt was based on alkane/repellent systems data acquired using DSC and hot stage microscopy.

Future developments can use this approach to make sandals or anklets. This conceptual study confirmed the viability and possibility of developing long-life mosquito repellent products that may assist in preventing infective outdoor mosquito bites, thereby decreasing malaria infections rates in malaria-endemic areas.

More experimental work is required in order to understand the mechanisms responsible for the formation of the outer skin, microporous scaffold and the release of the active ingredient depending on the design of the product. Ultimately, extensive field trials will be required in order to determine whether the wearing of such personal protection can, in fact, reduce outdoor malaria transmission.

REFERENCES

AKHTAR, M. U. & FOCKE, W. W. 2015. Trapping citronellal in a microporous polyethylene matrix. *Thermochimica Acta,* 613**,** 61-65.

AKOVALI, G. 2005. *Polymers in Construction*, Rapra Technology.

AKOVALI, G. 2012. *Advances in Polymer Coated Textiles*, Smithers Information Limited.

ALLAN, S. A., BERNIER, U. R. & KLINE, D. L. 2006. Attraction of mosquitoes to volatiles associated with blood. *Journal of Vector Ecology,* 31**,** 71-79.

ALLEN, N. S., EDGE, M., RODRIGUEZ, M., LIAUW, C. M. & FONTAN, E. 2000. Aspects of the thermal oxidation of ethylene vinyl acetate copolymer. *Polymer Degradation and Stability,* 68**,** 363-371.

ALMEIDA, A., POSSEMIERS, S., BOONE, M. N., DE BEER, T., QUINTEN, T., VAN HOOREBEKE, L., REMON, J. P. & VERVAET, C. 2011. Ethylene vinyl acetate as matrix for oral sustained release dosage forms produced via hot-melt extrusion. *European Journal of Pharmaceutics and Biopharmaceutics,* 77**,** 297-305.

ALPHEY, L., BENEDICT, M., BELLINI, R., CLARK, G. G., DAME, D. A., SERVICE, M. W. & DOBSON, S. L. 2010. Sterile-insect methods for control of mosquito-borne diseases: an analysis. *Vector-Borne and Zoonotic Diseases,* 10**,** 295-311.

ATKINSON, M. P., SU, Z., ALPHEY, N., ALPHEY, L. S., COLEMAN, P. G. & WEIN, L. M. 2007. Analyzing the control of mosquito-borne diseases by a dominant lethal genetic system. *Proceedings of the National Academy of Sciences,* 104**,** 9540-9545.

BALCERZAK, J. & MUCHA, M. 2010. Analysis of model drug release kinetics from complex matrices of polylactide-chitosan. *Progress on Chemistry and Application of Chitin and its Derivatives,* 15**,** 117-126.

BARNARD, D. R. & XUE, R.-D. 2004. Laboratory evaluation of mosquito repellents against *Aedes albopictus*, *Culex nigripalpu*s, and *Ochlerotatus triseriatus* (Diptera: Culicidae). *Journal of Medical Entomology,* 41**,** 726-730.

BATTEN, S. R., CHAMPNESS, N. R., CHEN, X.-M., GARCIA-MARTINEZ, J., KITAGAWA, S., ÖHRSTRÖM, L., O'KEEFFE, M., SUH, M. P. & REEDIJK, J. 2012. Coordination polymers, metal–organic frameworks and the need for terminology guidelines. *CrystEngComm,* 14**,** 3001-3004.

BELMARES, M., BLANCO, M., GODDARD, W. A., ROSS, R. B., CALDWELL, G., CHOU, S. H., PHAM, J., OLOFSON, P. M. & THOMAS, C. 2004. Hildebrand and Hansen solubility parameters from molecular dynamics with applications to electronic nose polymer sensors. *Journal of Computational Chemistry,* 25**,** 1814-1826.

BELTRÁN-SILVA, S. L., CHACÓN-HERNÁNDEZ, S. S., MORENO-PALACIOS, E. & PEREYRA-MOLINA, J. Á. 2018. Clinical and differential diagnosis: Dengue, Chikungunya and Zika. *Revista Médica del Hospital General de México,* 81**,** 146-153.

BENELLI, G. 2016. Plant-mediated synthesis of nanoparticles: A newer and safer tool against mosquito-borne diseases? *Asian Pacific Journal of Tropical Biomedicine,* 6**,** 353-354.

BENELLI, G. & MEHLHORN, H. 2016. Declining malaria, rising of dengue and Zika virus: insights for mosquito vector control. *Parasitology Research,* 115**,** 1747-54.

BENELLI, G., MURUGAN, K., PANNEERSELVAM, C., MADHIYAZHAGAN, P., CONTI, B. & NICOLETTI, M. 2015. Old ingredients for a new recipe? Neem cake, a low-cost botanical by-product in the fight against mosquito-borne diseases. *Parasitology Research,* 114**,** 391-7.

BITTRICH, E., COMETA, S., DE GIGLIO, E., DI MUNDO, R., DITARANTO, N., EICHHORN, K. J., KELLER, B., LEDNICKÝ, F. & MANGOLINI, F. 2014. *Polymer Surface Characterization*, De Gruyter.

BOCKARIE, M. J. & REBOLLO, M. P. 2016. Reducing the population requiring interventions against lymphatic filariasis in Africa. *The Lancet Global Health,* 4**,** e154-e155.

BRAACK, L., HUNT, R., KOEKEMOER, L. L., GERICKE, A., MUNHENGA, G., HADDOW, A. D., BECKER, P., OKIA, M., KIMERA, I. & COETZEE, M. 2015. Biting behaviour of African malaria vectors: 1. where do the main vector species bite on the human body. *Parasites & Vectors,* 8**,** 76.

BRANNON-PEPPAS, L. & PEPPAS, N. A. 1989. Solute and penetrant diffusion in swellable polymers. IX. The mechanisms of drug release from pH-sensitive swelling-controlled systems. *Journal of Controlled Release,* 8**,** 267-274.

BRAZEL, C. S. & PEPPAS, N. A. 2000. Modeling of drug release from swellable polymers. *European Journal of Pharmaceutics and Biopharmaceutics,* 49**,** 47-58.

BURKI, T. 2016. Yellow fever in Africa: a disaster waiting to happen. *The Lancet Infectious Diseases,* 16**,** 896-897.

CAHN, J. W. 1961. On spinodal decomposition. *Acta Metallurgica,* 9**,** 795-801.

CAHN, J. W. & HILLIARD, J. E. 1971. Spinodal decomposition: a reprise. *Acta Metallurgica,* 19**,** 151-161.

CALLISTER, W. D. & RETHWISCH, D. G. 2013. *Materials Science and Engineering: An Introduction*, John Wiley and Sons, Incorporated.

CARTER, G. F. & PAUL, D. E. 1991. *Materials Science and Engineering*, ASM International.

CASTRO, A. J. 1981. *Methods for making microporous products*.

CHALMERS, J. M. & MEIER, R. J. 2008. *Molecular Characterization and Analysis of Polymers*, Elsevier Science.

CHANDAVASU, C., XANTHOS, M., SIRKAR, K. K. & GOGOS, C. G. 2003. Fabrication of microporous polymeric membranes by melt processing of immiscible blends. *Journal of Membrane Science,* 211**,** 167-175.

CHARARA, Z. N., WILLIAMS, J. W., SCHMIDT, R. H. & MARSHALL, M. R. 1992. Orange flavor absorption into various polymeric packaging materials. *Journal of Food Science,* 57**,** 963-968.

CHEN, G., LIN, Y. & WANG, X. 2007. Formation of microporous membrane of isotactic polypropylene in dibutyl phthalate-soybean oil via thermally induced phase separation. *Journal of Applied Polymer Science,* 105**,** 2000-2007.

CHEN, Y., ZOU, H., LIANG, M. & CAO, Y. 2014. Melting and crystallization behavior of partially miscible high density polyethylene/ethylene vinyl acetate copolymer (HDPE/EVA) blends. *Thermochimica Acta,* 586**,** 1-8.

CHOWDHURY, N., GHOSH, A. & CHANDRA, G. 2008. Mosquito larvicidal activities of *Solanum villosum* berry extract against the dengue vector *Stegomyia aegypti*. *BMC Complementary and Alternative Medicine,* 8**,** 10.

CISAK, E., WÓJCIK-FATLA, A., ZAJAC, V. & DUTKIEWICZ, J. 2012. Repellents and acaricides as personal protection measures in the prevention of tick-borne diseases. *Annals of Agricultural and Environmental Medicine,* 19**,** 625-630.

COFFEY, L. L. & REISEN, W. K. 2016. West Nile Virus fitness costs in different mosquito species. *Trends in Microbiology,* 24**,** 429-430.

COWMAN, A. F., HEALER, J., MARAPANA, D. & MARSH, K. 2016. Malaria: biology and disease. *Cell,* 167**,** 610-624.

CUNHA, L. M., OLIVEIRA, F. A. R., ILINCANU, L. A. & DRUMOND, M. C. Application of the probabilistic Weibull model to rehydration kinetics: relationship between the model parameters and the underlying physical mechanisms. Process Optimization and Minimal Processing of Foods, 1998a. 9-13.

CUNHA, L. M., OLIVEIRA, F. A. R. & OLIVEIRA, J. C. 1998b. Optimal experimental design for estimating the kinetic parameters of processes described by the Weibull probability distribution function. *Journal of Food Engineering,* 37**,** 175-191.

DASH, S., MURTHY, P. N., NATH, L. & CHOWDHURY, P. 2010. Kinetic modeling on drug release from controlled drug delivery systems. *Acta Pol Pharm,* 67**,** 217-223.

DAVID, J. P., ISMAIL, H. M., CHANDOR-PROUST, A. & PAINE, M. J. 2013. Role of cytochrome P450s in insecticide resistance: impact on the control of mosquito-borne diseases and use of insecticides on earth. *Philosophical Transactions of the Royal Society B: Biological Sciences,* 368**,** 20120429.

DAVIDSON, G. W. R. & PEPPAS, N. A. 1986a. Solute and penetrant diffusion in swellable polymers: V. Relaxation-controlled transport in P(HEMA-co-MMA) copolymers. *Journal of Controlled Release,* 3**,** 243-258.

DAVIDSON, G. W. R. & PEPPAS, N. A. 1986b. Solute and penetrant diffusion in swellable polymers: VI. The Deborah and swelling interface numbers as indicators of the order of biomolecular release. *Journal of Controlled Release,* 3**,** 259-271.

DE CASTRO, M. D. L., VALCARCEL, M. & TENA, M. T. 1994. *Analytical Supercritical Fluid Extraction*, Springer Berlin Heidelberg.

DEBBOUN, M. & STRICKMAN, D. 2013. Insect repellents and associated personal protection for a reduction in human disease. *Medical and Veterinary Entomology,* 27**,** 1-9.

DEKKER, T., TAKKEN, W., KNOLS, B. G., BOUMAN, E., VAN DE LAAK, S., DE BEVER, A. & HUISMAN, P. W. 1998. Selection of biting sites on a human host by *Anopheles gambiae s.s.*, *An. arabiensis* and *An. quadriannulatus*. *Entomologia Experimentalis et Applicata,* 87**,** 295-300.

ELIDRISSI, A., EL BARKANY, S., AMHAMDI, H., MAAROUFI, A. & HAMMOUTI, B. 2012. New approach to predict the solubility of polymers. Application: cellulose acetate

at various DS, prepared from alfa "*Stipa–tenassicima*" of Eastern Morocco. *Journal of Materials and Environmental Science,* 3**,** 270-285.

FAKIROV, S. 2017. *Fundamentals of Polymer Science for Engineers*, Wiley.

FAUCI, A. S. & MORENS, D. M. 2016. Zika virus in the Americas—yet another arbovirus threat. *New England Journal of Medicine,* 374**,** 601-604.

FAVIER, C., DEGALLIER, N., ROSA-FREITAS, M. G., BOULANGER, J. P., COSTA LIMA, J. R., LUITGARDS-MOURA, J. F., MENKES, C. E., MONDET, B., OLIVEIRA, C., WEIMANN, E. T. & TSOURIS, P. 2006. Early determination of the reproductive number for vector-borne diseases: the case of dengue in Brazil. *Tropical Medicine and International Health,* 11**,** 332-40.

FAVVAS, E. & MITROPOULOS, A. C. 2008. What is spinodal decomposition. *Journal of Engineering Science and Technology Review,* 1**,** 25-27.

FEDORS, R. F. 1974. A method for estimating both the solubility parameters and molar volumes of liquids. *Polymer Engineering and Science,* 14**,** 147-154.

FERNÁNDEZ, A., COLLADO, J., CUNHA, L. M., OCIO, M. J. & MARTíNEZ, A. 2002. Empirical model building based on Weibull distribution to describe the joint effect of pH and temperature on the thermal resistance of *Bacillus cereus* in vegetable substrate. *International Journal of Food Microbiology,* 77**,** 147-153.

FLORY, P. J. 1941. Thermodynamics of high polymer solutions. *The Journal of Chemical Physics,* 9**,** 660-660.

FRADIN, M. S. & DAY, J. F. 2002. Comparative efficacy of insect repellents against mosquito bites. *New England Journal of Medicine,* 347**,** 13-18.

FU, Y. & KAO, W. J. 2009. Drug release kinetics and transport mechanisms from semi-interpenetrating networks of gelatin and poly(ethylene glycol) diacrylate. *Pharmaceutical Research,* 26**,** 2115-2124.

FU, Y. & KAO, W. J. 2010. Drug release kinetics and transport mechanisms of non-degradable and degradable polymeric delivery systems. *Expert Opinion on Drug Delivery,* 7**,** 429-44.

GABRIELI, P., SMIDLER, A. & CATTERUCCIA, F. 2014. Engineering the control of mosquito-borne infectious diseases. *Genome Biology,* 15**,** 535.

GAIKWAD, E., KHABADE, S., SUTAR, T., BHAT, M. & PAYGHAN, S. A. 2017. Three-dimensional Hansen solubility parameters as predictors of miscibility in cocrystal formation. *Asian Journal of Pharmaceutics,* 11**,** 302-318.

GÅRDEBJER, S., ANDERSSON, M., ENGSTRÖM, J., RESTORP, P., PERSSON, M. & LARSSON, A. 2016. Using Hansen solubility parameters to predict the dispersion of nano-particles in polymeric films. *Polymer Chemistry,* 7**,** 1756-1764.

GENINA, N., HOLLANDER, J., JUKARAINEN, H., MAKILA, E., SALONEN, J. & SANDLER, N. 2016. Ethylene vinyl acetate (EVA) as a new drug carrier for 3D printed medical drug delivery devices. *European Journal of Pharmaceutical Sciences,* 90**,** 53-63.

GHOSH, A. 2015. *Technology of Polymer Packaging*, Hanser.

GILES, H. F., WAGNER, J. R. & MOUNT, E. M. 2013. *Extrusion: The Definitive Processing Guide and Handbook*, Elsevier Science.

GIOVINO, M., PRIBYL, J., BENICEWICZ, B., KUMAR, S. & SCHADLER, L. 2017. Linear rheology of polymer nanocomposites with polymer-grafted nanoparticles. *Polymer,* 131**,** 104-110.

GRUBAUGH, N. D. & EBEL, G. D. 2016. Dynamics of West Nile virus evolution in mosquito vectors. *Curr Opin Virol,* 21**,** 132-138.

GU, M., ZHANG, J., WANG, X., TAO, H. & GE, L. 2006. Formation of poly(vinylidene fluoride) (PVDF) membranes via thermally induced phase separation. *Desalination,* 192**,** 160-167.

GUBLER, D. J. 1997. Dengue and dengue hemorrhagic fever. *Seminars in Pediatric Infectious Diseases,* 8**,** 3-9.

HANSEN, C. M. 2002. *Hansen Solubility Parameters: A User's Handbook*, CRC Press.

HANSEN, C. M. & SMITH, A. L. 2004. Using Hansen solubility parameters to correlate solubility of C_{60} fullerene in organic solvents and in polymers. *Carbon,* 42**,** 1591-1597.

HARIHARAN, D., PEPPAS, N. A., BETTINI, R. & COLOMBO, P. 1994. Mathematical analysis of drug delivery from swellable systems with partial physical restrictions or impermeable coatings. *International Journal of Pharmaceutics,* 112**,** 47-54.

HARLAND, R. S. & PEPPAS, N. A. 1987. Solute diffusion in swollen membranes. *Polymer Bulletin,* 18**,** 553-556.

HARLAND, R. S. & PEPPAS, N. A. 1989. Solute diffusion in swollen membranes VII. Diffusion in semicrystalline networks. *Colloid and Polymer Science,* 267**,** 218-225.

HELLMAN, D. 2004. A novel process for membrane fabrication: thermally assisted evaporative phase separation (TAEPS). *Journal of Membrane Science,* 230**,** 99-109.

HEMINGWAY, J., BEATY, B. J., ROWLAND, M., SCOTT, T. W. & SHARP, B. L. 2006. The innovative vector control consortium: improved control of mosquito-borne diseases. *Trends in Parasitology,* 22**,** 308-12.

HONG, Y., GAO, C., SHI, Y. & SHEN, J. 2005. Preparation of porous polylactide microspheres by emulsion-solvent evaporation based on solution induced phase separation. *Polymers for Advanced Technologies,* 16**,** 622-627.

HOPFENBERG, H. B. & HSU, K. C. 1978. Swelling-controlled, constant rate delivery systems. *Polymer Engineering and Science,* 18**,** 1186-1191.

HOSSIN, B., RIZI, K. & MURDAN, S. 2016. Application of Hansen solubility parameters to predict drug-nail interactions, which can assist the design of nail medicines. *European Journal of Pharmaceutics and Biopharmaceutics,* 102**,** 32-40.

HRNJAK-MURGIĆ, Z., REŠČEK, A., KREHULA, L. K., SIROČIĆ, A. P. & KATANČIĆ, Z. 2015. *Nanoparticles in Active Polymer Food Packaging*, Smithers Information Limited.

HUANG, C. & CHENG, Q. 2017. Learning from nacre: constructing polymer nanocomposites. *Composites Science and Technology,* 150**,** 141-166.

HUBÁLEK, Z. & HALOUZKA, J. 1999. West Nile fever-a reemerging mosquito-borne viral disease in Europe. *Emerging Infectious Diseases,* 5**,** 643-650.

HUGGINS, M. L. 1941. Solutions of long chain compounds. *The Journal of Chemical Physics,* 9**,** 440-440.

HULL, T. R., PRICE, D., LIU, Y., WILLS, C. L. & BRADY, J. 2003. An investigation into the decomposition and burning behaviour of ethylene-vinyl acetate copolymer nanocomposite materials. *Polymer Degradation and Stability,* 82**,** 365-371.

HUSTON, E., CAHN, J. W. & HILLIARD, J. 1966. Spinodal decomposition during continuous cooling. *Acta Metallurgica,* 14**,** 1053-1062.

HUTH, M., CHEN, C.-W. & WAGNER, V. 2018. Measurement of Hansen solubility parameters for organophilic fluoromica and evaluation of potential solvents for exfoliation. *Applied Clay Science,* 155**,** 120-125.

ISIK, B. & KIS, M. 2004. Preparation and determination of swelling behavior of poly(acrylamide-co-acrylic acid) hydrogels in water. *Journal of Applied Polymer Science,* 94**,** 1526-1531.

ITURBE-ORMAETXE, I., WALKER, T. & SL, O. N. 2011. *Wolbachia* and the biological control of mosquito-borne disease. *EMBO Reports,* 12**,** 508-18.

IZDEBSKA, J. & THOMAS, S. 2015. *Printing on Polymers: Fundamentals and Applications*, Elsevier Science.

JONES, R. G., WILKS, E. S., METANOMSKI, W. V., KAHOVEC, J., HESS, M., STEPTO, R. & KITAYAMA, T. 2009. *Compendium of Polymer Terminology and Nomenclature: IUPAC Recommendations 2008*, Royal Society of Chemistry.

JUNG, J. T., KIM, J. F., WANG, H. H., DI NICOLO, E., DRIOLI, E. & LEE, Y. M. 2016. Understanding the non-solvent induced phase separation (NIPS) effect during the fabrication of microporous PVDF membranes via thermally induced phase separation (TIPS). *Journal of Membrane Science,* 514**,** 250-263.

KAPLAN, H. & GÜNER, A. 2000. Characterization and determination of swelling and diffusion characteristics of poly(n-vinyl-2-pyrrolidone) hydrogels in water. *Journal of Applied Polymer Science,* 78**,** 994-1000.

KIM, J. F., KIM, J. H., LEE, Y. M. & DRIOLI, E. 2016. Thermally induced phase separation and electrospinning methods for emerging membrane applications: a review. *AIChE Journal,* 62**,** 461-490.

KIM, M., KIM, G., KIM, J., LEE, D., LEE, S., KWON, J. & HAN, H. 2017. New continuous process developed for synthesizing sponge-type polyimide membrane and its pore size control method via non-solvent induced phase separation (NIPS). *Microporous and Mesoporous Materials,* 242**,** 166-172.

KIMANI, J., OSANJO, G., SANG, R., OCHANDA, J. & MULAA, F. 2016. Performance of methylcellulose and Avicel overlays in plaque and focus assays of Chikungunya virus. *African Journal of Pharmacology and Therapeutics,* 5**,** 54-58.

KINDHAUSER, M. K., ALLEN, T., FRANK, V., SANTHANA, R. S. & DYE, C. 2016. Zika: the origin and spread of a mosquito-borne virus. *Bulletin of the World Health Organization,* 94**,** 675-686C.

KITAK, T., DUMICIC, A., PLANINSEK, O., SIBANC, R. & SRCIC, S. 2015. Determination of solubility sarameters of Ibuprofen and Ibuprofen Lysinate. *Molecules,* 20**,** 21549-68.

KLIER, J. & PEPPAS, N. A. 1988. Solute and penetrant diffusion in swellable polymers: VIII. Influence of the swelling interface number on solute concentration profiles and release. *Journal of Controlled Release,* 7**,** 61-68.

KNOLS, B. & DE JONG, R. 1996. Limburger cheese as an attractant for the malaria mosquito *Anopheles gambiae s.s. Parasitology Today,* 12**,** 159-161.

KNOLS, B. G. 1996. On human odour, malaria mosquitoes, and limburger cheese. *The Lancet,* 348**,** 1322.

KNOLS, B. G., VAN LOON, J. J., CORK, A., ROBINSON, R. D., ADAM, W., MEIJERINK, J., DE JONG, R. & TAKKEN, W. 1997. Behavioural and electrophysiological responses of the female malaria mosquito *Anopheles gambiae* (Diptera: Culicidae) to Limburger cheese volatiles. *Bulletin of Entomological Research,* 87**,** 151-159.

KORSMEYER, R. W., LUSTIG, S. R. & PEPPAS, N. A. 1986a. Solute and penetrant diffusion in swellable polymers. I. Mathematical modeling. *Journal of Polymer Science Part B: Polymer Physics,* 24**,** 395-408.

KORSMEYER, R. W., VON MEERWALL, E. & PEPPAS, N. A. 1986b. Solute and penetrant diffusion in swellable polymers. II. Verification of theoretical models. *Journal of Polymer Science Part B: Polymer Physics,* 24**,** 409-434.

KOUADIO, I. K., ALJUNID, S., KAMIGAKI, T., HAMMAD, K. & OSHITANI, H. 2014. Infectious diseases following natural disasters: prevention and control measures. *Expert Review of Anti-infective Therapy,* 10**,** 95-104.

KRAEMER, M. U. G., FARIA, N. R., REINER, R. C., GOLDING, N., NIKOLAY, B., STASSE, S., JOHANSSON, M. A., SALJE, H., FAYE, O., WINT, G. R. W., NIEDRIG, M., SHEARER, F. M., HILL, S. C., THOMPSON, R. N., BISANZIO, D., TAVEIRA, N., NAX, H. H., PRADELSKI, B. S. R., NSOESIE, E. O., MURPHY, N. R., BOGOCH, I. I., KHAN, K., BROWNSTEIN, J. S., TATEM, A. J., DE OLIVEIRA, T., SMITH, D. L., SALL, A. A., PYBUS, O. G., HAY, S. I. & CAUCHEMEZ, S. 2017.

Spread of yellow fever virus outbreak in Angola and the Democratic Republic of the Congo 2015–16: a modelling study. *The Lancet Infectious Diseases,* 17**,** 330-338.

KRASUCKA, P., MERGO, P., WÓJCIK, G. & GOWOREK, J. 2018. Mechanical experiments as a tool for study of swelling-deswelling and structural properties of porous polymers. *Chemical Engineering Science,* 190**,** 21-27.

KUMAR, S., SARITA, NEHRA, M., DILBAGHI, N., TANKESHWAR, K. & KIM, K.-H. 2018. Recent advances and remaining challenges for polymeric nanocomposites in healthcare applications. *Progress in Polymer Science,* 80**,** 1-38.

KUSHWAHA, A. S., VERMA, K. C. & CARIAPPA, M. P. 2017. Filaria surveys in the Armed Forces: need for a revisit. *Medical Journal Armed Forces India,* 73**,** 332-337.

LAI, J. H., LIN, Y. L. & HSIEH, S. L. 2017. Pharmacological intervention for dengue virus infection. *Biochemical Pharmacology,* 129**,** 14-25.

LANGER, R. S. & PEPPAS, N. A. 1981. Present and future applications of biomaterials in controlled drug delivery systems. *Biomaterials,* 2**,** 201-214.

LI, D., KRANTZ, W. B., GREENBERG, A. R. & SANI, R. L. 2006. Membrane formation via thermally induced phase separation (TIPS): Model development and validation. *Journal of Membrane Science,* 279**,** 50-60.

LI, W., YUAN, Y. & CABASSO, I. 1995. Formation and microstructure of polyethylene microporous membranes through thermally induced phase separation. *Chinese Journal of Polymer Science,* 13**,** 7-19.

LI, X., WANG, Y., LU, X. & XIAO, C. 2008. Morphology changes of polyvinylidene fluoride membrane under different phase separation mechanisms. *Journal of Membrane Science,* 320**,** 477-482.

LICCIARDELLO, F., MURATORE, G., SUMA, P., RUSSO, A. & NERÍN, C. 2013. Effectiveness of a novel insect-repellent food packaging incorporating essential oils against the red flour beetle (*Tribolium castaneum*). *Innovative Food Science & Emerging Technologies,* 19**,** 173-180.

LINDVIG, T., MICHELSEN, M. L. & KONTOGEORGIS, G. M. 2002. A Flory–Huggins model based on the Hansen solubility parameters. *Fluid Phase Equilibria,* 203**,** 247-260.

LIU, K. & KIRAN, E. 1999. Kinetics of pressure-induced phase separation (PIPS) in solutions of polydimethylsiloxane in supercritical carbon dioxide: crossover from nucleation and growth to spinodal decomposition mechanism. *The Journal of Supercritical Fluids,* 16**,** 59-79.

LIU, M., LIU, S., XU, Z., WEI, Y. & YANG, H. 2016. Formation of microporous polymeric membranes via thermally induced phase separation: a review. *Frontiers of Chemical Science and Engineering,* 10**,** 57-75.

LLOYD, D. R., KIM, S. S. & KINZER, K. E. 1991. Microporous membrane formation via thermally-induced phase separation. II. Liquid—liquid phase separation. *Journal of Membrane Science,* 64**,** 1-11.

LLOYD, D. R., KINZER, K. E. & TSENG, H. 1990. Microporous membrane formation via thermally induced phase separation. I. Solid-liquid phase separation. *Journal of Membrane Science,* 52**,** 239-261.

LUSTIG, S. R. & PEPPAS, N. A. 1987. Solute and penetrant diffusion in swellable polymers. VII. A free volume-based model with mechanical relaxation. *Journal of Applied Polymer Science,* 33**,** 533-549.

MACIEL-DE-FREITAS, R., AGUIAR, R., BRUNO, R. V., GUIMARÃES, M. C., LOURENÇO-DE-OLIVEIRA, R., SORGINE, M. H., STRUCHINER, C. J., VALLE, D., O'NEILL, S. L. & MOREIRA, L. A. 2012. Why do we need alternative tools to control mosquito-borne diseases in Latin America? *Memórias do Instituto Oswaldo Cruz,* 107**,** 828-829.

MADARIAGA, M., TICONA, E. & RESURRECION, C. 2016. Chikungunya: bending over the Americas and the rest of the world. *Brazilian Journal of Infectious Diseases,* 20**,** 91-8.

MARABI, A., LIVINGS, S., JACOBSON, M. & SAGUY, I. S. 2003. Normalized Weibull distribution for modeling rehydration of food particulates. *European Food Research and Technology,* 217**,** 311-318.

MARTENS, P. & HALL, L. 2000. Malaria on the move: human population movement and malaria transmission. *Emerging Infectious Diseases,* 6**,** 103-109.

MARTÍN-ALFONSO, J. E. & FRANCO, J. M. 2014. Ethylene-vinyl acetate copolymer (EVA)/sunflower vegetable oil polymer gels: influence of vinyl acetate content. *Polymer Testing,* 37**,** 78-85.

MATEUS, M.-L., LINDINGER, C., GUMY, J.-C. & LIARDON, R. 2007. Release kinetics of volatile organic compounds from roasted and ground coffee: online measurements by PTR-MS and mathematical modeling. *Journal of Agricultural and Food Chemistry,* 55**,** 10117-10128.

MATSUYAMA, H., BERGHMANS, S. & LLOYD, D. R. 1999. Formation of anisotropic membranes via thermally induced phase separation. *Polymer,* 40**,** 2289-2301.

MATSUYAMA, H., TAKIDA, Y., MAKI, T. & TERAMOTO, M. 2002. Preparation of porous membrane by combined use of thermally induced phase separation and immersion precipitation. *Polymer,* 43**,** 5243-5248.

MATSUYAMA, H., TERAMOTO, M., KUDARI, S. & KITAMURA, Y. 2001. Effect of diluents on membrane formation via thermally induced phase separation. *Journal of Applied Polymer Science,* 82**,** 169-177.

MCCARROLL, L., PATON, M., KARUNARATNE, S., JAYASURYIA, H., KALPAGE, K. & HEMINGWAY, J. 2000. Insecticides and mosquito-borne disease. *Nature,* 407**,** 961-962.

MCGUIRE, K. S., LAXMINARAYAN, A. & LLOYD, D. R. 1994. A simple method of extrapolating the coexistence curve and predicting the melting point depression curve from cloud point data for polymer-diluent systems. *Polymer,* 35**,** 4404-4407.

MCKEEN, L. W. 2017. *Film Properties of Plastics and Elastomers*, Elsevier Science.

MEHTA, R. H., MADSEN, D. A. & KALIKA, D. S. 1995. Microporous membranes based on poly (ether ether ketone) via thermally-induced phase separation. *Journal of Membrane Science,* 107**,** 93-106.

MILLER, J. R. 2001. The control of mosquito-borne diseases in New York City. *Journal of Urban Health,* 78**,** 359-366.

MITTAL, V. 2015. *Manufacturing of Nanocomposites with Engineering Plastics*, Elsevier Science.

MOHAMMAD, M. A., ALHALAWEH, A. & VELAGA, S. P. 2011. Hansen solubility parameter as a tool to predict cocrystal formation. *International Journal of Pharmaceutics,* 407**,** 63-71.

MOLLA, E. 2016. Malaria: what are the needs for diagnosis, treatment and control. *Biology and Medicine,* 8**,** 320.

MONATH, T. P. & VASCONCELOS, P. F. 2015. Yellow fever. *Journal of Clinical Virology,* 64**,** 160-73.

MONATH, T. P., WOODALL, J. P., GUBLER, D. J., YUILL, T. M., MACKENZIE, J. S., MARTINS, R. M., REITER, P. & HEYMANN, D. L. 2016. Yellow fever vaccine supply: a possible solution. *The Lancet,* 387**,** 1599-1600.

MORENS, D. M. & FAUCI, A. S. 2016. Meeting the challenge of epidemic Chikungunya. *The Journal of Infectious Diseases,* 214**,** S434-S435.

MURALISRINIVASAN, N. S. 2014. *Introduction to Polymer Compounding: Raw Materials*, Smithers Information Limited.

MURUGAN, S. B. & SATHISHKUMAR, R. 2016. Chikungunya infection: a potential re-emerging global threat. *Asian Pacific Journal of Tropical Medicine,* 9**,** 933-937.

NDEFFO-MBAH, M. L. & GALVANI, A. P. 2017. Global elimination of lymphatic filariasis. *The Lancet Infectious Diseases,* 17**,** 358-359.

NETTO, M. J., BONFIM, C., BRANDAO, E., AGUIAR-SANTOS, A. M. & MEDEIROS, Z. 2016. Burden of lymphatic filariasis morbidity in an area of low endemicity in Brazil. *Acta Tropica,* 163**,** 54-60.

NICHOLSON, J. W. 2006. *The Chemistry of Polymers*, Royal Society of Chemistry.

NORRIS, D. E. 2004. Mosquito-borne diseases as a consequence of land use change. *EcoHealth,* 1**,** 19-24.

OMS-OLIU, G., ODRIOZOLA-SERRANO, I., SOLIVA-FORTUNY, R. & MARTÍN-BELLOSO, O. 2009. Use of Weibull distribution for describing kinetics of antioxidant potential changes in fresh-cut watermelon. *Journal of Food Engineering,* 95**,** 99-105.

OSSWALD, T. A. & MENGES, G. 2012. *Material Science of Polymers for Engineers*, Hanser Publishers.

PADESTE, C. & NEUHAUS, S. 2015. *Polymer Micro- and Nanografting*, Elsevier Science.

PANG, Y. P., EKSTROM, F., POLSINELLI, G. A., GAO, Y., RANA, S., HUA, D. H., ANDERSSON, B., ANDERSSON, P. O., PENG, L., SINGH, S. K., MISHRA, R. K., ZHU, K. Y., FALLON, A. M., RAGSDALE, D. W. & BRIMIJOIN, S. 2009. Selective and irreversible inhibitors of mosquito acetylcholinesterases for controlling malaria and other mosquito-borne diseases. *PLoS One,* 4**,** e6851.

PASCUAL-VILLALOBOS, M. J. & ROBLEDO, A. 1998. Screening for anti-insect activity in Mediterranean plants. *Industrial Crops and Products,* 8**,** 183-194.

PATEL, A. B., RATHOD, H., SHAH, P., PATEL, V., GARSONDIYA, J. & SHARMA, R. 2011. Perceptions regarding mosquito borne diseases in an urban area of Rajkot city. *National Journal of Medical Research,* 1**,** 45-7.

PATEL, M., PITTS, S., BEAVIS, P., ROBINSON, M., MORRELL, P., KHAN, N., KHAN, I., POCKETT, N., LETANT, S., VON WHITE, G. & LABOURIAU, A. 2013. Thermal stability of poly(ethylene-co-vinyl acetate) based materials. *Polymer Testing,* 32**,** 785-793.

PEACOCK, A. J. & CALHOUN, A. 2012. *Polymer Chemistry: Properties and Application*, Carl Hanser Verlag GmbH & Company KG.

PENG, H., SUN, X., WENG, W. & FANG, X. 2017. *Polymer Materials for Energy and Electronic Applications*, Elsevier Science.

PEPPAS, N. A. & FRANSON, N. M. 1983. The swelling interface number as a criterion for prediction of diffusional solute release mechanisms in swellable polymers. *Journal of Polymer Science: Polymer Physics Edition,* 21**,** 983-997.

PETERSEN, L. R., BRAULT, A. C. & NASCI, R. S. 2013. West Nile Virus: review of the literature. *Journal of the American Medical Association,* 310**,** 308-15.

PETHRICK, R. A. 2010. *Polymer Science and Technology for Engineers and Scientists*, Wiley.

PIALOUX, G., GAÜZÈRE, B.-A., JAURÉGUIBERRY, S. & STROBEL, M. 2007. Chikungunya, an epidemic arbovirosis. *The Lancet Infectious Diseases,* 7**,** 319-327.

QI, W., ZHANG, X. & WANG, H. 2018. Self-assembled polymer nanocomposites for biomedical application. *Current Opinion in Colloid & Interface Science,* 35**,** 36-41.

RANDOVÁ, A., BARTOVSKÁ, L., HOVORKA, Š., FRIESS, K. & IZÁK, P. 2009. The membranes (Nafion and LDPE) in binary liquid mixtures benzene+methanol – sorption and swelling. *European Polymer Journal,* 45**,** 2895-2901.

RANSON, H. & LISSENDEN, N. 2016. Insecticide resistance in african *Anopheles* mosquitoes: a worsening situation that needs urgent action to maintain malaria control. *Trends in Parasitology,* 32**,** 187-196.

RAO, K. V. R. & DEVI, K. P. 1988. Swelling controlled-release systems: recent developments and applications. *International Journal of Pharmaceutics,* 48**,** 1-13.

RASOULI, G. & REY, A. D. 2014. Viscoelastic effects on acousto-spinodal decomposition in polymer solutions: early stage analysis. *Journal of Non-Newtonian Fluid Mechanics,* 210**,** 12-28.

REITER, P. 2001. Climate change and mosquito-borne disease. *Environmental Health Perspectives,* 109**,** 141-161.

REVERCHON, E. & CARDEA, S. 2007. Production of controlled polymeric foams by supercritical CO_2. *The Journal of Supercritical Fluids,* 40**,** 144-152.

RHINE, W. D., HSIEH, D. S. T. & LANGER, R. 1980. Polymers for sustained macromolecule release: procedures to fabricate reproducible delivery systems and control release kinetics. *Journal of Pharmaceutical Sciences,* 69**,** 265-270.

RICCI, I., DAMIANI, C., ROSSI, P., CAPONE, A., SCUPPA, P., CAPPELLI, A., ULISSI, U., MOSCA, M., VALZANO, M., EPIS, S., CROTTI, E., DAFFONCHIO, D., ALMA, A., SACCHI, L., MANDRIOLI, M., BANDI, C. & FAVIA, G. 2011. Mosquito symbioses: from basic research to the paratransgenic control of mosquito-borne diseases. *Journal of Applied Entomology,* 135**,** 487-493.

RICCI, I., VALZANO, M., ULISSI, U., EPIS, S., CAPPELLI, A. & FAVIA, G. 2012. Symbiotic control of mosquito borne disease. *Pathogens and Global Health,* 106**,** 380-5.

RIOU, J., POLETTO, C. & BOELLE, P. Y. 2017. A comparative analysis of Chikungunya and Zika transmission. *Epidemics,* 19**,** 43-52.

RITGER, P. L. & PEPPAS, N. A. 1987a. A simple equation for description of solute release I. Fickian and non-fickian release from non-swellable devices in the form of slabs, spheres, cylinders or discs. *Journal of Controlled Release,* 5**,** 23-36.

RITGER, P. L. & PEPPAS, N. A. 1987b. A simple equation for description of solute release II. Fickian and anomalous release from swellable devices. *Journal of Controlled Release,* 5**,** 37-42.

RIVERO, A., VEZILIER, J., WEILL, M., READ, A. F. & GANDON, S. 2010. Insecticide control of vector-borne diseases: when is insecticide resistance a problem. *PLOS Pathogens,* 6**,** 1-9.

SAIZ, C. A., DARVISHMANESH, S., BUEKENHOUDT, A. & VAN DER BRUGGEN, B. 2018. Shortcut applications of the hansen solubility parameter for organic solvent nanofiltration. *Journal of Membrane Science,* 546**,** 120-127.

SALARI, E., AHMADI, K., DEHYAGHOBI, R. Z., PURHEMATY, A. & TAKALLOOZADEH, H. M. 2012. Toxic and repellent effect of harmal (*Peganum harmala L.*) acetonic extract on several aphids and *Tribolium castaneum* (herbst). *Chilean Journal of Agricultural Research,* 72**,** 147-151.

SAMPATHKUMAR, P. 2003. West Nile Virus: epidemiology, clinical presentation, diagnosis, and prevention. *Mayo Clinic Proceedings,* 78**,** 1137-1144.

SAVOVA, M., KOLUSHEVA, T., STOURZA, A. & SEIKOVA, I. 2007. The use of group contribution method for predicting the solubility of seed polyphenols of *Vitis vinifera L.* within a wide polarity range in solvent mixtures. *Journal of the University of Chemical Technology and Metallurgy,* 42**,** 295-300.

SCHNEIDER, C., LANGER, R., LOVEDAY, D. & HAIR, D. 2017. Applications of ethylene vinyl acetate copolymers (EVA) in drug delivery systems. *Journal of Controlled Release,* 262**,** 284-295.

SELKE, S. E. M. & CULTER, J. D. 2016. *Plastics Packaging: Properties, Processing, Applications, and Regulations*, Hanser Publications.

SELVARETNAM, A. A. P., SAHU, P. S., SAHU, M. & AMBU, S. 2016. A review of concurrent infections of malaria and dengue in Asia. *Asian Pacific Journal of Tropical Biomedicine,* 6**,** 633-638.

SHAMILOV, V., BABAYEV, E., KALBALIYEVA, E. & SHAMILOV, F. 2017. Polymer nanocomposites for enhanced oil recovery. *Materials Today: Proceedings,* 4**,** S70-S74.

SIEPMANN, J. & PEPPAS, N. A. 2011. Higuchi equation: derivation, applications, use and misuse. *International Journal of Pharmaceutics,* 418**,** 6-12.

SIGGIA, E. D. 1979. Late stages of spinodal decomposition in binary mixtures. *Physical Review A,* 20**,** 595-605.

SONG, S.-W. & TORKELSON, J. M. 1995. Coarsening effects on the formation of microporous membranes produced via thermally induced phase separation of polystyrene-cyclohexanol solutions. *Journal of Membrane Science,* 98**,** 209-222.

SONI, P., PATIDAR, P. J. & PATIDAR, P. K. 2016. West Nile Virus. *World Journal of Pharmacy and Pharmaceutical Sciences,* 5**,** 1740-1759.

STAIGER, C. L., CORNELIUS, C. J. & WHEELER, D. R. 2004. Hydrogen gas separations using a highly microporous polymer. *ACS Division of Fuel Chemistry, Preprints.* 2 ed.

STEFANIS, E. & PANAYIOTOU, C. 2012. A new expanded solubility parameter approach. *International Journal of Pharmaceutics,* 426**,** 29-43.

SUÁREZ, I. & COTO, B. 2016. GPC-VIS-MALS study of EVA copolymers: Quantification and interactions of SCB and LCB. *Polymer Testing,* 52**,** 265-271.

SUMROIPHON, S., YUWAREE, C., ARUNLERTAREE, C., KOMALAMISRA, N. & RONGSRIYAM, Y. 2006. Bioactivity of citrus seed for mosquito-borne diseases larval control. *The Southeast Asian Journal of Tropical Medicine and Public Health,* 37**,** 123-127.

SUNGKAPREECHA, C., BEILY, M. J., KRESSLER, J., FOCKE, W. W. & ANDROSCH, R. 2018. Phase behavior of the polymer/drug system PLA/DEET: effect of PLA molar mass on subambient liquid-liquid phase separation. *Thermochimica Acta,* 660**,** 77-81.

TANG, S., ZHANG, R., LIU, F. & LIU, X. 2015. Hansen solubility parameters of polyglycolic acid and interaction parameters between polyglycolic acid and solvents. *European Polymer Journal,* 72**,** 83-88.

TEWARY, V. K. & ZHANG, Y. 2015. *Modeling, Characterization and Production of Nanomaterials: Electronics, Photonics and Energy Applications*, Elsevier Science.

TIWARI, A. & SRIVASTAVA, R. B. 2012. *Biotechnology in Biopolymers: Developments, Applications & Challenging Areas*, Smithers Information Limited.

TIWARY, M., NAIK, S., TEWARY, D. K., MITTAL, P. & YADAV, S. 2007. Chemical composition and larvicidal activities of the essential oil of *Zanthoxylum armatum* DC (Rutaceae) against three mosquito vectors. *Journal of Vector Borne Diseases,* 44**,** 198-204.

TOLLE, M. A. 2009. Mosquito-borne diseases. *Current Problems in Pediatric and Adolescent Health Care,* 39**,** 97-140.

VAN DE WITTE, P., DIJKSTRA, P. J., VAN DEN BERG, J. W. A. & FEIJEN, J. 1996. Phase separation processes in polymer solutions in relation to membrane formation. *Journal of Membrane Science,* 117**,** 1-31.

VAN KREVELEN, D. W. & TE NIJENHUIS, K. 2009. *Properties of Polymers: Their Correlation with Chemical Structure; their Numerical Estimation and Prediction from Additive Group Contributions*, Elsevier Science.

VAN LAARHOVEN, J. A. H., KRUFT, M. A. B. & VROMANS, H. 2002. Effect of supersaturation and crystallization phenomena on the release properties of a controlled release device based on EVA copolymer. *Journal of Controlled Release,* 82**,** 309-317.

VAN ZYL, R. L. 2016. The malaria season is upon us. *South African Family Practice,* 58**,** 68-72.

VASENIN, R. M. 1964. The kinetics of swelling of polymers. *Polymer Science U.S.S.R.,* 6**,** 688-694.

VAY, K., SCHELER, S. & FRIESS, W. 2011. Application of hansen solubility parameters for understanding and prediction of drug distribution in microspheres. *International Journal of Pharmaceutics,* 416**,** 202-9.

VIJAYASHAKTHIVEL, A. T., KRISHNAMURTHY, R., RAVISANKAR, B. & KARUNAKARAN, C. 2018. Influence of nanoclay addition on the fatigue behavior of polymer nanocomposites. *Materials Today: Proceedings,* 5**,** 7225-7229.

WALKER, C. M. & PEPPAS, N. A. 1990. Solute and penetrant diffusion in swellable polymers: X. Swelling of multiethylene glycol dimethacrylate copolymers. *Journal of Applied Polymer Science,* 39**,** 2043-2054.

WANG, H., YU, J., BAI, H. & LI, L. 2016. Preparation of PAN nanofiltration membranes by supercritical-CO_2-induced phase separation. *The Journal of Supercritical Fluids,* 118**,** 89-95.

WANG, T., LIU, D. & XIONG, C. 2007. Synthesis of EVA-g-MAH and its compatibilization effect to PA11/PVC blends. *Journal of Materials Science,* 42**,** 3398–3407.

WANG, Z., YU, W. & ZHOU, C. 2015. Preparation of polyethylene microporous membranes with high water permeability from thermally induced multiple phase transitions. *Polymer,* 56**,** 535-544.

WEAVER, S. C. & LECUIT, M. 2015. Chikungunya virus and the global spread of a mosquito-borne disease. *New England Journal of Medicine,* 372**,** 1231-9.

WENJUN, L., ISRAEL, C., YOUXIN, Y. & ISRAEL, C. 1995. Formation and microstructure of polyethylene microporous membranes through thermally induced phase separation. *Chinese Journal of Polymer Science,* 13**,** 7-19.

WHO 2009. Guidelines for efficacy testing of mosquito repellents for human skin. Geneva: World Health Organisation.

WHO 2019. *World Malaria Report 2018*, WHO Regional Office for the Western Pacific.

WIJMANS, J., BAAIJ, J. & SMOLDERS, C. 1983. The mechanism of formation of microporous or skinned membranes produced by immersion precipitation. *Journal of Membrane Science,* 14**,** 263-274.

WINSTANLEY, P. 2001. Modern chemotherapeutic options for malaria. *The Lancet Infectious Diseases,* 1**,** 242-250.

YEWHALAW, D. & KWEKA, E. J. 2016. Insecticide Resistance in East Africa — History, Distribution and Drawbacks on Malaria Vectors and Disease Control. *In:* TRDAN, S. (ed.) *Insecticides Resistance.* IntechOpen.

YOUNG, R. J. & LOVELL, P. A. 2011. *Introduction to Polymers*, CRC Press.

ZHANG, G., XU, X., TANG, J., LIU, H., GE, X. & ZHANG, Z. 2000. Formation of microporous polymeric materials by microemulsion radiation polymerization of butyl acrylate. *Journal of Applied Polymer Science,* 77**,** 1989-1993.

ZHAO, J., WU, L., ZHAN, C., SHAO, Q., GUO, Z. & ZHANG, L. 2017. Overview of polymer nanocomposites: computer simulation understanding of physical properties. *Polymer,* 133**,** 272-287.

PUBLICATIONS

Journal Articles

Mapossa, A.B., Sibanda, M.M., Sitoe, A., Focke, W.W., Braack, L., Ndonyane, C., Moatcho, J., Smart, J., Muaimbo, H., Androsch, R., Loots, M.T. 2018. Microporous polyolefin strands as controlled-release devices for mosquito repellents. *Chemical Engineering Journal*. doi: https://doi.org/10.1016/j.cej. 2018.11.237

Mapossa, A.B., Focke, W.W., Sitoe, A., Androsch, R. (2019). Mosquito repellent thermal stability and air volatility. (Manuscript under review).

Sitoe, A., Mapossa, A.B., Focke, W.W., Muaimbo, H, Androsch, R., Wesley-Smith, J. (2019). Release of mosquito repellents from EVA polymer strands (Manuscript in progress).

Sitoe, A., Mapossa, A.B., Focke, W.W. (2019). Repellent/polyethelene phase equilibrium (Manuscript in progress).

Conferences participated in

Sitoe, A., Mapossa, A.B., Focke, W.W. Attempts to prepare microporous polymer repellent matrices. *14th Annual UNESCO/IUPAC Workshop & Conference on Macromolecules & Materials*, 11 – 13 April 2017, Stellenbosch, South Africa (Poster).

Mapossa, A.B., Sitoe, A., Focke, W.W. Designing microporous LLDPE mosquito repellent anklets. *3rd Southern Africa Malaria Research Conference*, 7 – 9 November 2017, Johannesburg, South Africa (Poster).

Sitoe, A., Mapossa, A.B., Focke, W.W. Designing microporous EVA mosquito repellent anklets. *3rd Southern Africa Malaria Research Conference*, 7 – 9 November 2017, Johannesburg, South Africa (Poster).

Sitoe, A., Focke, W.W., Mapossa, A.B., Braack, L., Androsch, R., Sibanda, M. Microporous polyolefin long-life insect repellent bracelets. *4th Southern Africa Malaria Research Conference*, 30 July to 1 August 2018, Johannesburg, South Africa (Poster).

Mapossa, A.B., Focke, W.W., Sitoe, A., Braack, L., Androsch, R., Sibanda, M.M. Modelling repellent release from long-life bracelets. *4th Southern Africa Malaria Research Conference*, 30 July to 1 August 2018, Johannesburg, South Africa (Poster).

Mapossa, A.B., Focke, W.W., Sitoe, A., Braack, L., Androsch, R., Muiambo, H., Salomé, G. Controlled release of volatile mosquito repellents from nano-structured polymers to reduce infectious tropical diseases. *German-African Cooperation Projects in Infectiology Conference.* 5 – 8 September 2018, Entebbe, Uganda.

Sitoe, A., Focke, W.W., Mapossa, A.B., Braack, L., Androsch, R., Sibanda, M. Microporous polymer matrix as a slow release of insect repellent. The 13th International Conference on Advanced Polymers via Macromolecular Engineering, 15-18 April 2019, Stellenbosch, South Africa (Oral).

APPENDICES

Appendix I: Group contributions

Table I.1: Group contributions to F for Small method

Group	Small	Van Krevelen	Hoy[a]
–CH$_3$	438	420	303.4
–CH$_2$–	272	280	269.0
$\overset{H}{\underset{|}{-\overset{|}{C}-}}$	57	140	176.0
$-\overset{|}{\underset{|}{C}}-$	−190	0	65.5
–CH(CH$_3$)–	495	560	(479.4)
–C(CH$_3$)$_2$–	686	840	(672.3)
—CH=CH—	454	444	497.4
$-\overset{|}{C}=\overset{H}{\underset{|}{C}}-$	266	304	421.5
–C(CH$_3$)=CH–	(704)	724	(724.9)
cyclopentyl	–	1384	1295.1
cyclohexyl	–	1664	1473.3
phenyl	1504	1517	1398.4
p-phenylene	1346	1377	1442.2
–F	(250)	164	84.5
–Cl	552	471	419.6
–Br	696	614	527.7
–I	870	–	–
–CN	839	982	725.5
–CHCN–	(896)	1122	(901.5)
–OH	–	754	462.0
–O–	143	256	235.3
–CO–	563	685	538.1
–COOH	–	652	(1000.1)
–COO–	634	512	668.2
—O-$\overset{O}{\overset{\|}{C}}$-O—	–	767	(903.5)
—$\overset{O}{\overset{\|}{C}}$-O-$\overset{O}{\overset{\|}{C}}$—	–	767	1160.7
—$\overset{O}{\overset{\|}{C}}$-$\overset{H}{\underset{\|}{N}}$—	–	1228	(906.4)
—O-$\overset{O}{\overset{\|}{C}}$-$\overset{H}{\underset{\|}{N}}$—	–	1483	(1036.5)
–S–	460	460	428.4

Table I.2: Group contributions to E_{coh} and V according to Fedors

Group	E_{coh} (J/mol)	V (cm³/mol)
–CH₃	4710	33.5
–CH₂–	4940	16.1
>CH–	3430	−1.0
>C<	1470	−19.2
=CH₂	4310	28.5
=CH–	4310	13.5
>C=	4310	−5.5
–HC≡	3850	27.4
–C≡	7070	6.5
Phenyl	31,940	71.4
Phenylene (o, m, p)	31,940	52.4
Phenyl (trisubstituted)	31,940	33.4
Phenyl (tetrasubstituted)	31,940	14.4
Phenyl (pentasubstituted)	31,940	−4.6
Phenyl (hexasubstituted)	31,940	−23.6
Ring closure 5 or more atoms	1050	16.0
Ring closure 3 or 4 atoms	3140	18.0
Conjugation in ring for each double bond	1670	−2.2
Halogen attached to carbon atom with double bond	−20% of E_{coh} of halogen	4.0
–F	4190	18.0
–F (disubstituted)	3560	20.0
–F (trisubstituted)	2300	22.0
–CF₂– (for perfluoro compounds)	4270	23.0
–CF₃ (for perfluoro compounds)	4270	57.5
–Cl	11,550	24.0
–Cl (disubstituted)	9630	26.0
–Cl (trisubstituted)	7530	27.3
–Br	15,490	30.0
–Br (disubstituted)	12,350	31.0
–Br (trisubstituted)	10,670	32.4
–I	19,050	31.5
–I (disubstituted)	16,740	33.5
–I (trisubstituted)	16,330	37.0
–CN	25,530	24.0
–OH	29,800	10.0
–OH (disubstituted or on adjacent C atoms)	21,850	13.0
–O–	3350	3.8
–CHO (aldehyde)	21,350	22.3
–CO–	17,370	10.8
–COOH	27,630	28.5
–CO₂–	18,000	18.0

(continued)

Table I.2 (continued)

Group	E_{coh} (J/mol)	V (cm^3/mol)
$-CO_3-$ (carbonate)	17,580	22.0
$-C_2O_3-$ (anhydride)	30,560	30.0
$-HCOO-$ (formate)	18,000	32.5
$-CO_2CO_2-$ (oxalate)	26,790	37.3
$-HCO_3$	12,560	18.0
$-COF$	13,400	29.0
$-COCl$	17,580	38.1
$-COBr$	24,150	41.6
$-COI$	29,300	48.7
$-NH_2$	12,560	19.2
$-NH-$	8370	4.5
$-N<$	4190	-9.0
$-N=$	11,720	5.0
$-NHNH_2$	21,980	–
$>NNH_2$	16,740	16
$>NHNH<$	16,740	16
$-N_2$ (diazo)	8370	23
$-N=N-$	4190	–
$>C=N-N=C<$	20,090	0
$-N=C=N-$	11,470	–
$-N=C$	18,840	23.1
$-NF_2$	7660	33.1
$-NF-$	5070	24.5
$-CONH_2$	41,860	17.5
$-CONH-$	33,490	9.5
$-CON<$	29,510	-7.7
$HCON<$	27,630	11.3
$HCONH-$	43,950	27.0
$-NHCOO-$	26,370	18.5
$-NHCONH-$	50,230	–
$-NHCON<$	41,860	–
$>NCON<$	20,930	-14.5
NH_2COO-	37,000	–
$-NCO$	28,460	35.0
$-ONH_2$	19,050	20.0
$>C=NOH$	25,120	11.3
$-CH=NOH$	25,120	24.0
$-NO_2$ (aliphatic)	29,300	24.0
$-NO_2$ (aromatic)	15,360	32.0
$-NO_3$	20,930	33.5
$-NO_2$ (nitrite)	11,720	33.5

(continued)
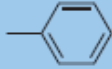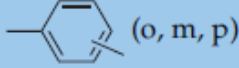
Table I.2 (continued)

Group	E_{coh} (J/mol)	V (cm^3/mol)
$-NH\ NO_2$	39,770	28.7
$-NNO-$	27,210	10
$-SH$	14,440	28.0
$-S-$	14,150	12
$-S_2-$	23,860	23.0
$-S_3-$	13,400	47.2
$>SO$	39,140	–
$-SO_3$	18,840	27.6
$-SO_4$	28,460	31.6
$-SO_2Cl$	37,070	43.5
$-SCN$	20,090	37.0
$-NCS$	25,120	40.0
P	9420	−1.0
$-PO_3$	14,230	22.7
$-PO_4$	20,930	28.0
$-PO_3(OH)$	31,810	32.2
Si	3390	0
SiO_4	21,770	20.0
B	13,810	−2.0
BO_3	0	20.4
Al	13,810	−2.0
Ga	13,810	−2.0
In	13,810	−2.0
Tl	13,810	−2.0
Ge	8080	−1.5
Sn	11,300	1.5
Pb	17,160	2.5
As	12,980	7.0
Sb	16,330	8.9
Bi	21,350	9.5
Se	17,160	16.0
Te	20,090	17.4
Zn	14,480	2.5
Cd	17,790	6.5
Hg	22,810	7.5

Table I.3: Solubility parameter component group contributions (Method of Hoftyzer and Van Krevelen)

Structural group	F_{di} $(MJ/m^3)^{1/2} \cdot mol^{-1}$	F_{pi} $(MJ/m^3)^{1/2} \cdot mol^{-1}$	E_{hi} J/mol
$-CH_3$	420	0	0
$-CH_2-$	270	0	0
$>CH-$	80	0	0
$>C<$	-70	0	0
$=CH_2$	400	0	0
$=CH-$	200	0	0
$=C<$	70	0	0
(cyclohexane ring)	1620	0	0
(benzene ring)	1430	110	0
(benzene ring, o, m, p)	1270	110	0
$-F$	(220)	–	–
$-Cl$	450	550	400
$-Br$	(550)	–	–
$-CN$	430	1100	2500
$-OH$	210	500	20,000
$-O-$	100	400	3000
$-COH$	470	800	4500
$-CO-$	290	770	2000
$-COOH$	530	420	10,000
$-COO-$	390	490	7000
$HCOO-$	530	–	–
$-NH_2$	280	–	8400
$-NH-$	160	210	3100
$>N-$	20	800	5000
$-NO_2$	500	1070	1500
$-S-$	440	–	–
$=PO_4$	740	1890	13,000
Ring	190	–	–
One plane of symmetry	–	$0.50\times$	–
Two planes of symmetry	–	$0.25\times$	–
More planes of symmetry	–	$0\times$	$0\times$

Table I.4: Values of increments in Hoy's system, for the molar attraction function

Groups	$F_{t,i}$ $((MJ/m^3)^{1/2}/mol)$	$F_{p,i}$	V_i (cm^3/mol)	$\Delta_{T,i}*$	$\Delta_{T,i}^{(P)}$	Groups		$F_{t,i}$ $((MJ/m^3)^{1/2}/mol)$	$F_{p,i}$	V_i (cm^3/mol)	$\Delta_{T,i}*$	$\Delta_{T,i}^{(P)}$
$-CH_3$	303.5	0	21.55	0.023	0.022	$-OH \rightarrow$ (H. bonded)		485	485	10.65	0.082	0.034
$-CH_2-$	269.0	0	15.55	0.020	0.020	$-OH$	prim.	675	675	12.45	0.082	0.049
$>CH-$	176.0	0	9.56	0.012	0.013		second.	591	591	12.45	0.082	0.049
$>C<$	65.5	0	3.56	0	0.040		tert.	(500)	(500)	12.45	0.082	0.049
$=CH_2$	259	67	19.17	0.018	0.019		phenolic	350	350	12.45	0.031	0.006
$=CH-$	249	59.5	13.18	0.018	0.0185	$-O-$	ether	235	216	6.45	0.021	0.018
$=C<$	173	63	7.18	0	0.013		acetal	236	102	6.45	0.018	0.018
CH_{ar}	241	62.5	13.42	0.011	0.018		epoxide	361	156	6.45	0.027	0.027
C_{ar}	201	65	7.42	0.011	0.015							
						$-NH_2$		464	464	17.0	0.031	0.035
$-HC=O$	600	532	23.3	0.048	0.045	$-NH-$		368	368	11.0	0.031	0.0275
$>C=O$	538	525	17.3	0.040	0.040	$>N-$		125	125	12.6	0.014	0.009
$-COOH$	565	415	26.1	0.039	0.039							
$-COO-$	640	528	23.7	0.047	0.050	$-S-$		428	428	18.0	0.015	0.032
$-CO-O-CO-$	1160	1160	41.0	0.086	0.086	$-F$		845	73.5	11.2	0.018	0.006
$-C\equiv N$	725	725	23.1	0.060	0.054	$-Cl$	prim.	419.5	307	19.5	0.017	0.031
$-N=C=O$	736	8.2	25.9	0.054	0.054		second.	426	315	19.5	0.017	0.032
$HCON<$	1020	725	35.8	0.062	0.055		arom.	330	81.5	19.5	0.017	0.025
$-CONH_2$	1200	900	34.3	0.071	0.084	$<(Cl)_2$ twinned		705	572	39.0	0.034	0.052
$-CONH-$	1131	895	28.3	0.054	0.073	$-Br$ aliph.		528	123	25.3	0.010	0.039
$-OCONH-$	1265	890	34.8	0.078	0.094		arom.	422	100	25.3	0.010	0.031

(continued)

Table I.4 (continued)

Configurations	$F_{t,i}$	$F_{p,i}$	V_i	$\Delta_{T,i}*$	$\Delta_{T,I}^{(P)}$	Configurations	$F_{t,I}$	$F_{p,i}$	V_i	$\Delta_{T,i}*$	$\Delta_{T,I}^{(P)}$
Base value (**B**)	277	–	–	–	–	Conjugation isomerism	47.5	−19.8	–	0	0.0035
Ring size (non-aromatic)						cis	−14.6	−14.6	–	0	−0.001
						trans	−27.6	−27.6	–	0	−0.002
4-membered	159	203	–	0	0.012	Aromatic substitution					
5-membered	43	85	–	0	0.003	ortho	20.2	−13.3	–	0	0.0015
6-membered	−48	61	–	0	−0.0035	meta	13.5	−24.3	–	0	0.0010
7-membered	92	0	–	0	0.007	para	83	−34.0	–	0	0.006

For bi-, tri- and tetra-valent groups in saturated rings the Δ_T - values must be multiplied by a factor 2/3

156

Appendix II: Calibration of setting feeder for polymers: EVA and LLDP; and pump feed for repellents: DEET and Icaridin;

The calibration setting feeder for the polymers and pump feeder for repellents shows on the chart that the value of the R^2 is approximately 1, indicating accurate calibration.

Icaridin

DEET

$y = 0.0598x - 4E-15$

$R^2 = 1$
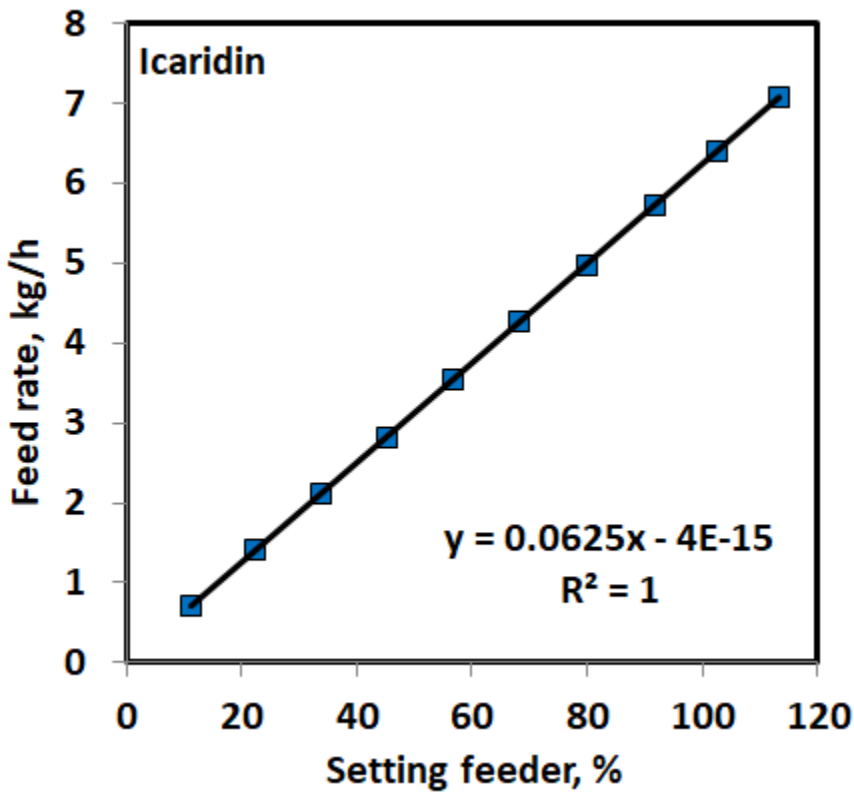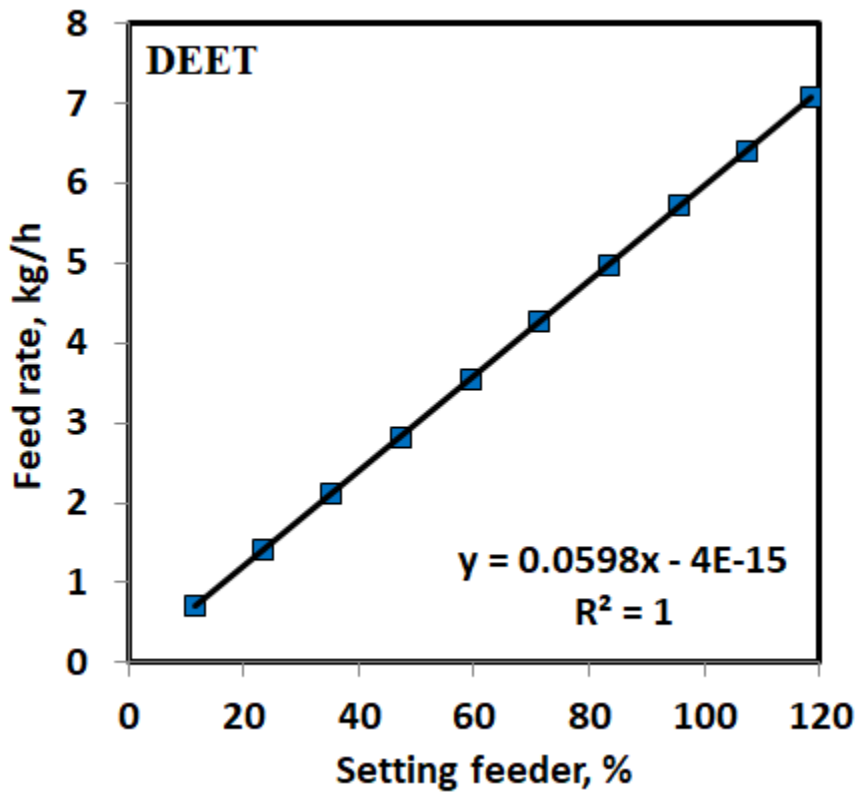
EVA
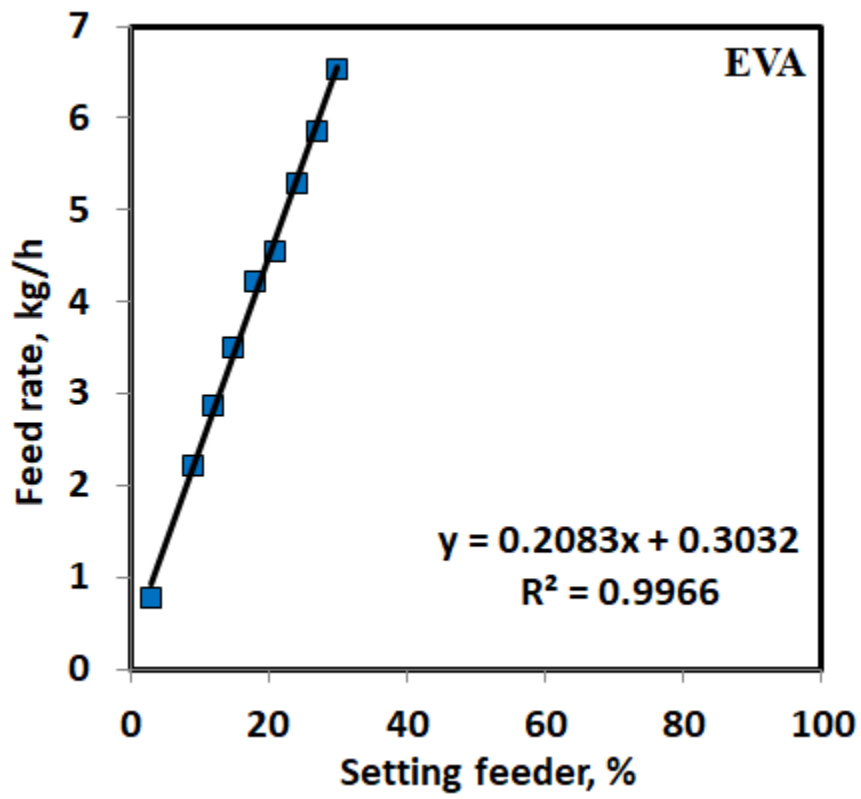
LLDPE
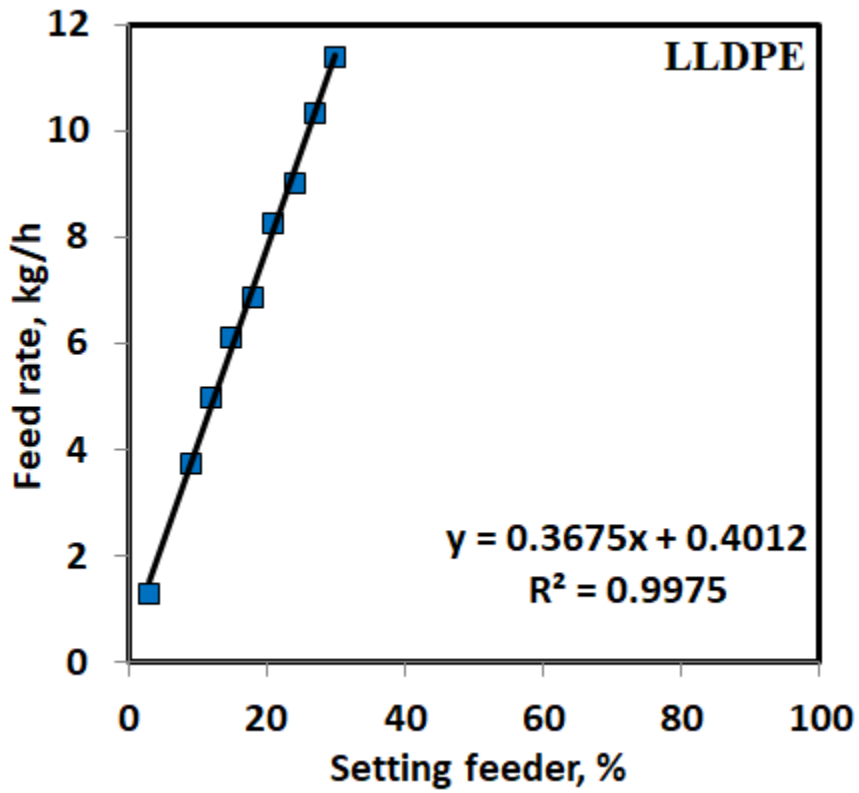
Appendix III: Conditions of compounding of the polymer strands impregnated with repellent without nanofiller

Table III.1: Conditions of compounding of the EVA strands impregnated with repellent without nanofiller

Samples	Vacuum (bar)	Setting Feeder	Kg/h	Pump Feed	Kg/h	LLDPE (wt %)	Repellent (wt %)	Screw speed (rpm)	T*/(°C)	T#/(°C)
EVA Virgin	0.12	5.0	1.34470	0	0	100	0	200	170	2
EVA/DEET	0.12	7.5	1.86545	25	1.7653	51	59	80	170	2
EVA/Icaridin	0.12	5.0	1.34470	20	1.4050	49	51	46.65	170	2

T* = processing temperature; T# = water bath temperature

Table III.2: Conditions of compounding of the LLDPE strands impregnated with repellent without nanofiller

Samples	Vacuum (bar)	Setting Feeder	Kg/h	Pump Feed	Kg/h	LLDPE (wt %)	Repellent (wt %)	Screw speed (rpm)	T*/(°C)	T#/(°C)
LLDPE Virgin	0.12	4.0	1.87212	0	0	100	0	147.74	210	2
LLDPE /DEET	0.12	4.0	1.87212	20	1.324	59	41	46.65	210	2
LLDPE /Icaridin	0.12	4.0	1.87212	20	1.3359	58	42	46.65	210	2

T* = processing temperature; T# = water bath temperature

Appendix IV: Typical compounder settings, i.e. temperature profiles from hopper to die and screw speed used to compound polymer strands

Table IV.1: TX28P extrusion conditions used to compound a composition comprising EVA (60 wt-%), fumed silica (5 wt-%), Dellite 43B (5 wt-%) and DEET (30 wt-%).

Conditions	Zone 1 (ºC)	Zone 2 (ºC)	Zone 3 (ºC)	Die (ºC)	Screw speed (rpm)
Set	140	160	160	160	100
Read	146.5	159.7	160.7	160.3	100

Table IV.2: TX28P extrusion conditions used to compound a composition comprising EVA (50 wt-%), fumed silica (5 wt-%), Dellite 43B (5 wt-%) and DEET (40 wt-%).

Conditions	Zone 1 (ºC)	Zone 2 (ºC)	Zone 3 (ºC)	Die (ºC)	Screw speed (rpm)
Set	140	160	160	160	100
Read	146.5	159.7	160.7	160.3	100

Table IV.3: TX28P extrusion conditions used to compound a composition comprising EVA (60 wt-%), fumed silica (5 wt-%), Dellite 43B (5 wt-%) and Icaridin (30 wt-%).

Conditions	Zone 1 (ºC)	Zone 2 (ºC)	Zone 3 (ºC)	Die (ºC)	Speed screw (rpm)
Set	140	160	160	160	100
Read	143.4	160.2	159.1	160.4	100

Table IV.4: TX28P extrusion conditions used to compound a composition comprising EVA (50 wt-%), fumed silica (5 wt-%), Dellite 43B (5 wt-%) and Icaridin (40 wt-%).

Conditions	Zone 1 (^{o}C)	Zone 2 (^{o}C)	Zone 3 (^{o}C)	Die (^{o}C)	Screw speed (rpm)
Set	140	160	160	160	100
Read	143.4	160.2	159.1	160.4	100

Table IV.5: TX28P extrusion conditions used to compound a composition comprising EVA (75 wt-%), Dellite 43B (5 wt-%) and DEET (20 wt-%).

Conditions	Zone 1 (^{o}C)	Zone 2 (^{o}C)	Zone 3 (^{o}C)	Die (^{o}C)	Screw speed (rpm)
Set	140	160	160	160	100
Read	146.5	159.7	160.7	160.3	100

Table IV.6: TX28P extrusion conditions used to compound a composition comprising EVA (65 wt-%), Dellite 43B (5 wt-%) and DEET (30 wt-%).

Conditions	Zone 1 (^{o}C)	Zone 2 (^{o}C)	Zone 3 (^{o}C)	Die (^{o}C)	Screw speed (rpm)
Set	140	160	160	160	100
Read	146.5	159.7	160.7	160.3	100

Table IV.7: TX28P extrusion conditions used to compound a composition comprising EVA (75 wt-%), Dellite 43B (5 wt-%) and Icaridin (20 wt-%).

Conditions	Zone 1 (^{o}C)	Zone 2 (^{o}C)	Zone 3 (^{o}C)	Die (^{o}C)	Screw speed (rpm)
Set	140	160	160	160	100
Read	143.4	160.2	159.1	160.4	100

Table IV.8: TX28P extrusion conditions used to compound a composition comprising EVA (65 wt-%), Dellite 43B (5 wt-%) and Icaridin (30 wt-%).

Conditions	Zone 1 (ºC)	Zone 2 (ºC)	Zone 3 (ºC)	Die (ºC)	Screw speed (rpm)
Set	140	160	160	160	100
Read	143.4	160.2	159.1	160.4	100

Table IV.9: TX28P extrusion conditions used to compound a composition comprising EVA (65 wt-%), fumed silica (5 wt-%) and DEET (30 wt-%).

Conditions	Zone 1 (ºC)	Zone 2 (ºC)	Zone 3 (ºC)	Die (ºC)	Screw speed (rpm)
Set	140	160	160	160	100
Read	146.5	159.7	160.7	160.3	100

Table IV.10: TX28P extrusion conditions used to compound a composition comprising EVA (55 wt-%), fumed silica (5 wt-%) and DEET (40 wt-%).

Conditions	Zone 1 (ºC)	Zone 2 (ºC)	Zone 3 (ºC)	Die (ºC)	Screw speed (rpm)
Set	140	160	160	160	100
Read	146.5	159.7	160.7	160.3	100

Table IV.11: TX28P extrusion conditions used to compound a composition comprising EVA (65 wt-%), fumed silica (5 wt-%) and Icaridin (30 wt-%).

Conditions	Zone 1 (ºC)	Zone 2 (ºC)	Zone 3 (ºC)	Die (ºC)	Screw speed (rpm)
Set	140	160	160	160	100
Read	143.4	160.2	159.1	160.4	100

Table IV.12: TX28P extrusion conditions used to compound a composition comprising EVA (55 wt-%), fumed silica (5 wt-%) and Icaridin (40 wt-%).

Conditions	Zone 1 (ºC)	Zone 2 (ºC)	Zone 3 (ºC)	Die (ºC)	Screw speed (rpm)
Set	140	160	160	160	100
Read	143.4	160.2	159.1	160.4	100

Table IV.13: TX28P extrusion conditions used to compound a composition comprising LLDPE (60 wt-%), fumed silica (5 wt-%), Dellite 43B (5 wt-%) and DEET (30 wt-%).

Conditions	Zone 1 (ºC)	Zone 2 (ºC)	Zone 3 (ºC)	Die (ºC)	Screw speed (rpm)
Set	140	175	180	190	150
Read	140.6	175.2	178.6	190.5	150

Table IV.14: TX28P extrusion conditions used to compound a composition comprising LLDPE (50 wt-%), fumed silica (5 wt-%), Dellite 43B (5 wt-%) and DEET (40 wt-%).

Conditions	Zone 1 (ºC)	Zone 2 (ºC)	Zone 3 (ºC)	Die (ºC)	Screw speed (rpm)
Set	140	175	180	190	150
Read	138.6	175	180.1	190	150

Table IV.15: TX28P extrusion conditions used to compound a composition comprising LLDPE (60 wt-%), fumed silica (5 wt-%), Dellite 43B (5 wt-%) and Icaridin (30 wt-%).

Conditions	Zone 1 (ºC)	Zone 2 (ºC)	Zone 3 (ºC)	Die (ºC)	Speed screw (rpm)
Set	140	175	180	190	150
Read	141.3	174.3	179.5	189.6	150

Table IV.16: TX28P extrusion conditions used to compound a composition comprising LLDPE (50 wt-%), fumed silica (5 wt-%), Dellite 43B (5 wt-%) and Icaridin (40 wt-%).

Conditions	Zone 1 (ºC)	Zone 2 (ºC)	Zone 3 (ºC)	Die (ºC)	Screw speed (rpm)
Set	140	160	170	170	150
Read	148.5	157.8	165.3	172.1	150

Table IV.17: TX28P extrusion conditions used to compound a composition comprising LLDPE (75 wt-%), Dellite 43B (5 wt-%) and DEET (20 wt-%).

Conditions	Zone 1 (ºC)	Zone 2 (ºC)	Zone 3 (ºC)	Die (ºC)	Screw speed (rpm)
Set	140	175	180	190	150
Read	140.6	175.2	178.6	190.5	150

Table IV.18: TX28P extrusion conditions used to compound a composition comprising LLDPE (65 wt-%), Dellite 43B (5 wt-%) and DEET (30 wt-%).

Conditions	Zone 1 (ºC)	Zone 2 (ºC)	Zone 3 (ºC)	Die (ºC)	Screw speed (rpm)
Set	140	175	180	190	150
Read	141.6	175.2	178.6	190.5	150

Table IV.19: TX28P extrusion conditions used to compound a composition comprising LLDPE (75 wt-%), Dellite 43B (5 wt-%) and Icaridin (20 wt-%).

Conditions	Zone 1 (ºC)	Zone 2 (ºC)	Zone 3 (ºC)	Die (ºC)	Screw speed (%)
Set	140	160	170	170	150
Read	148.5	157.8	165.3	172.1	150

Table IV.20: TX28P extrusion conditions used to compound a composition comprising LLDPE (65 wt-%), fumed silica (5 wt-%) and Icaridin (30 wt-%).

Conditions	Zone 1 (ºC)	Zone 2 (ºC)	Zone 3 (ºC)	Die (ºC)	Screw speed (%)
Set	140	160	170	170	150
Read	148.5	157.8	165.3	172.1	150

Table IV.21: TX28P extrusion conditions used to compound a composition comprising LLDPE (65 wt-%), fumed silica (5 wt-%) and DEET (30 wt-%).

Conditions	Zone 1 (ºC)	Zone 2 (ºC)	Zone 3 (ºC)	Die (ºC)	Screw speed (rpm)
Set	140	175	180	190	150
Read	141.6	175.2	178.6	190.5	150

Table IV.22: TX28P extrusion conditions used to compound a composition comprising LLDPE (55 wt-%), fumed silica (5 wt-%) and DEET (40 wt-%).

Conditions	Zone 1 (ºC)	Zone 2 (ºC)	Zone 3 (ºC)	Die (ºC)	Screw speed (rpm)
Set	140	175	180	190	150
Read	141.6	175.2	178.6	190.5	150

Table IV.23: TX28P extrusion conditions used to compound a composition comprising LLDPE (65 wt-%), fumed silica (5 wt-%) and Icaridin (30 wt-%).

Conditions	Zone 1 (ºC)	Zone 2 (ºC)	Zone 3 (ºC)	Die (ºC)	Screw speed (%)
Set	140	160	170	170	150
Read	148.5	157.8	165.3	172.1	150

Table IV.24: TX28P extrusion conditions used to compound a composition comprising LLDPE (55 wt-%), fumed silica (5 wt-%) and Icaridin (40 wt-%).

Conditions	Zone 1 (ºC)	Zone 2 (ºC)	Zone 3 (ºC)	Die (ºC)	Screw speed (%)
Set	140	160	170	170	150
Read	148.5	157.8	165.3	172.1	150

Appendix V: Diameter size of strands measured by Mutotoyo Vernier caliper
Table V.1: EVA strands

Samples	Diameter size (mm)	Sample No.
EVA-DEET (40)-SiO$_2$ (5)	3.32±0.54	AS100
EVA-Icaridin (40)- SiO$_2$ (5)	3.51±0.24	AS101
EVA-DEET (30)-SiO$_2$ (5)	3.84±0.32	AS200
EVA-DEET (40)-SiO$_2$ (5)	3.60±0.28	AS201
EVA-DEET (30)-43B (5)- SiO$_2$ (5)	3.42±0.28	AS202
EVA-DEET (40)-43B (5)- SiO$_2$ (5)	3.22±0.22	AS203
EVA-Icaridin (30)-SiO$_2$ (5)	4.84±0.30	AS204
EVA-Icaridin (40)-SiO$_2$(5)	3.95±0.38	AS205
EVA-Icaridin (30)-43B (5)-SiO$_2$ (5)	3.72±0.42	AS206
EVA-Icaridin (40)-43B (5)-SiO$_2$ (5)	4.15±0.41	AS207
EVA-DEET (30)-43B (5)	3.96±0.33	AS208
EVA-Icaridin (30)-43B (5)	3.94±0.42	AS209
EVA-Icaridin (20)-43B (5)	2.49±0.21* or 5.76±0.15	AS300
EVA-Icaridin (20)-43B (5)	2.99±0.12* or 3.13±0.11	AS301
EVA-Icaridin (30)-43B (5)	3.88±0.24* or 5.00±0.16	AS302
EVA-Icaridin (30)-43B (5)	4.16±0.21* or 2.89±0.06	AS303
EVA-DEET (20)-43B (5)	2.86±0.19* or 6.01±0.35	AS304
EVA-DEET (20)-43B (5)	2.59±0.22* or 3.39±0.28	AS305
EVA-DEET (30)-43B (5)	6.09±0.14* or 5.50±0.29	AS306
EVA-DEET (30)-43B (5)	3.37±0.20* or 3.27±0.23	AS307
EVA-Icaridin (20)-43B (5)	6.15±0.19	AS400
EVA-Icaridin (30)-43B (5)	5.82±0.16	AS401
EVA-DEET (20)-43B (5)	6.37±0.55	AS402
EVA-DEET (30)-43B (5)	6.22±0.37	AS403

EVA-Icaridin (20)-43B (0)	2.49±0.21	AS500
EVA-Icaridin (20)-43B (1)	2.99±0.12	AS501
EVA-Icaridin (20)-43B (2.5)	3.88±0.24	AS502
EVA-Icaridin (20)-43B (5)	4.16±0.21	AS503
EVA-Icaridin (30)-43B (5)	2.86±0.18	AS504

* Oven-ageing at 30 ℃

Table V.2: LLDPE strands

Samples	Diameter size (mm)	Sample No.
LLDPE-DEET (50)-SiO$_2$ (5)	3.21±0.34	BM100
LLDPE-DEET (40)- SiO$_2$ (5)	3.29±0.52	BM101
LLDPE-DEET (30)-SiO$_2$ (5)	3.93±0.54	BM102
LLDPE-DEET (30)-SiO$_2$ (5)	3.17±0.41	BM103
LLDPE-IR3535 (40)-SiO$_2$ (5)	3.31±0.44	BM104
LLDPE-Icaridin (40)-SiO$_2$ (5)	3.74±0.66	BM105
LLDPE-EA (40)-SiO$_2$ (5)	3.34±0.51	BM106
LLDPE-DEET (30)- 43B (5)- SiO$_2$ (5)	3.64±0.54	BM200
LLDPE-DEET (40)- 43B (5)- SiO$_2$ (5)	3.64±0.41	BM201
LLDPE-Icaridin (30)-43B (5)- SiO$_2$ (5)	3.64±0.25	BM202
LLDPE-Icaridin (40)-43B (5)- SiO$_2$ (5)	3.24±0.33	BM203
LLDPE-IR3535 (30)-43B (5)-SiO$_2$ (5)	3.39±0.44	BM204
LLDPE-IR3535 (40)-43B (5)-SiO$_2$(5)	3.38±0.29	BM205
LLDPE-Icaridin (30)-43B (5)	3.74±0.21	BM206
LLDPE-EA (30)-43B (5)-SiO$_2$ (5)	2.63±0.73	BM207
LLDPE-IR3535 (30)-43 (5)	3.59±0.39	BM208

Appendix VI: Nominal repellent content (in wt-%) and values estimated

Table VI.1: EVA strands

Samples	Solvent extraction	Sample No.
EVA-DEET (40)-SiO$_2$ (5)	37.92±0.19	AS100
EVA-Icaridin (40)- SiO$_2$ (5)	40.30±0.19	AS101
EVA-DEET (30)-SiO$_2$ (5)	29.63±0.06	AS200
EVA-DEET (40)-SiO$_2$ (5)	39.15±0.30	AS201
EVA-DEET (30)-43B (5)- SiO$_2$ (5)	29.33±0.08	AS202
EVA-DEET (40)-43B (5)- SiO$_2$ (5)	36.35±0.11	AS203
EVA-Icaridin (30)-SiO$_2$ (5)	30.25±0.04	AS204
EVA-Icaridin (40)-SiO$_2$(5)	38.76±0.06	AS205
EVA-Icaridin (30)-43B (5)-SiO$_2$ (5)	31.22±0.03	AS206
EVA-Icaridin (40)-43B (5)-SiO$_2$ (5)	38.09±0.10	AS207
EVA-DEET (30)-43B (5)	29.25±0.10	AS208
EVA-Icaridin (30)-43B (5)	25.72±0.04	AS209
EVA-Icaridin (20)-43B (5)	20.34±0.25	AS300
EVA-Icaridin (20)-43B (5)	18.84±0.47	AS301
EVA-Icaridin (30)-43B (5)	29.35±0.05	AS302
EVA-Icaridin (30)-43B (5)	26.83±0.49	AS303
EVA-DEET (20)-43B (5)	17.97±0.66	AS304
EVA-DEET (20)-43B (5)	18.72±0.18	AS305
EVA-DEET (30)-43B (5)	29.12±0.13	AS306
EVA-DEET (30)-43B (5)	29.03±0.21	AS307
EVA-Icaridin (20)-43B (0)	20.19±0.05	AS500
EVA-Icaridin (20)-43B (1)	20.05±0.28	AS501
EVA-Icaridin (20)-43B (2.5)	20.66±0.88	AS502

EVA-Icaridin (20)-43B (5)	19.55±0.19	AS503
EVA-Icaridin (30)-43B (5)	30.11±0.47	AS504

Table VI.2: LLDPE strands

Samples	TGA	Solvent extraction	Sample No.
LLDPE-DEET (50)-SiO_2 (5)	50.55	49.07±0.05	BM100
LLDPE-DEET (40)- SiO_2 (5)	39.25	36.89±0.05	BM101
LLDPE-DEET (30)-SiO_2 (5)	30.67	27.56±0.34	BM102
LLDPE-Icaridin (30)-43B (5)-SiO_2 (5)	29.69	29.42±0.08	BM202
LLDPE-Icaridin (40)-43B (5)- SiO_2 (5)	35.24	36.00±0.07	BM203
LLDPE-Icaridin (42)	-	39.41±0.70	-
LLDPE-DEET (41)	-	40.41±0.63	-

Appendix VII: Repellent release data from EVA polymer strands

Temp. (50 °C) Time (day)	AS100 X(t) (%)	AS101 X(t) (%)
0	0.00	0.00
1	0.20	2.55
4	6.49	4.38
8	12.97	6.47
11	22.52	9.27
12	24.77	9.63
12	24.77	9.63
15	34.16	12.17
18	42.84	17.33
22	50.62	22.09
25	58.04	27.40
26	59.90	28.77
26	59.90	28.77
29	67.12	33.48
32	74.62	39.17
35	79.31	45.24
38	82.82	49.23
39	83.41	50.77
39	83.41	50.77
42	87.76	56.01
45	89.49	63.42
49	91.89	68.70
52	92.42	73.50
56	93.16	78.63
59	93.61	81.71
61	93.81	82.81
61	93.81	82.81

Temp. (50 °C) Time (day)	AS200 X(t) (%)	AS201 X(t) (%)	AS202 X(t) (%)	AS203 X(t) (%)	AS204 X(t) (%)
0	0.00	0.00	0.00	0.00	0.00
3	18.38	8.29	26.11	13.61	0.40
7	31.24	22.23	35.66	31.90	1.33
10	37.73	32.41	42.65	41.54	3.37
14	43.42	39.92	48.87	51.66	6.87
17	49.00	43.87	53.47	56.56	9.26
22	53.66	48.03	58.18	59.09	15.06
25	56.69	50.29	64.09	60.24	17.65
29	59.73	53.77	69.98	62.36	21.18
32	63.98	56.82	69.98	62.36	21.18
36	68.24	58.53	72.48	65.99	26.43
39	69.66	60.74	76.29	67.90	34.03
43	73.11	63.27	77.58	68.59	38.06

Temp. (50 °C) Time (day)	AS205 X(t) (%)	AS206 X(t) (%)	AS207 X(t) (%)	AS208 X(t) (%)	AS209 X(t) (%)
0	0.00	0.00	0.00	0.00	0.00
3	1.68	1.15	0.42	5.36	1.02
7	2.16	2.72	1.12	13.78	1.06
10	4.16	4.88	3.88	17.86	1.66
14	8.06	7.79	8.31	22.41	3.62
17	10.42	12.09	10.38	25.37	4.87
22	14.27	16.29	13.86	28.65	6.50
25	18.03	19.70	16.22	31.20	8.27
29	22.80	19.70	18.60	32.73	9.34
32	22.80	20.29	18.60	32.73	9.34
36	26.62	20.29	21.65	36.17	10.92
39	31.31	23.45	27.35	40.36	13.04
43	34.78	27.01	36.05	45.56	16.29

| Temp. (30 °C) | AS204 | AS205 | AS206 | AS207 |
Time (day)	X(t) (%)	X(t) (%)	X(t) (%)	X(t) (%)
0	0.00	0.00	0.00	0.00
3	2.04	2.79	1.42	2.22
7	3.43	5.29	3.00	4.22
10	4.64	7.38	3.81	5.49
14	5.80	9.51	5.04	7.32
17	6.82	11.23	5.88	8.47
21	7.81	12.94	6.64	10.01
24	8.53	14.41	7.25	11.06
28	9.70	16.39	8.09	12.38
31	10.43	17.74	8.84	13.27
35	11.37	19.29	9.56	14.29
38	12.30	20.69	10.33	15.11
42	13.46	21.98	11.25	16.11
45	14.07	22.96	11.87	17.11
49	14.96	24.13	12.68	18.05
52	15.69	25.41	13.20	18.78
56	16.77	26.86	14.13	19.86
59	17.41	27.63	14.72	20.58
63	18.14	28.39	15.46	21.41
66	18.86	29.36	16.08	22.23
70	19.72	30.35	16.65	23.07
73	20.24	30.80	17.05	23.65
77	20.79	31.53	17.53	24.11
80	21.33	32.15	17.93	24.68
84	21.88	32.94	18.34	25.46
87	22.45	33.64	18.85	26.15
91	22.93	34.57	19.42	26.69
94	23.37	34.95	19.73	27.11

Temp. (50 °C) Time (day)	AS300 X(t) (%)	AS301 X(t) (%)	AS302 X(t) (%)	AS303 X(t) (%)
0	0.00	0.00	0.00	0.00
3	0.36	0.56	-0.19	1.16
7	3.03	1.31	-0.17	1.78
10	5.48	6.10	1.02	3.70
14	7.92	16.86	2.37	6.25
17	8.31	18.37	2.91	7.15
21	9.03	19.63	3.62	8.15
28	11.13	23.67	5.42	10.49
31	12.38	26.13	6.36	12.03
35	13.80	28.84	7.88	13.64
38	14.99	31.26	8.86	14.92
42	16.41	34.34	10.12	16.54
45	17.58	36.67	11.53	18.22
49	19.85	39.98	13.26	19.88
52	21.00	43.20	14.46	21.36
56	22.90	45.82	16.25	23.07
59	24.04	47.15	16.99	24.52
63	25.30	48.83	18.17	25.78
66	26.27	50.41	19.33	26.73
70	27.56	52.28	20.66	29.08
73	28.59	53.56	21.38	29.66
77	30.04	54.87	22.76	31.11
80	31.41	55.90	23.93	32.18
84	32.30	57.61	24.70	34.17
87	33.83	58.81	25.44	35.25
91	35.63	59.98	26.63	37.18
94	36.23	60.98	27.18	37.47

| Temp. (50 °C) | AS304 | AS305 | AS306 | AS307 |
Time (day)	X(t) (%)	X(t) (%)	X(t) (%)	X(t) (%)
0	0.00	0.00	0.00	0.00
3	6.89	11.82	6.66	11.02
7	12.52	17.43	12.48	23.67
10	16.27	20.25	16.00	30.45
14	19.43	23.25	24.97	36.99
17	20.45	24.84	27.18	38.65
21	21.46	26.08	29.18	41.02
28	23.98	28.19	32.74	44.16
31	24.97	29.17	35.61	45.70
35	26.07	30.59	36.34	48.07
38	26.90	31.56	37.79	50.20
42	28.16	32.29	39.53	51.64
45	28.98	33.12	40.94	53.00
49	29.65	33.78	42.48	55.49
52	30.45	34.42	43.57	57.03
56	31.44	35.04	45.01	58.19
59	32.21	35.26	46.52	59.03
63	33.31	35.67	48.28	61.03
66	34.06	36.36	49.69	61.67
70	34.96	36.64	51.39	62.68
73	35.44	36.87	52.54	64.01
77	36.14	37.63	54.13	64.86
80	36.58	37.93	55.06	65.48
84	37.18	38.46	56.46	66.71
87	37.62	38.90	57.58	67.47
91	38.16	39.21	58.82	68.34
94	38.31	39.80	59.22	68.66

Temp. (50 °C) Time (day)	AS400 X(t) (%)	AS401 X(t) (%)	Temp. (50 °C) X(t) (%)	AS402 X(t) (%)	AS403 X(t) (%)
0	0.00	0.00	0	0.00	0.00
2	0.91	0.51	2	5.49	1.06
6	0.91	0.63	6	14.16	4.41
9	1.82	0.86	9	16.87	6.96
13	2.58	1.29	9*	16.87	6.96
13*	2.58	1.29	13	21.13	12.15
16	3.96	2.10	16	23.90	14.11
20	5.08	3.00	20	28.30	17.47
23	6.38	4.04	23	32.02	18.90
27	7.69	5.10	27	37.37	20.76
30	9.01	6.07	27*	37.37	20.76
30*	9.01	6.07	30	40.38	22.94
34	11.26	7.41	34	43.33	27.59
37	13.02	8.30	37	45.02	29.89
40	15.10	9.35	40	46.63	32.09
43	16.15	10.26	40*	46.63	32.09
43*	16.15	10.26	43	49.51	34.88
48	19.41	11.99	48	52.54	39.38
51	21.06	13.48	51	54.91	42.01
54	22.47	14.40	54	57.05	43.71
57	24.92	15.46	54*	57.05	43.71
57*	24.92	15.46	57	59.05	47.03
62	28.68	18.47	62	61.78	50.73
65	30.33	20.17	65	63.24	53.60
69	33.35	21.55	69	65.14	55.69
72	35.72	23.65	69*	65.14	55.69
72*	35.72	23.65	72	66.87	57.92

* after removing three meters for repellence test.

Temp. (50 °C) Time (day)	AS500 X(t) (%)	AS501 X(t) (%)	AS502 X(t) (%)	AS503 X(t) (%)	AS504 X(t) (%)
0	0.00	0.00	0.00	0.00	0.00
1	1.62	2.01	1.01	1.11	1.11
5	4.44	5.62	2.77	2.20	2.54
8	6.55	7.76	3.40	3.13	4.01
12	9.56	9.91	4.59	4.51	5.81
15	11.90	13.38	5.60	5.53	7.13
19	15.79	16.28	6.55	7.02	9.09
22	17.85	19.01	7.48	7.87	10.09
26	22.26	22.19	8.73	9.70	11.58
29	24.48	24.05	10.28	11.01	12.95
33	26.52	28.18	12.12	13.17	15.24
36	28.40	30.24	13.14	14.01	16.77
40	31.66	34.09	13.93	15.44	18.61
43	34.75	35.02	14.70	16.68	20.31
50	39.17	40.30	16.93	18.63	24.04
54	43.21	44.75	17.71	19.95	25.17
57	47.26	46.32	19.21	20.98	26.65
60	50.38	48.84	20.31	22.24	27.87
65	55.12	52.20	21.32	23.33	29.76
70	58.93	55.38	22.75	26.34	32.58

**Appendix VIII: Modelling for repellent released from EVA polymer strands
Hill model**

Sample	Oven temperature (°C)	τ	n	R^2	Error
AS100	50	20.29	2.327	0.9968	16847
AS101	50	36.56	2.589	0.9948	24858
AS200	50	17.29	0.932	0.9944	3514
AS201	50	23.96	0.954	0.9947	3379
AS202	50	12.79	0.974	0.9827	12428
AS203	50	15.38	0.916	0.9899	6827
AS204	50	48.88	2.293	0.9966	1716
AS205	50	51.72	2.047	0.9960	1925
AS206	50	49.43	2.124	0.9908	4661
AS207	50	46.72	2.481	0.9931	4028
AS208	50	44.71	1.138	0.9826	8417
AS209	50	79.75	2.051	0.9978	333
AS400	50	99.97	1.914	0.9989	895
AS401	50	144.47	1.769	0.9985	590
AS402	50	41.99	1.144	0.9967	6888
AS403	50	61.76	1.535	0.9963	7614
AS204	30	369.33	0.856	0.9995	118
AS205	30	189.69	0.849	0.9994	305
AS206	30	497.33	0.832	0.9994	100
AS207	30	310.81	0.817	0.9998	44
AS300	50	156.16	1.185	0.9968	1913
AS301	50	66.12	1.300	0.9952	8839
AS302	50	176.43	1.488	0.9985	668
AS303	50	139.96	1.309	0.9989	749
AS304	50	220.18	0.555	0.9973	945
AS305	50	244.55	0.428	0.9982	469
AS306	50	65.21	0.840	0.9951	5186
AS307	50	35.06	0.747	0.9951	5375
AS500	50	61.47	1.523	0.9936	7859
AS501	50	63.56	1.375	0.9971	3450
AS502	50	226.79	1.047	0.9982	335
AS503	50	180.35	1.136	0.9987	321
AS504	50	130.69	1.223	0.9988	518

Weibull model

Sample	Oven temperature (°C)	τ	n	R^2	Error
AS100	50	26.99	1.525	0.9989	5731
AS101	50	45.62	1.887	0.9987	6354
AS200	50	30.85	0.687	0.9980	1263
AS201	50	40.86	0.727	0.9900	6387
AS202	50	23.03	0.690	0.9926	5350
AS203	50	28.32	0.649	0.9815	12471
AS204	50	56.94	1.999	0.9978	1069
AS205	50	60.93	1.801	0.9974	1193
AS206	50	58.21	1.851	0.9933	3313
AS207	50	54.17	2.136	0.9949	2864
AS208	50	62.76	0.969	0.9876	6000
AS209	50	88.54	1.918	0.9983	256
AS400	50	117.12	1.716	0.9995	413
AS401	50	157.69	1.703	0.9983	307
AS402	50	65.71	0.874	0.9990	1902
AS403	50	82.63	1.250	0.9983	3204
AS204	30	479.70	0.797	0.9994	102
AS205	30	273.91	0.755	0.9985	622
AS206	30	628.29	0.785	0.9993	99
AS207	30	424.91	0.749	0.9996	90
AS300	50	202.97	1.056	0.9977	1305
AS301	50	95.43	1.032	0.9944	10766
AS302	50	210.45	1.361	0.9978	1007
AS303	50	179.16	1.158	0.9993	435
AS304	50	418.38	0.478	0.9971	1024
AS305	50	595.85	0.362	0.9969	829
AS306	50	113.19	0.671	0.9961	4160
AS307	50	71.31	0.553	0.9953	5219
AS500	50	81.12	1.268	0.9966	4139
AS501	50	86.27	1.143	0.9988	1387
AS502	50	280.36	0.976	0.9984	289
AS503	50	222.97	1.050	0.9987	291
AS504	50	164.82	1.106	0.9992	310

Peppas model (2 factors: Diffusion and Relaxation)

Sample	Oven temperature (°C)	τ_1	τ_2	R^2	Error
AS100	50	67.90857	2.22E+12	0.9817	262366
AS101	50	2.23E+12	75.74477	0.9946	50351
AS200	50	77.77561	2.81E+08	0.9977	1762.004
AS201	50	102.2796	2.81E+08	0.9839	12160.32
AS202	50	61.56501	8.97E+16	0.9975	5335.107
AS203	50	72.64648	35461848	0.9609	27675.74
AS204	50	1.96E+13	118.001	0.9826	24185.6
AS205	50	1.96E+13	119.2807	0.9852	15368.32
AS206	50	1.96E+13	115.8026	0.9788	20573.47
AS207	50	1.96E+13	116.2912	0.9719	33197.21
AS208	50	1717.714	119.8739	0.9931	3291.151
AS209	50	1.97E+13	241.2331	0.9710	6921.846
AS400	50	2E+13	232.8559	0.9876	21062.22
AS401	50	2E+13	349.3268	0.9885	12703.32
AS402	50	176.2283	2E+13	0.9980	29245.62
AS403	50	2E+13	125.3823	0.9971	5759.819
AS204	30	2018.075	2E+13	0.9959	7245.245
AS205	30	828.3166	2E+17	0.9987	10035.67
AS206	30	2834.098	2E+13	0.9964	5153.104
AS207	30	1436.59	2E+13	0.9989	6448.133
AS300	50	2E+13	253.5347	0.9981	1595.929
AS301	50	292.0231	2E+13	0.9962	92781.75
AS302	50	4E+13	352.1995	0.9975	5243.644
AS303	50	2E+13	246.8261	0.9993	528.1393
AS304	50	565.6635	2E+13	0.9934	6461.131
AS305	50	476.2086	2E+31	0.9830	33868.9
AS306	50	266.5796	2E+13	0.9957	5484.248
AS307	50	170.5082	2E+13	0.9860	36375.96
AS500	50	2E+13	121.5162	0.9985	1707.361
AS501	50	1E+28	122.2625	0.9994	1832.698
AS502	50	5E+21	295.9447	0.9985	653.8034
AS503	50	2E+13	267.6763	0.9987	361.1363
AS504	50	2E+13	214.8298	0.9994	223.0149

Peppas model (general equation)

Sample	Oven temperature (°C)	τ	n	R^2	Error
AS100	50	57.29	0.716	0.9751	126377
AS101	50	68.47	1.248	0.9971	10739
AS200	50	82.20	0.475	0.9981	1204
AS201	50	94.86	0.530	0.9820	11520
AS202	50	68.18	0.444	0.9974	1823
AS203	50	85.73	0.428	0.9674	21988
AS204	50	69.04	1.720	0.9983	812
AS205	50	74.64	1.566	0.9985	678
AS206	50	71.58	1.592	0.9953	2248
AS207	50	65.53	1.814	0.9959	2189
AS208	50	98.13	0.808	0.9921	3820
AS209	50	99.45	1.789	0.9987	195
AS400	50	141.45	1.528	0.9997	198
AS401	50	195.33	1.495	0.9980	789
AS402	50	136.86	0.625	0.9974	5173
AS403	50	130.23	0.953	0.9976	4643
AS204	30	664.66	0.731	0.9992	179
AS205	30	443.42	0.655	0.9972	1430
AS206	30	842.40	0.729	0.9990	154
AS207	30	625.37	0.677	0.9991	266
AS300	50	278.35	0.933	0.9983	970
AS301	50	164.51	0.789	0.9907	18403
AS302	50	257.75	1.240	0.9969	1484
AS303	50	242.03	1.016	0.9993	493
AS304	50	943.61	0.408	0.9963	1314
AS305	50	1911.84	0.301	0.9949	1376
AS306	50	252.91	0.518	0.9953	5102
AS307	50	233.92	0.386	0.9920	9021
AS500	50	118.35	1.031	0.9987	1480
AS501	50	130.77	0.930	0.9995	567
AS502	50	355.26	0.907	0.9984	269
AS503	50	283.48	0.967	0.9986	303
AS504	50	216.42	0.995	0.9994	221

Appendix IX: Protection Analysis

Repellence test Data

Product	Polymer	Repellent	Level wt.%	Ageing weeks	Test person	Treated foot (L/R)	Time to 1st bite (s)	Number of bites Untreated foot #	Treated foot #	Protection
A	LLDPE	DEET	20	1	X	R	10	49	6	0.78
A	LLDPE	DEET	20	3	Z	L	23	39	4	0.81
A	LLDPE	DEET	20	5	Z	L	48	16	0	1.00
A	LLDPE	DEET	20	7	Z	R	103	20	6	0.54
A	LLDPE	DEET	20	9	Y	R	30	11	0	1.00
A	LLDPE	DEET	20	11	Y	L	54	26	6	0.63
B	LLDPE	DEET	30	1	Z	R	20	26	8	0.53
B	LLDPE	DEET	30	3	Z	R	21	98	12	0.78
B	LLDPE	DEET	30	5	X	R	62	7	0	1.00
B	LLDPE	DEET	30	7	X	R	79	40	1	0.95
B	LLDPE	DEET	30	9	Y	R	27	7	2	0.56
B	LLDPE	DEET	30	11	X	L	26	47	4	0.84
C	LLDPE	Icaridin	20	1	Z	L	13	47	1	0.96
C	LLDPE	Icaridin	20	3	X	R	10	24	3	0.78
C	LLDPE	Icaridin	20	5	X	L	51	45	0	1.00
C	LLDPE	Icaridin	20	7	Z	R	35	18	1	0.89
C	LLDPE	Icaridin	20	9	X	R	27	27	6	0.64
C	LLDPE	Icaridin	20	11	X	L	43	41	15	0.46
D	LLDPE	Icaridin	30	1	X	L	105	18	1	0.89
D	LLDPE	Icaridin	30	3	X	L	15	62	0	1.00

D	LLDPE	Icaridin	30	5	Z	L	29	24	0	1.00
D	LLDPE	Icaridin	30	7	Z	L	57	20	0	1.00
D	LLDPE	Icaridin	30	9	X	L	24	7	0	1.00
D	LLDPE	Icaridin	30	11	Y	L	54	48	1	0.96
E	EVA	DEET	20	2	Z	R	45	36	0	1.00
E	EVA	DEET	20	4	X	R	50	33	0	1.00
E	EVA	DEET	20	6	X	L	32	11	0	1.00
E	EVA	DEET	20	8	Z	L	115	65	13	0.67
E	EVA	DEET	20	10	X	L	57	28	8	0.56
E	EVA	DEET	20	12	X	R	21	29	2	0.87
F	EVA	DEET	30	2	X	L	25	21	0	1.00
F	EVA	DEET	30	4	Z	R	36	17	0	1.00
F	EVA	DEET	30	6	Z	L	25	11	1	0.83
F	EVA	DEET	30	8	X	R	90	20	1	0.90
F	EVA	DEET	30	10	Y	L	75	43	16	0.46
F	EVA	DEET	30	12	Y	R	13	55	8	0.75
G	EVA	Icaridin	20	2	Z	L	20	22	0	1.00
G	EVA	Icaridin	20	4	Z	L	115	7	1	0.75
G	EVA	Icaridin	20	6	Z	R	34	78	4	0.90
G	EVA	Icaridin	20	8	Z	L	28	24	0	1.00
G	EVA	Icaridin	20	10	Y	R	29	13	0	1.00
G	EVA	Icaridin	20	12	Y	L	6	62	6	0.82
H	EVA	Icaridin	30	2	X	L	40	23	0	1.00
H	EVA	Icaridin	30	4	X	L	170	7	0	1.00
H	EVA	Icaridin	30	6	X	R	40	57	3	0.90
H	EVA	Icaridin	30	8	X	R	51	50	0	1.00
H	EVA	Icaridin	30	10	X	R		24	5	0.66

| H | EVA | Icaridin | 30 | 12 | X | L | 6 | 71 | 12 | 0.71 |

Parametric analysis of variance

Mr. Theodor Loots
Department of Statistics, Faculty of Natural and Agricultural Sciences, University of Pretoria

17 September 2018

The factors influencing the efficiency of a mosquito repellent are analyzed below. All the

analyses were performed using R Core Team (2018), and in particular the ANOVA functionality

from the *car* package by Fox and Weisberg (2011).

The following data were received (See Table below):

'data.frame':   48 obs. of 11 variables:

 $ Product   : Factor w/ 8 levels "A","B","C","D",..: 1 1 1 1 1 1 2 2 2 2 ...

 $ Polymer   : Factor w/ 2 levels "EVA","LLDPE": 2 2 2 2 2 2 2 2 2 2 ...

 $ Repellent   : Factor w/ 2 levels "DEET", "Icaridin": 1 1 1 1 1 1 1 1 1 1 ...

 $ Level   : int 20 20 20 20 20 20 30 30 30 30 ...

 $ Week   : int 1 3 5 7 9 11 1 3 5 7 ...

 $ Test.person : Factor w/ 3 levels "AS","BM","RT": 2 1 1 1 3 3 1 1 2 2 ...

 $ Treated.foot: Factor w/ 2 levels "L","R": 2 1 1 2 2 1 2 2 2 2 ...

 $ Time.1st.bite: int 10 23 48 103 30 54 20 21 62 79 ...

 $ Untreated.foot: int 49 39 16 20 11 26 26 98 7 40 ...

 $ Treated.foot.1: int 6 4 0 6 0 6 8 12 0 1 ...

$ Protection: num 0.78 0.81 1 0.54 1 0.63 0.53 0.78 1 0.95 ...

Summary statistics for the measurement variable:

  Min. 1st Qu. Median   Mean 3rd Qu.   Max.

 0.4600 0.7500 0.9000 0.8496 1.0000 1.0000

A parametric analysis of variance (ANOVA) was performed in order to detect significant factors that might have an influence on the protection measurement of the repellent. This ensures that the effect of multiple testing is sufficiently dealt with, i.e. that the probability of detecting an effect does not increase simply because more tests are performed. Following this, a non-parametric ANOVA was performed using the Kruskal-Wallis test, which makes no assumptions of the underlying data structure. In all these tests, the null hypothesis was that no effect was observed.

ANOVA Models

	Sum Sq	Df	F value	Pr(>F)
(Intercept)	0.98	1	36.39	0.0000
Polymer	0.05	1	1.70	0.1997
Repellent	0.08	1	2.83	0.1005
Level	0.01	1	0.50	0.4817
Week	0.11	1	4.05	0.0514
Test.person	0.01	2	0.13	0.8761
Treated.foot	0.00	1	0.01	0.9330
Time.1st.bite	0.02	1	0.61	0.4378
Residuals	1.02	38		

All the variables were tested simultaneously to minimize the effect of multiple testing. The product was not included as a variable, since it leads to an inversion problem of the hessian matrix. From this the following conclusions were possible: Neither product, polymer, repellent, level, test person, treated foot, nor time to first bite had a significant effect on the level of protection. The week seemed to indicate a slight relation to the level of protection. This was damped somewhat by the addition of "time to 1st bite", which is not really an input variable to the model and may be excluded.

These variables were now analysed separately in a non-parametric model.

Kruskal-Wallis Test

	Kruskal.Wallis.chi.squared	df	p.value
Product	7.05	7	0.42
Polymer	0.59	1	0.44
Repellent	2.10	1	0.15
Level	0.32	1	0.57
Week	18.90	11	0.06
Test person	1.67	2	0.43
Treated foot	0.51	1	0.47

These results confirm the results of the ANOVA tests, and furthermore show that the "Week" effect is not significant at a 5% level of significance.

Analysing pre-post data

Since the treated foot did not appear to be a significant effect in the model, the untreated foot was regarded as a control group. Here the number of probes were entered as a dependent variable, and not the protection measurement.

Paired t-test

Data: Count by Group t = 34.417, df = 47, p-value < 2.2e-16

Alternative hypothesis: true difference in means is greater than 0

95% confidence interval:

 0.8082174   Inf

Sample estimates:

Mean of the differences

        0.84964

 Wilcoxon signed rank test with continuity correction

Data: Count by Group

V = 1176, p-value = 6.335e-10

Alternative hypothesis: true location shift is greater than 0

95% confidence interval:

0.8125206   Inf

Sample estimates:

(pseudo)median

0.8729766

Therefore, although no significant effects could be detected between the different treatments, they all differed significantly from the untreated feet, indicating that being treated differed significantly from not being treated, i.e. had significantly fewer probes.

Fox, John and Sanford Weisberg. 2011. *An R Companion to Applied Regression*. 2nd edition. Thousand Oaks CA: Sage. http://socserv.socsci.mcmaster.ca/jfox/Books/Companion

R Core Team. 2018. *R: A language and environment for statistical computing*. Vienna, Austria: R Foundation for Statistical Computing. https://www.R-project.org/.

Appendix X: Specification sheets of polymers, fumed silica and Dellite 43B organoclay considered in this study

Specification of EVA (760)

DuPont Performance Materials

DuPont™ The miracles of science™

DuPont™ Elvax® 760A

Elvax® resins Product Data Sheet

Description	
Product Description	DuPont™ Elvax® 760A is an ethylene-vinyl acetate copolymer resin for use in industrial applications.
Restrictions	
Material Status	Commercial: Active
Typical Characteristics	
Composition	9.3% By Weight Vinyl Acetate comonomer content Thermal Stabilizer: BHT antioxidant
Features	Low level BHT antioxidant
Applications	Elvax® resins can be used in a variety of applications involving molding, compounding, extrusion, adhesives, sealants, and wax blends. For additional information and properties associated with specific applications, please refer to the Grade Selector Guides found on the Elvax® website for industrial applications. http://www.dupont.com/industrial-polymers/elvax/index.html.

Typical Properties			
Physical	**Nominal Values**	**Test Method(s)**	
*Density ( )	0.93 g/cm³	ASTM D792	ISO 1183
*Melt Flow Rate (190°C/2.16kg)	2 g/10 min	ASTM D1238	ISO 1133
Thermal	**Nominal Values**	**Test Method(s)**	
*Melting Point (DSC)	98 °C (208.4 °F)	ASTM D3418	ISO 3146
Freezing Point (DSC)	82 °C (179.6 °F)	ASTM D3418	ISO 3146
Vicat Softening Point ( )	75 °C (167 °F)	ASTM D1525	ISO 306

Processing Information	
*Maximum Processing Temperature	235 °C (455 °F)
General Processing Information	Elvax® resins can be processed by conventional thermoplastic processing techniques, including injection molding, structural foam molding, sheet and shape extrusion, blow molding and wire coating. They can also be processed using conventional rubber processing techniques such as Banbury, two-roll milling and compression molding. Elvax can be used in conventional extrusion equipment designed to process polyethylene resins. However, corrosion-protected barrels, screws, adapters, and dies are recommended, since, at sustained melt temperatures above 455°F (235°C), ethylene vinyl acetate (EVA) resins may thermally degrade and release corrosive by-products.
FDA Status Information	ELVAX® 760A EVA Resin complies with Food and Drug Administration Regulation 21 CFR 177.1350(a)(1) - - Ethylene-vinyl acetate copolymers, subject to the limitations and requirements therein. This Regulation describes polymers that may be used in contact with food, subject to the finished food-contact article meeting the extractive limitations under the intended conditions of use, as shown in paragraph (b)(1) of the Regulation.

Specification of LLDPE (HR411)

LLDPE - Product Data Sheet

HR 411   **LLDPE**

Date of Issue: February 2002   *Print Date: July 2002*

Information
Polymer technology centre
P O Box 72
Modderfontein 1645
South Africa

Tel: +27 (0) 11 458 0700
Fax: +27 (0) 11 458 0734

Polyethylene sales
Sasol Polymers
Johannesburg
Tel: +27 (0) 11 790 1250
Cape Town
Tel: +27 (0) 21 686 7740
Durban
Tel: +27 (0) 31 267 0777

www.sasol.com/polymers

Sasol Polymers
Polythene Business

Rotational moulding/injection moulding

Melt index: 3.5   Density: 0.939

Features	Additives	Applications
High rigidity	Antioxidant	Large mouldings
Excellent impact strength		Thick walled containers
Excellent chemical resistance		Articles for indoor use
Good ESCR		
Tough and abrasion resistant		
Colourable		
Hexene copolymer		

Performance properties – HR 411

Test	Value	Unit	Test method
MFI (190°C/2.16kg)	3.5	g/10min	ASTM D1238
Nominal density	0.939	g/cm^3	ASTM D1505
Tensile strength at yield	19	MPa	ASTM D638 [1]
Tensile strength at break	24	MPa	ASTM D638 [1]
Elongation at break	820	%	ASTM D638 [1]
Flexural modulus	846	MPa	ASTM D790
ESCR F_{50}	>500	hr	ASTM D1693 [2]
Impact energy at –40°C	35	J/mm	ASTM D3029 [3]
Vicat softening temperature	121	°C	ASTM D1525
Shore D hardness	61	Shore D	ASTM D2240

[1] Crosshead speed 50mm/min
[2] 100% Igepal C0630
[3] Tested on rotomoulded product

ARMSA
MEMBER

LLDPE - Product Data Sheet

sasol
reaching new frontiers

Processing (Rotomoulding)

An air temperature of 270˚C to 300˚C is recommended for processing of HR 411. Temperatures above 300˚C should be avoided as this would narrow the processing window considerably and could result in poor physical properties.

Processing (Injection moulding)

HR 411 has a medium melt viscosity making it unsuitable for moulds with long flow paths. Typical melt temperatures would be 200˚C – 280˚C. Parts can be demoulded at relatively high temperatures due to the material's high melting point and rigidity.

Typical temperature profile (Injection moulding)

˚C	H	1	2	3	4	N	M
220							
200							
180							
160							
140							
120							

	H	1	2	3	4	N	M
	Cooled						Cooled
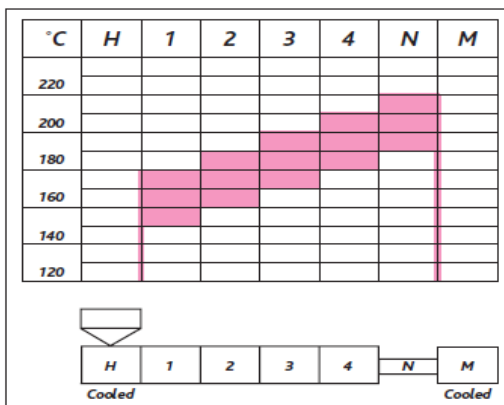
Presentation

Supplied in pellet form packed in 25kg bags. Grinding of pellets is required to make it suitable for rotomoulding.

Handling

Workers should be protected from the possibility of skin or eye contact with molten polymer. Safety glasses are suggested as a minimal precaution to prevent possible mechanical or thermal injury to the eyes. Fabrication areas should be ventilated to carry away fumes or vapours.

Combustibility

Polyethylene resins will burn when supplied with adequate heat and oxygen. They should be handled and stored away from contact with direct flames and/or other ignition sources. In burning, polyethylene resins contribute high heat and may generate a dense black smoke. Fires can be extinguished by conventional means, with water and water mist preferred. In enclosed areas, fire fighters should be provided with self-contained breathing apparatus.

Pigmentation (Rotomoulding)

For colouring purposes inorganic pigments should be added at the lowest possible concentration and mixed in using a high speed mixer or a tumble blender, prior to moulding. Pigment preparations should contain only minimal amounts of dispersants.

Food Packaging

This material complies with F&DA regulation 177.1520 when used unmodified and according to good manufacturing practices for food contact applications. Accordingly, this material may be used in all food contact applications (except holding food during cooking).

Conveying

Conveying equipment should be designed to prevent accumulation of fines and dust particles that are contained in all polyethylene resins. These fines and dust particles can, under certain conditions, pose an explosion hazard. We recommend the conveying system used:
1. be equipped with adequate filters;
2. is operated and maintained in such a manner to ensure no leaks develop;
3. that adequate grounding exists at all times.
We further recommend good housekeeping be practised throughout the facility.

Storage

As ultraviolet light may cause a change in the material, all resins should be protected from direct sunlight during storage.

Specification of Pyrogenic Silica (HDK® N20)

WACKER | **SILICONES**   **HDK®**

HDK® N20
PYROGENIC SILICA

Product description

Synthetic, hydrophilic amorphous silica, produced via flame hydrolysis.

Special features

White colloidal powder of high purity.

Application

HDK® N20 is applied as a thickening and thixotropic agent in many organic systems, e.g. in unsaturated polyesters, coatings, printing inks, adhesives, cosmetics and others. It is used as a reinforcing filler in elastomers, mainly silicone-elastomers. HDK® N20 acts as a free flow additive in the production of technical powders, in food and feed and in pharmaceutical products.

Processing

A good dispersion of HDK® N20 is a must to assure optimum performance.

More detailed information about the application and processing of HDK® N20 is available in our HDK-brochures and on the WACKER web site (http://www.wacker.com/hdk).

Storage

The 'Best use before end' date of each batch is shown on the shipping label and the certificate of analysis.

HDK® N20 should be stored in the original packaging in dry storage areas.

Storage beyond the date specified on the label does not necessarily mean that the product is no longer usable. In this case however, the properties required for the intended use must be checked for quality assurance reasons.

Packaging

HDK® N20 is offered in following packaging:

- paper bags on pallet:
   10 kg bags

- Big bags:
   150 kg (big bags on pallets)

- Silotruck:
   depending on size of truck, approx. 3.5 to 5 tons

Details about packaging and handling:
(http://www.wacker.com/hdk).

Safety notes

Comprehensive instructions are given in the corresponding Material Safety Data Sheets. They are available on request from WACKER subsidiaries or may be printed via the WACKER web site (http://www.wacker.com/hdk).

During transportation and processing HDK® N20 may cause electrostatic charges. Like other amorphous silicas HDK® N20 does not show either carcinogenic (IARC classification, Volume 68, 1997) or mutagenic properties.

WACKER | **SILICONES**   **HDK®**

Product data

Typical general characteristics	Inspection Method	Value
SiO_2 content (based on the substance heated at 1000 °C for 2 h)	DIN EN ISO 3262-19	> 99,8 %
Loss of weight at 1000 °C / 2h (based on the substance dried at 105 °C for 2 h)	DIN EN ISO 3262-19	< 2 %
Density at 20 °C (SiO_2)	DIN 51757	approx. 2,2 g/cm³
Refraction index at 20 °C		1,46
Silanol group density		2 $SiOH/nm^2$
INCI name		Silica

Physical-chemical properties		
BET surface	DIN ISO 9277/ DIN 66132	170 - 230 m²/g
pH-Value (in 4 % aqueous dispersion)	DIN EN ISO 787-9	3,8 - 4,3
Tamped density	DIN EN ISO 787-11	approx. 40 g/l
Loss on drying , ex works (2h at 105 °C)	DIN EN ISO 787-2	< 1,5 %
Sieve residue , acc. to Mocker > 40 µm	DIN EN ISO 787-18	< 0,04 %

199

Specification of Organoclay DELLITE® 43B

DELLITE® 43B
Nanoclay for nanocomposites

Description

DELLITE® 43B is a nanoclay deriving from a naturally occurring montmorillonite especially purified and modified with a quaternary ammonium salt (dimethyl benzylhydrogenated tallow ammonium).
DELLITE® 43B is an additive for polymer application, used to improve various physical and thermo-mechanical properties.

Applications

- Polyolefins
- Polyester
- Polystyrene
- Ethylene Vinyl Acetate
- Polyamides
- Epoxy and acrylic resins
- Rubbers and Elastomers
- (...)

Advantages of Dellite® 43B in Polymeric Systems

- Oxygen, CO_2 and water vapour barrier
- Thermal stability
- Stiffness
- Melt fracture reduction
- Solvent/Chemical resistance
- Weight reduction
- Fiberglas reduction
- Rheology control
- UV transmission
- Flame retardant and Antidropping
- (...)

Chemical and physical data

		DELLITE® 43B
Colour		off white
Moisture	%	3 (max)
Loss of ignition	weight %	32 – 35
Particle size (dry)	micron	7-9 (medium)
Particle size after dispersion	nm	1x500 (medium)
Modifier		dimethyl benzylhydrogenated tallow ammonium
Specific weight	g/cc	1.6
Bulk density	g/cc	0.40

Incorporation

- **Thermoplastic Systems**

According to the application the incorporation of Dellite® 43B into a thermoplastic system is usually carried out as follows:
a) Adding up to 50% of Dellite® 43B in a masterbatch and diluting the master in the final compound
b) Adding directly the Dellite® 43B to the compound.

- **Thermoset Systems**

The incorporation of Dellite® 43B into a thermoset system may be obtained using the following methods:
a) Mixing the desired amount of Dellite® with the resin. Then the curing agent and other additives may be added.
b) Mixing the desired amount of Dellite® with the curing agent. Then the resin and other additives may be added.
c) Resin, curing agent and additives are mixed and then Dellite® 43B is added.

Dosage

The typical levels of use are included in the range 1-5% based on total system weight .

Storage Stability and Packing

Product does not deteriorate in a significant way in a twelve months period.
Storage is advisable in a dry sheltered place in closed bags.
Packing is 25kg net paper bags on wood pallets of 1200kg each. Different packing is possible if required.

All information contained here in is believed to be accurate but is not warranted. It doesn't represent any assurance of properties and fitness for use of the product. Above mentioned specifications may be changed without any notice.

LAVIOSA CHIMICA MINERARIA S.p.A.

I-57123 LIVORNO • Via Leonardo da Vinci, 21
Tel. (+39) 0586 434000 - Fax (+39) 0586 410852
www.laviosa.it • E-mail: additives@laviosa.it

COMPANY WITH QUALITY SYSTEM CERTIFIED BY DNV
Pag. 1 of 1 = ISO 9001/2000=